Ultrafine Particles in California
– Weekly Trends, Source Apportionment, and Sampling Implications

By

Wei Xue

DISSERTATION

Submitted in partial satisfaction of the requirements for the degree of

DOCTOR OF PHILOSOPHY

in

Agricultural and Environmental Chemistry

in the

OFFICE OF GRADUATE STUDIES

of the

UNIVERSITY OF CALIFORNIA

DAVIS

Approved:

Michael J. Kleeman, Chair

Anthony S. Wexler

Qi Zhang

Committee in Charge

2021

ABSTRACT

Ultrafine particulate matter (UFP; airborne particles with diameter < 0.1 μm) is an emerging air quality concern because particles in this size range are potentially more toxic than larger airborne particles. Measurement networks that can support source apportionment calculations for UFPs have been limited in the past by the high costs for equipment, supplies, and labor. The lack of UFP sampling and chemical analysis limits the understanding of spatial and temporal trends, source contributions and health effects of ambient UFP. In the current study, two co-located cascade impactors collected 3-day averaged UFP mass ($PM_{0.1}$) for a full year at four sites in California, United States for the measurement of carbonaceous components and elements, respectively. Monthly samples of particles in the diameter range 0.1 – 1.8 μm were also collected. Statistical analyses of the day-of-week trends for $PM_{0.1}$ components revealed location-specific patterns along with important general trends for UFP concentrations. Source apportionment calculations by Positive Matrix Factorization (PMF) using $PM_{0.1}$ elements as unique tracers identified seven sources. The major source contributions to total $PM_{0.1}$ mass were consistent with results generated by Chemical Mass Balance (CMB) using molecular markers as tracers. The feasibility of employing a single cascade impactor loaded with foil substrates for future $PM_{0.1}$ sampling networks was explored by modifying the extraction method for elements to work on foil substrates. The results of PMF source apportionment calculations carried out with two impactors vs. one impactor were compared. The analyses performed in this study will provide information for understanding $PM_{0.1}$ emission patterns, investigating their health effects and reducing the costs of sampling to enable larger scale $PM_{0.1}$ studies in the future.

ACKNOWLEDGEMENTS

I would like to thank Professor Michael J. Kleeman for his guidance and support. I would like to thank Agricultural and Environmental Chemistry graduate group for their partial financial support and help throughout the process. I would like to thank Professor Anthony S. Wexler, Professor Qi Zhang, and Professor Cort Anastasio for their professionalism and technical expertise. I would like to specially thank Doctor Peter Green for his guidance in the ICP-MS lab. I would like to thank former group mates Eric Jian Xue, Toshi Kuwayama, Melissa A Venecek and Xin Yu for their academic assistance. I would also like to thank Yiting Li, Yin Li and Zhengzao Wang for their friendship and company along this journey. Most importantly, I would like to thank my parents and husband, who have always been there for me. Finally, I would like to thank colleagues at University of Southern California and California State University – Fresno for their collaboration during sampling campaign and California Air Resources Board for partially funding this research under contract #13-418.

Table of Contents

LIST OF TABLES

LIST OF FIGURES

1.0 Introduction

1.1 Motivation

Airborne particulate matter (PM) is hazardous to human health. Many studies have found that exposure to elevated $PM_{2.5}$ (particles with diameter smaller than 2.5 μm) is associated with respiratory and cardiovascular diseases and increased cardiac mortality[1]. Ultrafine particles (UFPs) (particles that are smaller than 100 nm) account for the majority of total suspended particle number concentration and a significant portion of $PM_{2.5}$ surface area. These particle features are at the core of several proposed mechanisms of injury associated with airborne particles, making it important to study to what extent ultrafine particles are contributing to the total toxicity of $PM_{2.5}$. Ultrafine particles are small enough to penetrate cell membranes in the lung and circulate in the blood, giving them the ability to translocate to other organs in the human body [2]. Larger particles in the $PM_{2.5}$ size fraction do not have this ability which limits their possible mechanisms of toxicity.

There have been multiple toxicological studies showing the potential hazards associated with exposure to UFPs [3]. Previous studies have also found that short-term exposure to UPFs may be associated with respiratory and cardiovascular effects [4]. However, the majority of the epidemiological studies investigating the relationship between long-term exposure to UFPs and health effects have not found conclusive associations with human health [5]. These previous epidemiological studies are limited by the lack of a UFP monitoring network that can properly characterize UFP concentrations and composition, including temporal and spatial trends.

Measurements of UFP mass and chemical composition are difficult to obtain because of the high cost of instrumentation and human labor as well as chemical analysis. Measurements of UFP number concentration are easier to make with commercial instruments but the spatial gradients for

UFP number are even more extreme than the spatial gradients for UFP mass, making it difficult to deploy enough measurement sites for exposure analysis. Measuring either UFP mass or number for epidemiological studies therefore faces challenges. The current work attempts to establish improvements in sampling networks for UFP mass measurements that can support future epidemiological studies.

The doctoral research described in this dissertation analyzes the temporal and spatial trends of UFP components and investigates the source contributions to $PM_{0.1}$ It also provides an alternative sampling method to reduce costs of sampling campaign. The research results presented here will aid $PM_{0.1}$ emission regulation and support $PM_{0.1}$ health effect studies.

1.2 Research Objectives

The overall objective of this doctoral research is to characterize the day-of-week trends and source contributions to $PM_{0.1}$ and to test effects of modified extraction method that can potentially reduce sampling costs. The objective was achieved by (i) collecting 3-day average $PM_{0.1}$ samples and monthly average PM samples with size range 0.1 – 1.8 μm at four sites in California for a year, (ii) analyzing the carbonaceous content (OC/EC) and elements concentrations, and (iii) analyzing the measurement data using source apportionment tools. A new element extraction method was evaluated with samples in the 0.1 – 1.8 μm diameter range and tested by calculating the source contributions of simulated $PM_{0.1}$ for comparison with the traditional $PM_{0.1}$ analysis.

1.2.1 Day-of-Week Patterns for Ultrafine Particulate Matter Components at Four Sites in California

The purpose of Chapter 2 is to explore weekly pattern for measured $PM_{0.1}$ components by collecting 3-day $PM_{0.1}$ samples over an annual cycle at four sites across California: Los Angeles,

East Oakland, San Pablo, and Fresno. Statistical analyses are performed, and weekly trends are compared between sites and between species. Since day-of-week patterns of $PM_{0.1}$ have been scarcely studied before, this chapter contributes important information to this field and identifies the unique day-of-week concentration profiles for UFP components that reflect the surrounding sources. These factors must be considered when estimating population exposure to ultrafine particles during future health effects studies.

Note: Material in this chapter has been published in Atmospheric Environment and should be referenced as:

Xue, W., Xue, J., Shirmohammadi, F., Sioutas, C., Lolinco, A., Hasson, A., & Kleeman, M. J. (2020). Day-of-week patterns for ultrafine particulate matter components at four sites in California. *Atmospheric Environment*, *222*, 117088.

1.2.2 Positive Matrix Factorization of Ultrafine Particle Mass ($PM_{0.1}$) at Three Sites in California

Chapter 3 aims to investigate $PM_{0.1}$ sources by performing source apportionment studies using $PM_{0.1}$ OC/EC and elements at Los Angeles, San Pablo and East Oakland. Unique elements tracer (EC3 for Diesel, V for Shipping, Sb for Brake Wear, Rb for Wood Burning) for $PM_{0.1}$ are used because tracers (Na, Cl, Fe, Cu, and Mn) for larger particles, for example, $PM_{2.5,}$ are usually hard to measure on particles smaller than 0.1 μm due to background interferences. Comparable results with source apportionment study using molecular tracers show the validity of the element tracers used. The $PM_{0.1}$ source apportionment results contained in the current study further characterize the seasonal and spatial patterns of ultrafine particle sources and could aid $PM_{0.1}$ emission regulation.

Note: Material in this chapter has been published in Science of Total Environment and should be referenced as:

Xue, W., Xue, J., Mousavi, A., Sioutas, C., & Kleeman, M. J. (2020). Positive matrix factorization of ultrafine particle mass (PM0. 1) at three sites in California. *Science of The Total Environment*, *715*, 136902.

1.2.3 Comparison of size-resolved PM elements measured using aluminum foil and Teflon impaction substrates: implications for ultrafine particle source apportionment and future sampling networks

The goal of Chapter 4 is to test the effects of a modified extraction method for elemental analysis by: 1) comparing the extraction efficiency and measurement accuracy for the traditional and modified method; 2) generating a simulated dataset based on the uncertainty introduced by the modified method,; and 3) comparing the source contributions with results from original datasets at three sites as described in Chapter 2. This modified method could fulfil the measurement of both OC/EC and elements using only one substrate, thus a single sampling device is needed instead of two at each sampling site. Sampling costs could be reduced in half so that the sampling network could be expanded if this method is adopted.

Note: Material in this chapter will be submitted to a research journal and may be cited as "Xue, W., Xue, J., Shirmohammadi, F., Sioutas, C., Lolinco, A., Hasson, A., & Kleeman, M. J. (2021). (in preparation)", until accepted and published.

1.3 References

1. Schwarze, P., et al., *Particulate matter properties and health effects: consistency of epidemiological and toxicological studies.* Human & experimental toxicology, 2006. **25**(10): p. 559-579.

2. Elder, A. and G. Oberdörster, *Translocation and effects of ultrafine particles outside of the lung.* Clinics in occupational and environmental medicine, 2005. **5**(4): p. 785-796.
3. Oberdorster, G., *Toxicology of ultrafine particles: in vivo studies.* Philosophical Transactions of the Royal Society of London Series a-Mathematical Physical and Engineering Sciences, 2000. **358**(1775): p. 2719-2739.
4. Delfino, R.J., C. Sioutas, and S. Malik, *Potential Role of Ultrafine Particles in Associations between Airborne Particle Mass and Cardiovascular Health.* Environmental Health Perspectives, 2005. **113**(8): p. 934-946.
5. Frampton, M., et al., *Understanding the health effects of ambient ultrafine particles.* Boston, MA: Health Effects Institute, 2013.

2.0 Day-of-Week Patterns for Ultrafine Particulate Matter Components at Four Sites in California

Wei Xue[a], Jian Xue[a], Farimah Shirmohammadi[b], Constantinos Sioutas[b], Annabelle Lolinco[c], Alam Hasson[c], and Michael J. Kleeman[a,*]

[a] Department of Civil and Environmental Engineering, University of California – Davis, Davis, California, USA

bDepartment of Civil and Environmental Engineering, University of Southern California, Los Angeles, California, USA

cDepartment of Chemistry, California State University – Fresno, Fresno, California, USA

2.1 Introduction

Many studies have found that exposure to elevated concentrations of airborne particulate matter with diameter smaller than 2.5 μm ($PM_{2.5}$) is associated with respiratory and cardiovascular morbidity and mortality (see for example [1, 2]). Ultrafine particles (UFPs) (particles with aerodynamic diameter smaller than 100 nm) are a sub-fraction of $PM_{2.5}$ that accounts for the majority of total suspended particle number concentration [3, 4] and a significant portion of $PM_{2.5}$ surface area. Toxicological studies suggest that inhaled UFPs deposit deep into the lung where they may penetrate cellular membranes and translocate to other compartments in human body in ways that larger particles do not [5, 6]. Given the potential toxicity of UFPs, exposure assessments are needed to characterize the spatial and temporal trends of UFP concentrations, chemical composition, and source contributions.

UFPs have been measured during multiple short-term studies in California over the past 20 years as summarized in Table 4.2. Early work carried out in Southern California in 1995-1997

determined that $PM_{0.1}$ concentrations were composed of organic compounds (50%), elemental carbon (8.7%), metal oxides (14%), and small portions of nitrate (6.8%), sulfate (8.2%), and ammonium ion (3.7%) [7]. Later UFP studies in Southern California starting in 2002 characterized the organic and inorganic components in quasi-ultrafine particles ($PM_{0.25}$) focusing on source and receptor locations over timescales ranging from weeks to months [8-12]. UFP studies began in California's Central Valley in 2000 with short term studies conducted every few years to measure concentrations and perform source apportionment calculations [13, 14]. Kuwayama et al [15] collected daily UFP mass samples for a full year in Sacramento, CA, but only monthly trends of particle components were reported with no analysis of trends at higher time frequency.

An important gap in the studies summarized in Table 2.1 is the absence of any analysis for day-of-week trends in UFP concentrations. The importance of day-of-week cycles in ambient pollutants has long been recognized for ozone (O_3) concentrations in Los Angeles which are higher on weekends than weekdays [16, 17]. A series of studies followed up on the O_3 finding to analyze the weekly trends of carbon dioxide, $PM_{2.5}$ and its components (OC, EC, NO_x, NH_4^+, NO_3^-, SO_4^{2-}, and metals) to analyze the association between day-of-week cycles and the activity of gasoline / diesel vehicles and other human activities [18-25]. The net results of this work show that day-of-week patterns provide insight on the important sources, chemical pathways, and atmospheric processes that influence pollutant concentrations. Day-of-week cycles also provide an opportunity to better understand the public health impacts of pollutants. Multiple epidemiological studies find that hospital admissions exhibit weekly patterns. For example, acute admissions to hospitals peak on Monday [26], and emergency room visits for asthmatic children are better correlated with a week cycle than daily cycle [27]. These patterns are likely influenced by a range of socioeconomic

factors, but the possible effects of weekly trends in air pollutant concentrations also merits consideration.

Table 2.1. Summary of previous UFP studies in California that measured ultrafine particles.

Location	Date Range and # of sampling days	Particle Size Range	Reference
Pasadena, CA	One month, January/February, 1996	0.017 – 0.250 µm	[28]
Long Beach, Fullerton, and Riverside, CA	Two weeks, September/October, 1996	0.017 – 0.250 µm	[29]
Modesto and Bakersfield, CA	15 days, December 2000 – January 2001	0.056 – 0.1 µm	[13]
Ten sites in urban LA and remote location, CA	Weekly samples, April 2008 – March 2009	<0.25 µm	[30]
Sacramento, CA	Daily sampling, October 2009 – November 2010	0.056 – 0.1 µm	[31]
Central LA and Anaheim, CA	Five-day sampling, July 2012 – February 2013	<0.18 µm	[8]

The purpose of the current study is to analyze day-of-week patterns in UFP concentrations at four locations across California's most heavily polluted air basins. Measurements of UFP chemical composition were made for a period of one year so that trends could be analyzed in all seasons.

Day-of-week patterns are identified for individual chemical species within UFP size fraction at each measurement site. Statistical analysis is conducted to examine similarities between weekly trends for different elements at the same site, and for similarities between trends for the same elements at different sites. Likely combination of sources, chemical reactions, and atmospheric processes that yield the observed day-of-week patterns are discussed.

2.2 Methods

2.2.1 Sampling and chemical analysis

Ultrafine particulate matter samples were collected at four locations in the current study: (i) San Pablo and (ii) East Oakland in the San Francisco Bay Area, (iii) the USC campus in Los Angeles, and (iv) the CSUF campus in Fresno. These locations span the diverse sub-regions of California that experience heavy air pollution. The San Francisco Bay Area has one of the highest population densities in California, and the San Pablo site (SP) and East Oakland (EO) sites are separated by a distance of 30 km within this region. A comparison between these locations enables an evaluation of the sharp spatial gradients for UFP driven by the influence of local sources. Both SP and EO are surrounded by vehicular, industrial, commercial and residential sources. The SP location is within 5 km of a major chemical refinery while the EO location is within 5km of the Oakland International Airport and within 15 km of the Port of Oakland. The greater Los Angeles (LA) region is one of the largest population and economic hubs in the United States. The USC campus in Los Angeles is near major freeways and downwind of important sources including Los Angeles International Airport and the trucking routes connecting the Port of Los Angeles and the Port of Long Beach to the interstate freeway system. Fresno (FR) is the largest city in the heavily polluted San Joaquin Valley, which has some of the worst air quality in the state because of the topography that encourages long stagnation events. The Fresno sampling location is surrounded by

commercial/residential neighborhood and agricultural fields. The FR sampling location was within 3 km of a moderately busy state highway (99) that is a major route for the movement of agricultural goods.

Sample collection at SP, EO and LA started August 2015 and ended July 2016 (duration of twelve months). Due to scheduling difficulties, sampling at FR was conducted during Jan, Feb, Apr, Jun, Jul of 2016 (five months of sampling). Each sampling site was equipped with two Micro-Orifice Uniform Deposit Impactor (MOUDIs) that were operated in parallel to obtain samples averaged over three days. The three-day sample windows were selected in order to collect enough $PM_{0.1}$ on sampling substrates for subsequent chemical analysis. UFP samples in the diameter range 56 – 100 nm were collected on the last stage of each MOUDI accounting for ~80% of the UFP mass [32]. The first MOUDI was loaded with pre-baked aluminum substrates (Foil 0100-96-0573A-X; MSP Corp., Shoreview, MN, USA) for subsequent analysis of elemental carbon and organic carbon. The second MOUDI used Teflon membrane filters (Teflo R2PJ047; Pall Corp., Port Washington, NY, USA) that were later extracted and analyzed for the concentration of elements.

A 1.5 cm^2 portion of each foil substrate was analyzed with Sunset Laboratory EC/OC analyzer following the National Institute for Occupational Safety and Health (NIOSH) temperature protocol [33] modified to avoid melting the aluminum in the sample by reducing the final temperature below 800ºC [32]. Teflon samples were extracted by sonicating them in a mixture of nitric acid and acetone followed by evaporation under nitrogen [34]. Samples were then analyzed using Inductively Coupled Plasma Mass Spectrometry (Agilent ICP-MS 7900) for 60 elements. Instrument minimum detection limits [35] and method minimum detection limits based on filter blanks were calculated. Precision of the OC/EC and elemental analysis was assessed by re-analysis of 10% of total samples (shown in Table 2.2.). Table 2.3 summarizes the components quantified in

the current analysis, along with potential sources and health effects of those components.

Table 2.2. Instrument detection limits, field blank method detection limits, slope and R squared of 10% re-analyzed samples of selected ultrafine species.

Element	Field blank filter method detection limit (ng/m^3)	Instrument detection limit (ng/m^3)	Slope	RSQ
OC	24.39	2.31	1.048	0.973
EC	13.73	2.31	1.052	0.820
Li	6.65E-04	1.04E-04	1.088	0.972
Mg	9.94E-02	6.75E-03	0.990	0.981
S	2.53E+00	3.95E+00	2.025	0.762
K	5.85E-01	1.05E-01	1.087	0.990
V	1.47E-03	1.83E-03	1.036	0.973
As	2.38E-03	2.13E-03	1.029	0.989
Se	3.36E-03	2.15E-03	0.989	0.991
Br	5.00E-03	1.96E-03	0.992	0.963
Rb	4.44E-04	5.07E-05	1.095	0.947
Mo	2.56E-03	6.24E-04	1.133	0.940
Sn	9.39E-03	1.62E-03	0.978	0.996
Sb	1.01E-03	4.04E-04	1.069	0.970
Pb	5.41E-02	1.92E-03	1.099	0.944

Table 2.3. Ultrafine particulate matter components measured in the current study, potential sources for these components, and potential health effects.

Component	Sources	Health effects
OC	Fossil fuel, biomass burning, meat cooking, agricultural [36]	Cardiovascular, respiratory, heart rate variability [37, 38]
EC	Fossil fuel, biomass burning, diesel vehicles, incomplete combustion [36]	Cardiovascular, respiratory, heart rate variability [37, 38]
Li	Glazed ceramic production [39]	Respiratory [40]
Mg	Fossil fuels	No measurable pulmonary toxicity [41]
S	Diesel fuels, marine fuels, oil refining	Cardiovascular [38]

Component	Sources	Health effects
K	Biomass burning, meat cooking [42, 43]	Respiratory [37, 38]
V	Fossil fuels, smelting	Cardiovascular, respiratory [38, 44-46]
As	Fossil fuels, automotive, smelting	Vasospasticity, cell function, heart rate variability, cancer, chronic arsenic poisoning [47, 48]
Se	Fossil fuels, steel production, glazed ceramic production[39]	Selenium poisoning[48]
Br	Marine aerosol, biomass burning, pesticides[49]	Cell function, heart rate variability[37]
Rb	Biomass burning [42, 43]	Respiratory[37]
Mo	Steel production [39]	Respiratory [50]
Sn	Fossil fuels, steel production [39, 51]	Respiratory [52]
Sb	Fossil fuels, crustal dust, smelting[51, 53, 54]	Cell function, heart rate variability, respiratory[53]
Pb	Fossil fuels, smelting, glazed ceramic production[39, 51]	Metabolic disorder and neuropsychological problems [51]

2.2.2 Data analysis

Average day-of-week concentrations of ultrafine particulate matter components were created at each sampling location using successive 3-day average measurements falling on the target day. Table 2.4 illustrates an example based on a ~five-week sampling schedule starting on a Monday. The values illustrated in the table correspond to the 3-day average sample number. In this example, the Monday concentration of the sampling period would be calculated as the average of samples 1,3,5,8,10, and 12. The Wednesday concentrations would be calculated as the average of samples 1,4,6,8, and 11. As the length of the sampling period increases, the accuracy of each daily average

also increases.

Table 2.4. Example sampling schedule over a ~five-week period.

Mon	Tue	Wed	Thu	Fri	Sat	Sun
1	1	1	2	2	2	3
3	3	4	4	4	5	5
5	6	6	6	7	7	7
8	8	8	9	9	9	10
10	10	11	11	11	12	12
12						

The deconvolution algorithm described above was characterized using a Monte Carlo simulation, which creates a dataset of daily concentrations assuming each day of week follows a lognormal distribution (trend A in Figure 2.1). Using the 3-day sampling method illustrated in Table 2.4, the day-of-week pattern (trend B in Figure 2.1) is calculated and compared to the original trend A to quantify the effect of the 3-day averaging sampling method. More specifically, trend A (dashed line in Figure 2.1) represents the true day-of-week concentrations for a candidate UFP species (based on measured EC in this case). The true concentrations follow a unique lognormal distribution on each day of the week characterized by the error bars about the mean value on that day. In this example, the highest true concentrations occur on a Wednesday. During each realization of the Monte Carlo simulation, a synthetic dataset of daily average concentrations spanning the target number of weeks was randomly generated from the true lognormal distribution describing the concentrations on each sample day. The sampling pattern summarized in Table 2.4 was then applied to the synthetic dataset and the deconvolution algorithm was used to reconstruct the day-of-week concentration patterns as they would have been measured in the current study.

Trend B (solid line in Figure 2.1) illustrates the results of our sampling and calculation based on the true ambient concentration described by Trend A. A paired-t test applied to the highest and lowest concentrations in the deconvoluted data was able to detect day-of-week trends with increasing statistical accuracy as the length of the sampling period increased. The p-value for the paired-t test decreased from 0.0228 based on ten weeks of sampling to 0.0131 based on 30 weeks of sampling. In the current study, more than 30 weeks of samples were collected at SP, EO and LA, which should enable the detection of day-of-week trends in UFP concentrations. Less than 20 weeks of samples were collected at FN, which increases the uncertainty of the analysis at this location. It should also be noted that the difference between the highest and lowest concentrations within each week shrinks from 20 ng/m^3 in the true distribution to 10 ng/m^3 in the deconvoluted distribution. This suggests that any day-of-week trends detected in the current study are likely a low estimate of the true weekly profile.

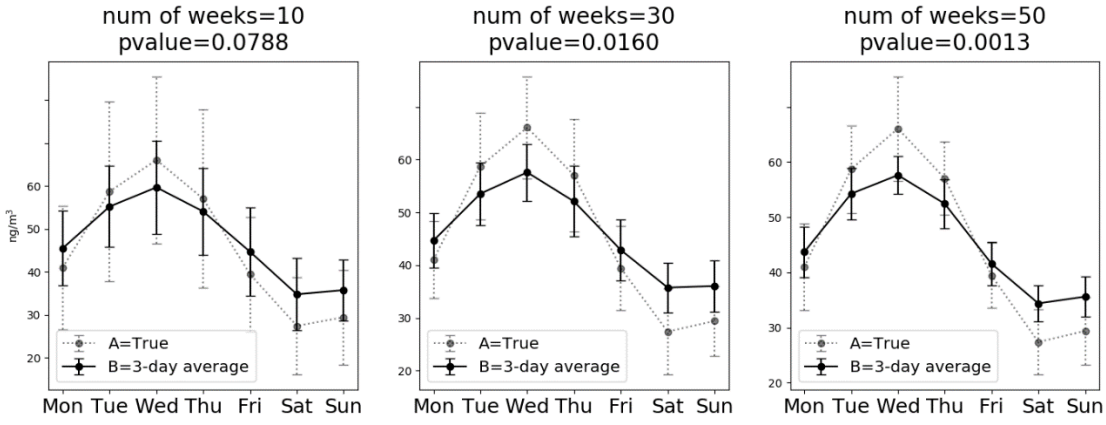

Figure 2.1. Comparison of actual day-of-week-trend (A, dashed line) and deconvoluted 3-day averaged trend (B, solid line). Each scenario based on 30 sets of data-generation and sampling. Error bar represents standard error of the mean for the indicated number of weeks. p-value is the result of paired t-test for the highest concentration and lowest concentration within a week.

2.3 Results

2.3.1 Annual mean concentration and weekly trends

Table 2.5 shows the annual mean concentrations of UFP species at SP, EO, LA, and FR. Organic carbon (OC) and elemental carbon (EC) make up the majority of the UFP mass. Trace elements lithium (Li), magnesium (Mg), sulfur (S), potassium (K), vanadium (V), arsenic (As), selenium (Se), bromine (Br), rubidium (Rb), molybdenum (Mo), tin (Sn), antimony (Sb) and lead (Pb) analyzed here were measured above detection limits and previous studies have shown that they can be measured in the UFP size fraction with reasonable accuracy and precision [34]. Sulfur is the most abundant trace ultrafine element measured in the current study, with annual mean concentration ranging from 2.75 ng/m^3 to 16.34 ng/m^3. Potassium (0.94 – 2.41 ng/m^3) and magnesium (0.14 – 0.29 ng/m^3) are the second and third most abundant elements measured. Potassium has been used as a tracer for residential wood burning [42, 43]; it could also be present in other forms of biomass burning, such as wildfire, campfire, and meat cooking. Comparing the four sites in the current study, Los Angeles (LA) had the highest OC and EC concentrations. FR had the highest annual mean sulfur concentration, which may indicate a local sulfur source near that site. FR also had the highest magnesium, potassium, arsenic, bromine, rubidium and tin concentrations.

Table 2.5. Annual mean concentrations of ultrafine particle components at San Pablo (SP), East Oakland (EO), Los Angeles (LA) and Fresno (FR) in ng/m^3.

Component	SP	EO	LA	FN
OC	97.70 ± 58.74	129.40 ± 81.77	142.22 ± 82.32	125.04 ± 35.00
EC	37.82 ± 21.30	37.45 ± 24.07	55.89 ± 25.96	30.62 ± 16.95
Li	0.0004 ± 0.0004	0.0008 ± 0.0011	0.0014 ± 0.0010	0.0010 ± 0.0007
Mg	0.1730 ± 0.3863	0.1407 ± 0.1495	0.1518 ± 0.1534	0.2863 ± 0.3113

S	7.3721 ± 15.2410	7.8765 ± 14.2216	3.0061 ± 5.8652	17.2568 ± 13.8350
K	0.9407 ± 0.9506	1.1861 ± 1.2987	1.0633 ± 0.8214	2.4134 ± 3.3398
V	0.0080 ± 0.0067	0.0067 ± 0.0086	0.0132 ± 0.0133	0.0019 ± 0.0028
As	0.0125 ± 0.0095	0.0170 ± 0.0258	0.0205 ± 0.0119	0.0267 ± 0.0176
Se	0.0272 ± 0.1460	0.0207 ± 0.0426	0.0458 ± 0.0353	0.0165 ± 0.0159
Br	0.0804 ± 0.0635	0.0883 ± 0.0759	0.1729 ± 0.0765	0.1980 ± 0.1634
Rb	0.0015 ± 0.0013	0.0020 ± 0.0013	0.0018 ± 0.0013	0.0035 ± 0.0031
Mo	0.0087 ± 0.0149	0.0147 ± 0.0219	0.0196 ± 0.0120	0.0024 ± 0.0039
Sn	0.0360 ± 0.1263	0.0691 ± 0.1585	0.1229 ± 0.1121	0.1069 ± 0.1006
Sb	0.0169 ± 0.0160	0.0393 ± 0.0420	0.0949 ± 0.0768	0.0182 ± 0.0085
Pb	0.0592 ± 0.0579	0.0967 ± 0.0997	0.0514 ± 0.0495	0.0630 ± 0.0722

The day-of-week trends for ultrafine species based on a full year of measurements are shown in Figures 2.2 through 2.5 for the four sites considered in the current analysis. All day-of-week profiles are normalized to the annual mean concentrations shown in the title of each sub-panel. Student t-tests were performed on the highest and lowest day-of-week for each subpanel displayed. Asterisks (*) denote significant difference ($p < 0.05$) between the highest and lowest day of the week, while plus signs (+) denote strong ($0.05 < p < 0.1$) difference. Among all the species, OC and EC display similar patterns for highly urbanized locations SP, EO and LA. The weekly trends of OC are relatively flat with slightly higher values in the middle of the week or on the 5th day of the week, while EC values start to rise on Monday, peak on Wednesday and then decline through the weekend. Previous studies also found that the weekly pattern for $PM_{2.5}$ OC is much smaller than the weekly pattern for $PM_{2.5}$ EC[23-25]. The observation of the higher $PM_{0.1}$ EC concentrations on weekdays vs. weekends is consistent with $PM_{2.5}$ EC weekly patterns and is due to greater activity level of diesel vehicles on weekdays as found in previous studies (see for

example, [18, 20, 25]). It is interesting to note that these day-of-week EC trends are still apparent despite the widespread adoption of diesel particle filters (DPFs) in California which remove 99% of EC emissions from diesel vehicles [31]. The EC difference between the highest and lowest days of the week are statistically significant at SP (p = 0.0001), EO (p = 0.0040), and FN (p = 0.015). The p value at LA is 0.056, which indicates a "close to significant" difference.

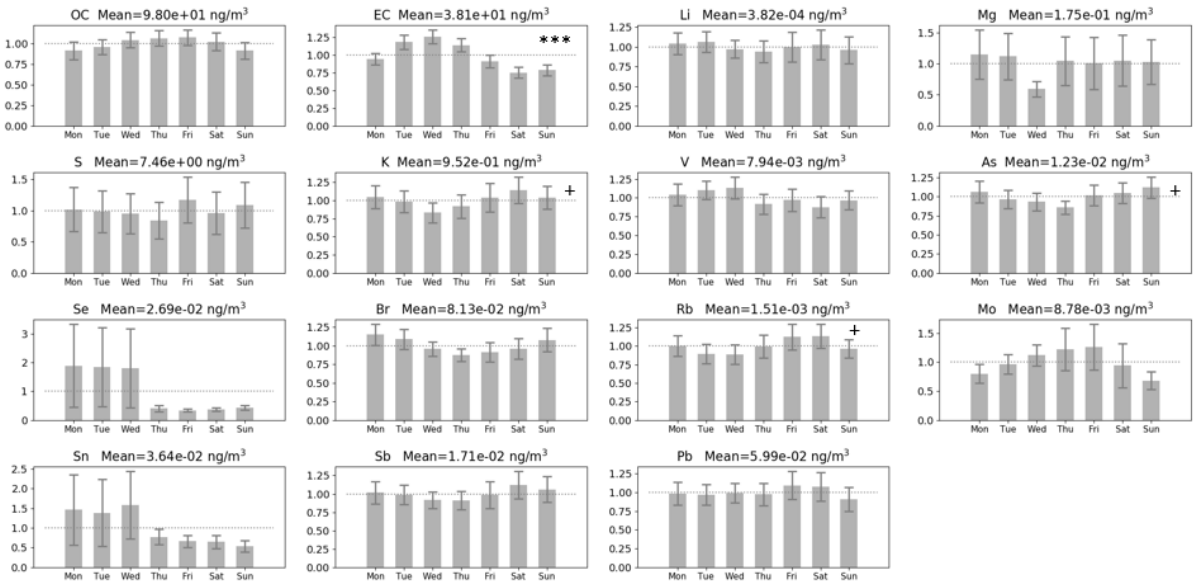

Figure 2.2. Annually averaged weekly profiles normalized to annual mean concentrations for ultrafine components at San Pablo. Error bars represent 1 standard deviation of the mean concentrations. * denotes $p < 0.05$, ** $p < 0.01$, *** $p < 0.001$. + denotes $0.05 < p < 0.1$.

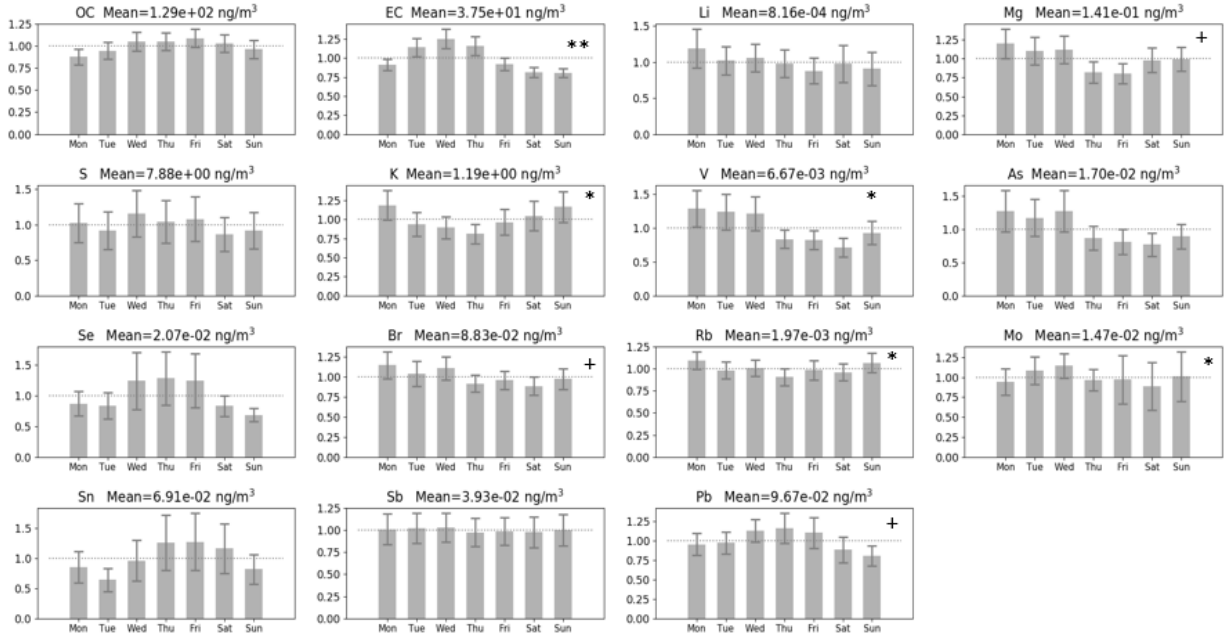

Figure 2.3. Annually averaged weekly profiles normalized to annual mean concentrations for ultrafine components at East Oakland. Error bars represent 1 standard deviation of the mean concentrations. * denotes $p < 0.05$, ** $p < 0.01$, *** $p < 0.001$. + denotes $0.05 < p < 0.1$.

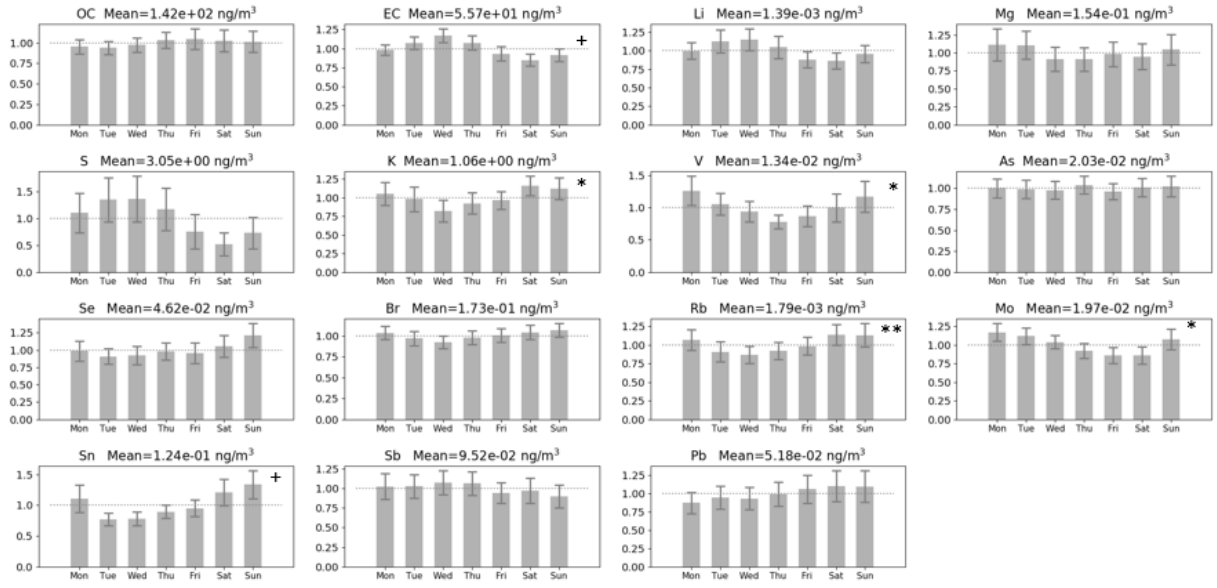

Figure 2.4. Annually averaged weekly profiles normalized to annual mean concentrations for ultrafine components at Los Angeles. Error bars represent 1 standard deviation of the mean concentrations. * denotes $p < 0.05$, ** $p < 0.01$, *** $p < 0.001$. + denotes $0.05 < p < 0.1$.

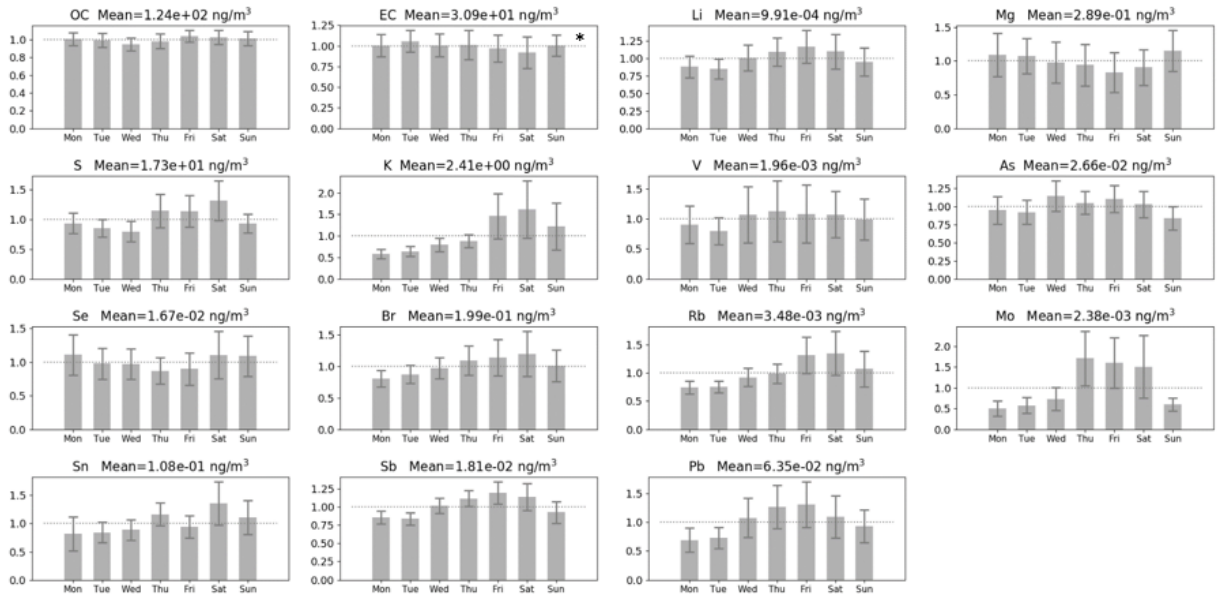

Figure 2.5. Annually averaged weekly profiles normalized to annual mean concentrations for ultrafine components at Fresno. Error bars represent 1 standard deviation of the mean concentrations. * denotes $p < 0.05$, ** $p < 0.01$, *** $p < 0.001$. + denotes $0.05 < p < 0.1$.

Concentrations of Mg, K, and Rb follow similar day-of-week trends at all four sampling sites, with higher concentrations on Friday, Saturday and Sunday. These trends are visually apparent, and statistically significant at EO and LA for K and Rb. $PM_{0.1}$ K and Rb are correlated [13] and both elements have been found in woodsmoke [42]. K and Rb can therefore be treated as tracers for UFP biomass burning sources, such as residential woodsmoke, wildfires, and campfires. The measured day-of-week trends suggest greater activity from these sources on weekends. This finding is consistent with higher $PM_{2.5}$ levoglucosan concentrations (a tracer for wood combustion) on weekends [21].

2.3.2 Correlation analysis

The similarity in two day-of-week profiles ("A" and "B") was quantified using a dotproduct (Eq 2.1) to better compare the trends between sites and species.

$$\text{dotproduct} = \frac{\sum_{i=1}^{7} C_i^{(A)} \cdot C_i^{(B)}}{\sqrt{\sum_{i=1}^{7} (C_i^{(A)})^2} \cdot \sqrt{\sum_{i=1}^{7} (C_i^{(B)})^2}} \quad \text{(Eq. 2.1)}$$

where $C_i^{(A)}$ denotes the concentration of the i^{th} day of the week of trend A, and $C_i^{(B)}$ denotes the concentration of the i^{th} day of the week of trend B. Dotproduct values of 1.0 indicate perfect agreement between two day-of-week profiles, while dotproduct values of 0.0 indicate no agreement. Comparisons can be made where "A" and "B" represent different elements at the same site, or where "A" and "B" represent the same element at different sites.

2.3.3 Correlation between different elements at the same site

Tables 2.6 through 2.9 display the correlation between weekly trends for different elements at the same site. Values greater than 0.9 are marked in bold to represent strong similarity in day-of-week trends. The weekly trends for various species at each site can be grouped based on the dotproducts in combination with the plots in Figures 2 through 5.

In Table 2.6 (site SP), UFP species OC, Mo, and Pb are assigned to be Group I(M-F) because these species all follow the pattern with concentration increasing from Monday, peaking on Friday and then declining through weekend. Trends for OC and Pb are very flat while Mo has much more obvious difference between highest and lowest day of the week. UFP species K, As, Br, Rb and Sb are assigned to Group II(S-M). Each of these UFP elements has minimum concentrations during the middle of the week and higher concentrations on the weekend or immediately following the weekend. Timing is slightly different for subsets of Group II(S-M) species since K, Rb and Sb (Group IIa) peak on Saturday while As and Br (Group IIb) peak on Sunday / Monday. Group III(M-W) (V, Sn, and Se) features higher concentrations from Monday to Wednesday and decreasing concentration thereafter. Sn and Se are abnormally high on Mondays to Wednesday which could

be driven by unusual events. Several refinery flares occurred in the San Francisco Bay Area during June 2016 that may have released ultrafine metals to the atmosphere.

In Table 2.7 (site EO), OC, S, Se, Sn and Pb are assigned to Group I(M-F) because of the higher concentrations on Fridays. Consistent with site SP, Group II(S-M) at EO also demonstrates higher concentrations on weekends, but the elements in this group are different at EO and SP. Group II(S-M) elements at EO include K and Rb, while Group III(M-W) elements (concentrations higher Monday to Wednesday) include Li, Mg, V, As, and Br. It should be noted that SP and EO are separated by a distance of approximately 30 km and so they can be used to investigate the spatial gradients in UFP concentrations. Although SP and EO both have three day-of-week trends (Groups I(M-F), II(S-M), and III(M-W)), the species contained in each group varies between sites. This finding is consistent with past measurements indicating that UFPs are dominated by fresh emissions and therefore more influenced by emissions sources around the measurement site as opposed to $PM_{2.5}$ concentrations that are strongly influenced by secondary concentrations.

Tables 2.6 and 2.7 identify OC and Pb as species in Group I(M-F) for both SP and EO. UFP day-of-week profiles for Pb were somewhat correlated with Group I species at both locations. Pb was phased-out of motor-vehicle gasoline over 40 years ago, but Pb is still present in paved road dust and Pb is still used in general-aviation gasoline for piston-engine aircraft. Pb is also emitted from metal recycling facilities and from waste incinerators. K and Rb belong to Group II(S-M) at both SP and EO, reflecting the higher incidence of biomass burning activities such as fireplaces (winter) or campfires (summer) on weekends. The higher concentration at the beginning of the week is likely associated with lingering $PM_{0.1}$ from Sunday. V present in Group III(M-W) for both SP and EO is associated with shipping activities during weekdays, because both SP and EO are adjacent to the Port of Oakland.

Table 2.6. Dot products between ultrafine constituents at the same site. Dot product is calculated based on one (1) year of measurements at San Pablo (SP).

SP	OC	EC	Li	Mg	S	K	V	As	Se	Br	Rb	Mo	Sn	Sb	Pb
OC	1	-	-	-	-	-	-	-	-	-	-	-	-	-	-
EC	0.747	1	-	-	-	-	-	-	-	-	-	-	-	-	-
Li	0.627	0.629	1	-	-	-	-	-	-	-	-	-	-	-	-
Mg	0.647	0.610	0.830	1	-	-	-	-	-	-	-	-	-	-	-
S	0.649	0.512	0.738	0.789	1	-	-	-	-	-	-	-	-	-	-
K	0.636	0.408	0.837	**0.926**	0.835	1	-	-	-	-	-	-	-	-	-
V	0.529	0.865	0.742	0.674	0.707	0.536	1	-	-	-	-	-	-	-	-
As	0.454	0.453	0.764	0.868	0.885	0.898	0.727	1	-	-	-	-	-	-	-
Se	0.367	0.801	0.730	0.562	0.498	0.413	**0.938**	0.596	1	-	-	-	-	-	-
Br	0.325	0.579	0.785	0.820	0.735	0.748	0.856	**0.921**	0.823	1	-	-	-	-	-
Rb	0.792	0.364	0.715	0.795	0.774	**0.910**	0.348	0.695	0.203	0.467	1	-	-	-	-
Mo	**0.979**	0.831	0.684	0.713	0.692	0.641	0.639	0.501	0.488	0.425	0.756	1	-	-	-
Sn	0.536	0.882	0.753	0.595	0.537	0.456	**0.939**	0.583	**0.978**	0.772	0.318	0.636	1	-	-
Sb	0.497	0.240	0.751	0.793	0.737	**0.949**	0.425	0.868	0.316	0.692	0.825	0.459	0.339	1	-
Pb	**0.911**	0.600	0.822	0.755	0.786	0.832	0.542	0.645	0.422	0.494	**0.930**	0.893	0.552	0.726	1

Table 2.7. Dot products between ultrafine constituents at the same site. Dot product is calculated based on one (1) year of measurements at East Oakland (EO).

EO	OC	EC	Li	Mg	S	K	V	As	Se	Br	Rb	Mo	Sn	Sb	Pb
OC	1	-	-	-	-	-	-	-	-	-	-	-	-	-	-
EC	0.743	1	-	-	-	-	-	-	-	-	-	-	-	-	-
Li	0.495	0.712	1	-	-	-	-	-	-	-	-	-	-	-	-
Mg	0.505	0.672	**0.930**	1	-	-	-	-	-	-	-	-	-	-	-
S	0.823	0.845	0.710	0.651	1	-	-	-	-	-	-	-	-	-	-
K	0.532	0.341	0.730	0.823	0.534	1	-	-	-	-	-	-	-	-	-
V	0.521	0.792	**0.908**	**0.944**	0.761	0.714	1	-	-	-	-	-	-	-	-
As	0.484	0.801	**0.923**	**0.939**	0.764	0.654	**0.989**	1	-	-	-	-	-	-	-
Se	**0.915**	0.855	0.602	0.501	**0.940**	0.407	0.607	0.600	1	-	-	-	-	-	-
Br	0.528	0.743	**0.914**	**0.934**	0.810	0.747	**0.982**	**0.980**	0.630	1	-	-	-	-	-
Rb	0.559	0.508	0.805	0.897	0.689	**0.956**	0.857	0.814	0.512	0.893	1	-	-	-	-
Mo	0.724	0.892	0.680	0.793	0.818	0.555	0.874	0.857	0.728	0.838	0.723	1	-	-	-
Sn	**0.941**	0.614	0.532	0.451	0.781	0.577	0.438	0.404	0.889	0.477	0.550	0.530	1	-	-
Sb	0.565	0.775	0.818	**0.937**	0.743	0.705	**0.963**	**0.954**	0.578	**0.946**	0.854	**0.934**	0.417	1	-
Pb	0.892	**0.907**	0.682	0.586	**0.938**	0.450	0.698	0.686	**0.988**	0.701	0.561	0.781	0.857	0.653	1

Table 2.8 summarizes correlations between day-of-week profiles for different UFP elements at LA. Group I(M-F) consists of OC and Pb, with relatively flat weekly trends and a slight increase starting Friday. Group II(S-M) exhibits lower concentration in the middle of the week and contains Mg, V, Mo, K, Br, Rb, Sn and Se. Among these Group II(S-M) species, only K and Rb have similar values on Saturday and Sunday, with other species having Saturday concentrations lower than Sunday concentrations. Group III(M-F) at LA includes EC, Li and S which peak on Wednesday and then decrease throughout the week.

Table 2.8. Dot products between ultrafine constituents at the same site. Dot product is calculated based on one (1) year of measurements at Los Angeles (LA).

LA	OC	EC	Li	Mg	S	K	V	As	Se	Br	Rb	Mo	Sn	Sb	Pb
OC	1	-	-	-	-	-	-	-	-	-	-	-	-	-	-
EC	0.543	1	-	-	-	-	-	-	-	-	-	-	-	-	-
Li	0.435	**0.978**	1	-	-	-	-	-	-	-	-	-	-	-	-
Mg	0.499	0.575	0.641	1	-	-	-	-	-	-	-	-	-	-	-
S	0.525	**0.987**	**0.984**	0.672	1	-	-	-	-	-	-	-	-	-	-
K	0.755	0.449	0.474	0.844	0.510	1	-	-	-	-	-	-	-	-	-
V	0.519	0.579	0.648	**0.930**	0.647	0.884	1	-	-	-	-	-	-	-	-
As	0.687	0.786	0.810	0.775	0.826	0.825	0.825	1	-	-	-	-	-	-	-
Se	0.757	0.326	0.334	0.645	0.346	0.871	0.750	0.731	1	-	-	-	-	-	-
Br	0.803	0.457	0.459	0.842	0.513	**0.981**	0.880	0.817	**0.904**	1	-	-	-	-	-
Rb	0.697	0.334	0.360	0.791	0.390	**0.972**	0.889	0.749	0.888	**0.970**	1	-	-	-	-
Mo	0.368	0.781	0.857	0.879	0.840	0.670	**0.904**	0.838	0.542	0.674	0.630	1	-	-	-
Sn	0.767	0.324	0.330	0.721	0.362	**0.946**	0.829	0.749	**0.961**	**0.968**	**0.976**	0.576	1	-	-
Sb	0.615	**0.946**	**0.914**	0.575	**0.947**	0.553	0.598	0.844	0.347	0.539	0.441	0.725	0.406	1	-
Pb	**0.936**	0.467	0.417	0.610	0.467	0.866	0.634	0.702	0.866	0.874	0.806	0.433	0.858	0.516	1

Table 2.9 shows that OC belongs to Group I(M-F) at FR, with very flat day-of-week profiles. Mg and Se are placed in Group II(S-M) with lower concentrations in the middle of the week. Li, S, K, Br, Rb, Mo, Sn, Sb and Pb are grouped because their day-of-week profiles is low at the beginning of the week and then peaks on Thursday, Friday or Saturday. This profile is assigned as Group IV since it was not observed at the other sites.

Table 2.9. Dot products between ultrafine constituents at the same site. Dot product is calculated based on one (1) year of measurements at Fresno (FR).

FR	OC	EC	Li	Mg	S	K	V	As	Se	Br	Rb	Mo	Sn	Sb	Pb
OC	1	-	-	-	-	-	-	-	-	-	-	-	-	-	-
EC	0.557	1	-	-	-	-	-	-	-	-	-	-	-	-	-
Li	0.776	0.511	1	-	-	-	-	-	-	-	-	-	-	-	-
Mg	0.571	0.895	0.398	1	-	-	-	-	-	-	-	-	-	-	-
S	0.833	0.486	0.882	0.435	1	-	-	-	-	-	-	-	-	-	-
K	0.897	0.429	0.893	0.447	**0.900**	1	-	-	-	-	-	-	-	-	-
V	0.774	0.609	**0.972**	0.547	**0.897**	0.874	1	-	-	-	-	-	-	-	-
As	0.643	0.582	**0.917**	0.435	0.728	0.711	0.878	1	-	-	-	-	-	-	-
Se	0.763	0.644	0.501	0.855	0.635	0.660	0.610	0.480	1	-	-	-	-	-	-
Br	0.826	0.541	**0.956**	0.476	**0.946**	**0.958**	**0.952**	0.808	0.601	1	-	-	-	-	-
Rb	0.877	0.431	**0.939**	0.413	**0.911**	**0.992**	**0.912**	0.776	0.612	**0.974**	1	-	-	-	-
Mo	0.701	0.467	**0.948**	0.289	**0.929**	0.832	**0.923**	0.831	0.387	**0.940**	0.881	1	-	-	-
Sn	0.687	0.437	0.771	0.496	**0.913**	0.864	0.835	0.568	0.660	**0.902**	0.852	0.809	1	-	-
Sb	0.764	0.478	**0.997**	0.354	0.898	0.893	**0.962**	**0.907**	0.473	**0.960**	**0.940**	**0.965**	0.784	1	-
Pb	0.734	0.556	**0.986**	0.407	0.868	0.864	**0.969**	0.883	0.441	**0.954**	**0.912**	**0.960**	0.775	**0.984**	1

2.3.4 Correlation between different sites for the same element

Table 2.10 examines the similarity between day-of-week profiles for the same UFP elements at different sites. Dotproduct values greater than 0.90 are interpreted as strong agreement and are marked in bold. The only UFP species that have strong agreement between sites are OC, EC, K, V and Rb. As discussed previously, OC is in Group I(M-F) for all sites, showing relatively consistent weekly trend with slightly higher concentration on Friday for SP, EO and LA. This trend reflects the combined effect from vehicular emission, food cooking, biomass burning and industrial activities. K and Rb are in Group II for SP, EO and LA, with concentrations lowest in the middle of the week. This trend reflects higher biomass burning activity on weekends. The dotproduct for Rb day-of-week profiles between SP and EO are not as large as that for K, probably due to the

slightly different trend on Saturday and Sunday between the two sites. Weekend concentrations are still higher than weekday concentrations for both K and Rb. The proximity of site SP and EO leads to dotproducts as high as 0.980 for V, 0.971 for OC and 0.911 for EC.

Groups II(S-M), III(M-W), and IV identified in Tables 2.6 through 2.9 often contained different UFP species indicating that the same UFP species have different day-of-week patterns at different sites. This is reflected by the lack of strong correlations between these species at different locations in Table 2.10. For example, at SP the species As and Br are in Group II(S-M) together with K and Rb, while at EO they belong to Group III(M-W) with higher concentrations from Monday to Wednesday. Similarly, UFP Se is present in Group III(M-W) at SP, in Group I(M-F) at EO, and Group II(S-M) at LA. These day-of-week patterns reflect the emission pattern of nearby sources that varies from site to site.

Table 2.10. Dot products between four sites for same elements. Dotproduct is calculated based on annual mean concentrations of each day of a week.

OC	SP	EO	LA	FN
SP	1	-	-	-
EO	**0.971**	1	-	-
LA	**0.876**	**0.931**	1	-
FN	0.632	0.723	0.821	1

EC	SP	EO	LA	FN
SP	1	-	-	-
EO	**0.911**	1	-	-
LA	0.845	0.746	1	-
FN	0.795	0.715	0.886	1

Li	SP	EO	LA	FN
SP	1	-	-	-
EO	0.773	1	-	-
LA	0.641	0.823	1	-
FN	0.609	0.460	0.486	1

Mg	SP	EO	LA	FN
SP	1	-	-	-
EO	0.720	1	-	-
LA	0.891	0.813	1	-
FN	0.828	0.862	**0.915**	1

S	SP	EO	LA	FN
SP	1	-	-	-
EO	0.709	1	-	-
LA	0.574	0.846	1	
FN	0.655	0.504	0.412	1

K	SP	EO	LA	FN
SP	1	-	-	-
EO	0.876	1	-	-
LA	**0.969**	**0.926**	1	-
FN	0.877	0.669	0.814	1

V	SP	EO	LA	FN
SP	1	-	-	-
EO	**0.980**	1	-	-
LA	0.785	0.817	1	-
FN	0.517	0.480	0.566	1

As	SP	EO	LA	FN
SP	1	-	-	-
EO	0.648	1	-	-
LA	0.782	0.737	1	-
FN	0.554	0.645	0.655	1

Se	SP	EO	LA	FN
SP	1	-	-	-
EO	0.512	1	-	-
LA	0.185	0.340	1	-
FN	0.591	0.328	0.803	1

Br	SP	EO	LA	FN
SP	1	-	-	-
EO	0.875	1	-	-
LA	0.806	0.584	1	-
FN	0.435	0.359	0.791	1

Rb	SP	EO	LA	FN
SP	1	-	-	-
EO	0.562	1	-	-
LA	0.772	0.829	1	
FN	**0.936**	0.544	0.733	1

Mo	SP	EO	LA	FN
SP	1	-	-	-
EO	0.718	1	-	-
LA	0.443	0.800	1	-
FN	0.893	0.406	0.187	1

Sn	SP	EO	LA	FN
SP	1	-	-	-
EO	0.458	1	-	-
LA	0.296	0.667	1	-
FN	0.169	0.789	0.812	1

Sb	SP	EO	LA	FN
SP	1	-	-	-
EO	0.458	1	-	-
LA	0.420	0.770	1	-
FN	0.646	0.391	0.674	1

Pb	SP	EO	LA	FN
SP	1	-	-	-
EO	0.809	1	-	-
LA	0.790	0.601	1	-
FN	0.879	0.851	0.868	1

2.3.5 Day of week profiles in different seasons

In the previous sections, measured 3-day average concentrations at each site were used to build up

the day-of-week profiles. This approach increases the power of the analysis mapping 3-day averages to specific days of the week, but seasonal variations may also contribute to variation that masks important differences. Paired t-tests were carried out based on the original 3-day average data to study day-of-week variation while normalizing for seasonal variability. Samples spanning Friday to Sunday or Saturday to Monday were treated as weekend samples, and samples that are right before or after the weekend samples were regarded as paired weekday samples. Paired samples are likely to experience similar meteorological conditions which reduces the uncertainty in the paired comparison.

Table 2.11 summarizes the statistically-significant results from the paired t-test analysis across the entire 12 month measurement period. Statistically significant differences in paired weekend – weekday samples were identified for UFP EC, K and Rb. As discussed previously, K and Rb are markers for biomass combustion. Surveys of consumer behavior indicate that Friday, Saturday and Sunday night are the most frequent residential wood burning periods [55]. Therefore, weekend – weekday pairs including Friday in weekday samples were excluded in the later analysis for K and Rb. Pairs including Monday in weekday samples were also excluded from paired t test since Monday may have lingering effect carried from weekend. The number of pairs tested for K and Rb are about half the number of pairs tested for EC due to this data exclusion criteria. There is significant difference between weekday and weekend for Rb at SP, for K and Rb at EO, and for Rb at LA. The weekday/weekend difference is statistically significant for EC at SP, EO and LA. There are no statistically significant differences observed at FR since the number of available pairs is too limited.

Table 2.11. p values for paired t-test of weekend vs weekday K, Rb and EC values. * denotes $p < 0.05$, ** $p < 0.01$, *** $p < 0.001$.

Site	Number of pairs	K	Rb	Number of pairs	EC
SP	25	0.185	0.027*	43	7.509E-06***
EO	22	0.004**	0.022*	42	0.006**
LA	15	0.107	0.018*	29	0.019*
FR	4	0.306	0.270	8	0.080

The box plots of seasonal EC, K and Rb values on weekdays and weekends at EO are displayed in Figures 2.6 through 2.8, where statistical significance is denoted with an asterisk. In Figure 2.6, EC is significantly higher on weekdays than weekends in winter, and this trend is also visible for fall. The weekday concentrations are only slightly higher than weekend concentrations in spring and summer. This pattern could be explained by the annual cycle in mixing depth that amplifies the effects of changing emissions rates when mixing depth is low (fall and winter) with less amplification when mixing depth is higher (spring and summer). Another possible explanation is the effect of cold-start emissions from gasoline vehicles in the colder fall and winter seasons leading to higher UFP EC emissions. Gasoline vehicle activity decreases on weekends and also occurs later in the day when temperatures have increased.

Figures 2.7 and 2.8 display that K and Rb have the greatest difference in weekday vs. weekend concentrations during winter, reflecting the extensive use of wood burning as heating source in Northern California. The difference between weekend vs. weekday concentrations for UFP K and Rb are obvious for all seasons.

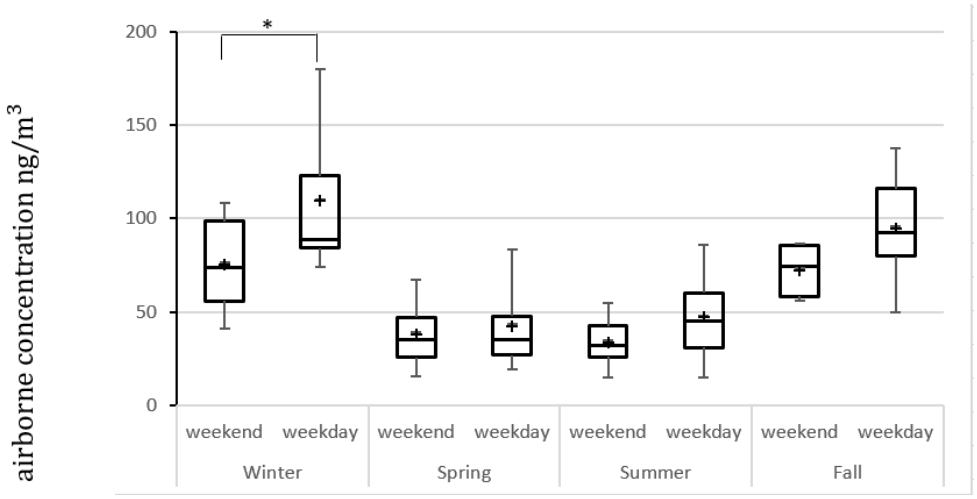

Figure 2.6. Weekend vs weekday concentrations for ultrafine EC at East Oakland in four seasons. * denotes $p < 0.05$. + represents the mean values. Boxes represent 25th and 75th percentile and whiskers represent 5th and 95th percentile.

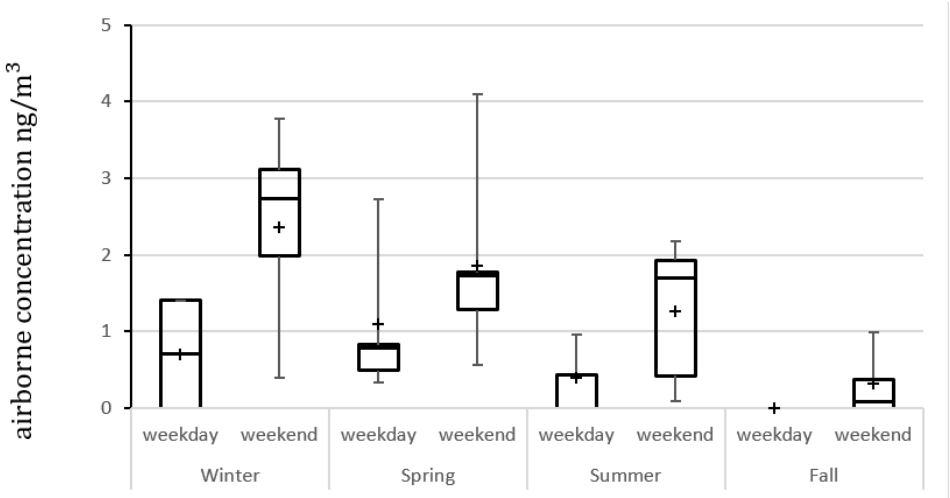

Figure 2.7. Weekend vs weekday concentrations for ultrafine K at East Oakland in four seasons. * denotes $p < 0.05$. + represents the mean values. Boxes represent 25th and 75th percentile and whiskers represent 5th and 95th percentile.

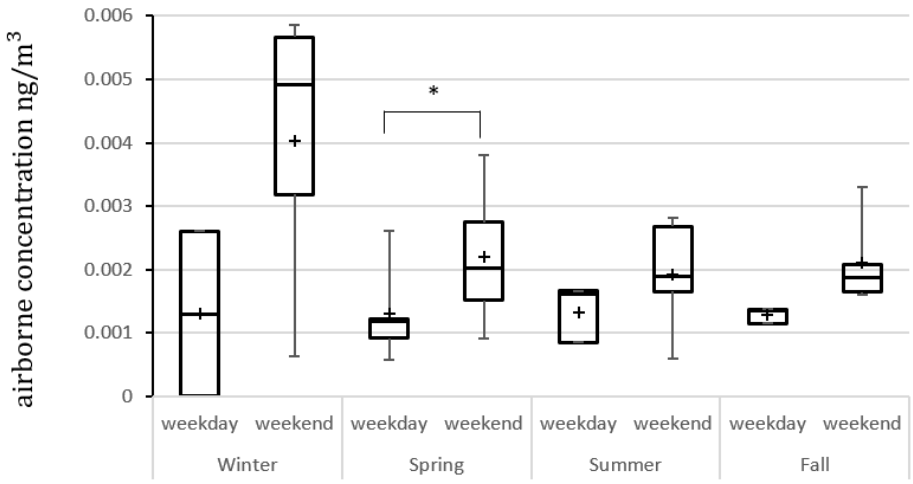

Figure 2.8. Weekend vs weekday concentrations for ultrafine Rb at East Oakland in four seasons. * denotes $p < 0.05$. + represents the mean values. Boxes represent 25th and 75th percentile and whiskers represent 5th and 95th percentile.

2.4 Discussion

The presence of a day-of-week trend for $PM_{0.1}$ EC and the absence of a day-of-week effect for $PM_{0.1}$ OC suggests that diesel engine emissions do not dominate $PM_{0.1}$ OC in the current study. Volatility measurements indicate that approximately 50-70% of the OC emitted by modern diesel engines may evaporate in the atmosphere [56] which suggests that particle evaporation does not completely mask the diesel $PM_{0.1}$ OC trend.

The presence of a minor day-of-week trend for $PM_{0.1}$ K and Rb, and the absence of a trend for $PM_{0.1}$ OC also suggests that wood combustion does not strongly dominate $PM_{0.1}$ concentrations. PM0.1 OC usually contains contribution from gasoline, diesel, food cooking, biomass burning, secondary organic aerosol (SOA) formation and biogenic emission [8, 57]. The overall results of the current study suggest that the mixing of common combustion sources of $PM_{0.1}$ OC mentioned above must be responsible for the observed weekly pattern. Within frame of current study, source biomass burning peaks on weekends, and source diesel engines peaks in the middle of week.

Another major source – gasoline vehicles – may also exhibit higher activities during weekdays. These sources, combined with other PM0.1 OC contributors, forms the $PM_{0.1}$ OC weekly trend with overall flat shape and slightly higher Friday values.

In the table showing similarity between weekly trends for the same element at different sites (Table 2.10), site SP and EO have three species (OC, EC and V) whose dotproducts are greater than 0.9. This suggests that the major sources for these species – common combustion sources for OC, diesel for EC, and shipping for V – show very similar weekly emission patterns. Site SP and EO are both located in the San Francisco Bay area separated by a distance of 35 km (Figure 2.9). These sites are surrounded by similar commercial, residential and traffic emission patterns which explains the similarity for OC and EC trends. Both Bay Area sites are adjacent to the Port of Oakland and San Francisco Bay that leads to similar weekly patterns for shipping (V). The other species don't exhibit great association between SP and EO sites, indicating that ultrafine particles have sharp spatial gradients and that local industrial emission patterns may vary between the two sites.

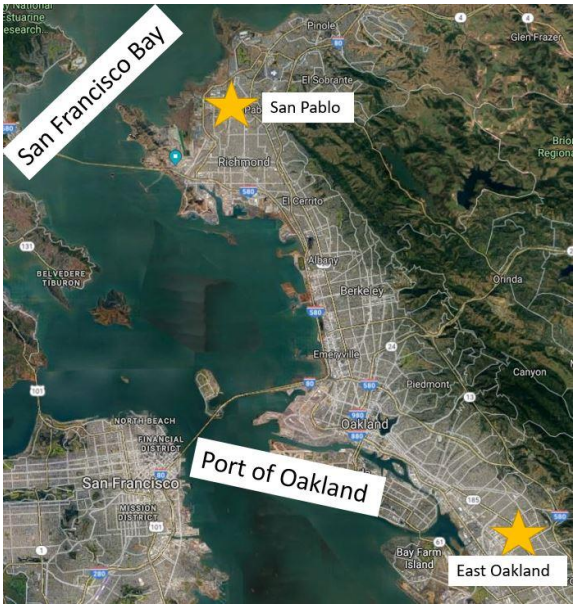

Figure 2.9. Location of site San Pablo and site East Oakland.

A distinct weekly trend was found for K and Rb at SP, EO and LA, which reveals that biomass burning displays a significant weekly emission pattern at these sites in California. The indoor exposure to wood smoke has been found to link significantly with early-life asthma [58]. A study carried out in Northern California also demonstrated association between increased asthma-caused emergency room (ER) visits and increased PM that was mainly attributed to excessive wood burning activities [59]. On the other hand, one study in Canada [60] and one study in Seattle, US [61] found consistently higher ER visit volume of children asthma during weekends and on Mondays. The researchers didn't specifically suggest the causes of this pattern, but based on our findings of weekly trends of wood burning tracers, and the fact that wood smoke exposure may cause children asthma, we suspect that the weekly burning pattern may contribute to the weekly trends of ER visits of asthma-suffering children. Future studies are needed to test this hypothesis.

2.5 Conclusions

A comprehensive analysis of the day-of-week trends for fifteen components of ultrafine particulate matter was carried out over an annual cycle at four sites in California. This analysis reveals location-specific patterns along with important general trends. A comparison between different elements at the same location identified ultrafine components with highest concentrations on weekdays (Group I(M-F)), weekends (Group II(S-M)), or during the early week (Group III(M-W)). Across the most heavily urban sites, Group III(M-W) always contains EC (diesel engines). Across all sites, Group II(S-M) always contains K and Rb (biomass combustion). Ultrafine OC, and 11 other trace components did not display strong day-of-week concentration patterns, suggesting that multiple sources contribute to these ultrafine components.

A paired t-test constructed using measurements on weekends compared to measurements immediately preceding or immediately following the weekend confirms that ambient ultrafine

particle concentrations associated with diesel engines (EC) are highest on weekdays while ambient ultrafine particle concentrations associated with biomass combustion (K and Rb) are highest on weekends in California. These weekly cycles in ultrafine particulate matter source contributions may have implications for public health.

A detailed trend analysis for the same element at different locations shows that the two closest sampling locations (SP and EO) have the great number of ultrafine particle components with identical weekly trends, but even at these locations only 3 out of 15 components displayed the exact same day-of-week profiles. Less similarity was observed in measured day-of-week profiles for ultrafine particle elements at other sites. This suggests that the details of ultrafine particle concentrations at each sampling site reflect the mixture of sources immediately adjacent to that site. By extension, individual neighborhoods across California will each experience unique day-of-week concentration profiles for ultrafine particle components that reflect the surrounding sources.

2.6 Acknowledgements

This work was funded by the California Air Resources Board under Project #13-418. The statements and conclusions in this paper are those of the authors and not necessarily those of the sponsors. The mention of commercial products, their source, or their use in connection with material reported herein is not to be construed as actual or implied endorsement of such products.

2.7 References

1. Schwarze, P., et al., *Particulate matter properties and health effects: consistency of epidemiological and toxicological studies.* Human & experimental toxicology, 2006. **25**(10): p. 559-579.
2. Pope III, C.A. and D.W. Dockery, *Health effects of fine particulate air pollution: lines that connect.* Journal of the air & waste management association, 2006. **56**(6): p. 709-742.

3. Kim, S., et al., *Size distribution and diurnal and seasonal trends of ultrafine particles in source and receptor sites of the Los Angeles basin.* Journal of the Air & Waste Management Association, 2002. **52**(3): p. 297-307.
4. Zhu, Y., et al., *Concentration and size distribution of ultrafine particles near a major highway.* Journal of the air & waste management association, 2002. **52**(9): p. 1032-1042.
5. Elder, A. and G. Oberdörster, *Translocation and effects of ultrafine particles outside of the lung.* Clinics in occupational and environmental medicine, 2005. **5**(4): p. 785-796.
6. Geiser, M., et al., *Ultrafine particles cross cellular membranes by nonphagocytic mechanisms in lungs and in cultured cells.* Environmental health perspectives, 2005. **113**(11): p. 1555.
7. Cass, G.R., et al., *The chemical composition of atmospheric ultrafine particles.* Philosophical Transactions of the Royal Society of London A: Mathematical, Physical and Engineering Sciences, 2000. **358**(1775): p. 2581-2592.
8. Shirmohammadi, F., et al., *Fine and ultrafine particulate organic carbon in the Los Angeles basin: Trends in sources and composition.* Sci Total Environ, 2016. **541**: p. 1083-1096.
9. Saffari, A., et al., *Seasonal and spatial variation of trace elements and metals in quasi-ultrafine (PM0. 25) particles in the Los Angeles metropolitan area and characterization of their sources.* Environmental pollution, 2013. **181**: p. 14-23.
10. Hasheminassab, S., et al., *Source apportionment and organic compound characterization of ambient ultrafine particulate matter (PM) in the Los Angeles Basin.* Atmospheric environment, 2013. **79**: p. 529-539.
11. Daher, N., et al., *Seasonal and spatial variability in chemical composition and mass closure of ambient ultrafine particles in the megacity of Los Angeles.* Environmental Science: Processes & Impacts, 2013. **15**(1): p. 283-295.
12. Ntziachristos, L., et al., *Fine, ultrafine and nanoparticle trace element compositions near a major freeway with a high heavy-duty diesel fraction.* Atmospheric Environment, 2007. **41**(27): p. 5684-5696.
13. Ham, W.A., et al., *Size Distribution of Health-Relevant Trace Elements in Airborne Particulate Matter During a Severe Winter Stagnation Event: Implications for Epidemiology and Inhalation Exposure Studies.* Aerosol Science and Technology, 2010. **44**(9): p. 753-765.
14. Ham, W.A. and M.J. Kleeman, *Size-resolved source apportionment of carbonaceous particulate matter in urban and rural sites in central California.* Atmospheric environment, 2011. **45**(24): p. 3988-3995.
15. Kuwayama, T., C.R. Ruehl, and M.J. Kleeman, *Daily trends and source apportionment of ultrafine particulate mass (PM0. 1) over an annual cycle in a typical California City.* Environmental science & technology, 2013. **47**(24): p. 13957-13966.
16. Austin, J. and H. Tran, *A Characterization of the Weekend-Weekday Behavior of Ambient Ozone Concentrations in California.* Technical Support and Planning Division, California Air Resources Board, Sacramento, CA, 1999.
17. Fujita, E.M., et al., *Evolution of the magnitude and spatial extent of the weekend ozone effect in California's South Coast Air Basin, 1981–2000.* Journal of the Air & Waste Management Association, 2003. **53**(7): p. 802-815.

18. Harley, R.A., et al., *Changes in motor vehicle emissions on diurnal to decadal time scales and effects on atmospheric composition.* Environmental Science & Technology, 2005. **39**(14): p. 5356-5362.
19. Chinkin, L.R., et al., *Weekday versus weekend activity patterns for ozone precursor emissions in California's South Coast Air Basin.* Journal of the Air & Waste Management Association, 2003. **53**(7): p. 829-843.
20. Motallebi, N., et al., *Day-of-week patterns of particulate matter and its chemical components at selected sites in California.* Journal of the Air & Waste Management Association, 2003. **53**(7): p. 876-888.
21. Lough, G., J.J. Schauer, and D. Lawson, *Day-of-week trends in carbonaceous aerosol composition in the urban atmosphere.* Atmospheric Environment, 2006. **40**(22): p. 4137-4149.
22. Zhao, N., et al., *Day-of-week and seasonal patterns of PM2. 5 concentrations over the United States: Time-series analyses using the Prophet procedure.* Atmospheric environment, 2018. **192**: p. 116-127.
23. Murphy, D., et al., *Weekly patterns of aerosol in the United States.* Atmospheric Chemistry and Physics, 2008. **8**(10): p. 2729-2739.
24. Sheesley, R.J., et al., *Daily variation in particle-phase source tracers in an urban atmosphere.* Aerosol Science and Technology, 2007. **41**(11): p. 981-993.
25. Bae, M.-S., et al., *Hourly and daily patterns of particle-phase organic and elemental carbon concentrations in the urban atmosphere.* Journal of the Air & Waste Management Association, 2004. **54**(7): p. 823-833.
26. Whynes, D.K., J. Falk-Whynes, and M. Pringle, *Trends in acute admissions: a study of one English district general hospital.* Journal of Public Health, 1999. **21**(4): p. 459-463.
27. Garty, B.Z., et al., *Emergency room visits of asthmatic children, relation to air pollution, weather, and airborne allergens.* Annals of Allergy, Asthma & Immunology, 1998. **81**(6): p. 563-570.
28. Hughes, L.S., et al., *Physical and chemical characterization of atmospheric ultrafine particles in the Los Angeles area.* Environmental Science & Technology, 1998. **32**(9): p. 1153-1161.
29. Hughes, L.S., et al., *Size and composition distribution of atmospheric particles in southern California.* Environmental science & technology, 1999. **33**(20): p. 3506-3515.
30. Saffari, A., et al., *Seasonal and spatial variation in reactive oxygen species activity of quasi-ultrafine particles (PM0.25) in the Los Angeles metropolitan area and its association with chemical composition.* Atmospheric Environment, 2013. **79**: p. 566-575.
31. Kuwayama, T., C.R. Ruehl, and M.J. Kleeman, *Daily Trends and Source Apportionment of Ultrafine Particulate Mass (PM0.1) over an Annual Cycle in a Typical California City.* Environmental Science & Technology, 2013. **47**(24): p. 13957-13966.
32. Herner, J.D., et al., *Size and composition distribution of airborne particulate matter in northern California: I-particulate mass, carbon, and water-soluble ions.* Journal of the Air & Waste Management Association, 2005. **55**(1): p. 30-51.
33. Eller, P.M., *NIOSH manual of analytical methods*. Vol. 94. 1994: Diane Publishing.
34. Herner, J.D., P.G. Green, and M.J. Kleeman, *Measuring the trace elemental composition of size-resolved airborne particles.* Environmental science & technology, 2006. **40**(6): p. 1925-1933.

35. USE, P., *Method 6020a: inductively coupled plasma—mass spectrometry.* United States Environmental Protection Agency, Washington, DC USA, 1998.
36. Seinfeld, J.H. and S.N. Pandis, *Atmospheric chemistry and physics: from air pollution to climate change*. 2012: John Wiley & Sons.
37. Naeher, L.P., et al., *Woodsmoke health effects: a review.* Inhalation toxicology, 2007. **19**(1): p. 67-106.
38. Ostro, B., et al., *The effects of components of fine particulate air pollution on mortality in California: results from CALFINE.* Environmental health perspectives, 2007. **115**(1): p. 13.
39. Querol, X., et al., *Source origin of trace elements in PM from regional background, urban and industrial sites of Spain.* Atmospheric Environment, 2007. **41**(34): p. 7219-7231.
40. Greenspan, B.J., et al., *Inhalation toxicity of lithium combustion aerosols in rats.* Journal of Toxicology and Environmental Health, Part A Current Issues, 1986. **18**(4): p. 627-637.
41. Kuschner, W.G., et al., *Human pulmonary responses to experimental inhalation of high concentration fine and ultrafine magnesium oxide particles.* Environmental health perspectives, 1997. **105**(11): p. 1234.
42. Kleeman, M.J., J.J. Schauer, and G.R. Cass, *Size and composition distribution of fine particulate matter emitted from wood burning, meat charbroiling, and cigarettes.* Environmental Science & Technology, 1999. **33**(20): p. 3516-3523.
43. McDonald, J.D., et al., *Fine particle and gaseous emission rates from residential wood combustion.* Environmental Science & Technology, 2000. **34**(11): p. 2080-2091.
44. Kiviluoto, M., et al., *Effects of vanadium on the upper respiratory tract of workers in a vanadium factory: A macroscopic and microscopic study.* Scandinavian journal of work, environment & health, 1979: p. 50-58.
45. Kiviluoto, M., *Observations on the lungs of vanadium workers.* Occupational and Environmental Medicine, 1980. **37**(4): p. 363-366.
46. Knecht, E.A., et al., *Pulmonary effects of acute vanadium pentoxide inhalation in monkeys.* American Review of Respiratory Disease, 1985. **132**(6): p. 1181-1185.
47. Lagerkvist, B., H. Linderholm, and G.F. Nordberg, *Vasospastic tendency and Raynaud's phenomenon in smelter workers exposed to arsenic.* Environmental research, 1986. **39**(2): p. 465-474.
48. Liu, G., et al., *Health effects of arsenic, fluorine, and selenium from indoor burning of Chinese coal*, in *Reviews of environmental contamination and toxicology*. 2007, Springer. p. 89-106.
49. Manö, S. and M.O. Andreae, *Emission of methyl bromide from biomass burning.* Science, 1994. **263**(5151): p. 1255-1257.
50. Barceloux, D.G. and D. Barceloux, *Molybdenum.* Journal of Toxicology: Clinical Toxicology, 1999. **37**(2): p. 231-237.
51. Nriagu, J.O., *Global metal pollution: poisoning the biosphere?* Environment: Science and Policy for Sustainable Development, 1990. **32**(7): p. 7-33.
52. Bomhard, E.M., *The toxicology of indium tin oxide.* Environmental toxicology and pharmacology, 2016. **45**: p. 282-294.
53. Registry., U.S.A.f.T.S.a.D., *Toxicological Profile for Antimony. Final Report. Atlanta, GA, U.S. Dept. of Health and Human Services Public Health Service Agency for Toxic Substances and Disease Registry.* 1992.

54. Moreno, T., et al., *Recreational atmospheric pollution episodes: inhalable metalliferous particles from firework displays.* Atmospheric Environment, 2007. **41**(5): p. 913-922.
55. Bay Area Air Quality Mangement District, *Winter Spare the Air Study, 2014-2015 Winter Wood Smoke Season.* 2015.
56. May, A.A., et al., *Gas-Particle Partitioning of Primary Organic Aerosol Emissions: (2) Diesel Vehicles.* Environmental Science & Technology, 2013. **47**(15): p. 8288-8296.
57. Xue, J., et al., *Seasonal and Annual Source Appointment of Carbonaceous Ultrafine Particulate Matter (PM0. 1) in Polluted California Cities.* Environmental science & technology, 2018. **53**(1): p. 39-49.
58. Ratnapradipa, D., A.G. Robins, and K. Ratnapradipa, *Preschool Children's Environmental Exposures: A Case-Control Epidemiological Study of the Presence of Asthma-Like Symptoms.* Journal of environmental health, 2013. **76**(4): p. 12-17.
59. Lipsett, M., S. Hurley, and B. Ostro, *Air pollution and emergency room visits for asthma in Santa Clara County, California.* Environmental Health Perspectives, 1997. **105**(2): p. 216-222.
60. Rosychuk, R.J., et al., *Asthma presentations by children to emergency departments in a Canadian province: A population‐based study.* Pediatric pulmonology, 2010. **45**(10): p. 985-992.
61. Schwartz, J., et al., *Particulate air pollution and hospital emergency room.* Am Rev Respir Dis, 1993. **147**(4): p. 826-831.

3.0 Positive Matrix Factorization of Ultrafine Particle Mass ($PM_{0.1}$) at Three Sites in California

Wei Xue[a], Jian Xue[a], Amirhosein Mousavi [b], Constantinos Sioutas[b], and Michael J. Kleeman[a,*]

[a] Department of Civil and Environmental Engineering, University of California – Davis, Davis, California, USA

[b]Department of Civil and Environmental Engineering, University of Southern California, Los Angeles, California, USA

3.1 Introduction

Ultrafine particulate matter (UFP; airborne particles with diameter < 0.1 μm) is an emerging environmental pollutant of concern. Epidemiological studies have found associations between UFPs and increased mortality [1] and adverse birth outcomes [2, 3]. UFPs may also be more toxic than larger airborne particles because they are more likely to induce oxidative stress upon inhalation [4, 5] and have potential to enter deeper into respiratory system and translocate to other organs of human bodies[6, 7]. Characterization of UFP's concentrations, chemical composition and source contributions is urgently needed to better understand health effects and mitigate emissions. The current study focuses on analyzing sources of UFPs based on a one-year UFP sampling campaign in California, US.

There has been limited number of UFPs measurement campaigns worldwide because the sampling devices are expensive and require frequent maintenance. Most of UFP source apportionment studies were based in California [8-12] and northeastern [13] of United States, Europe [14, 15], and parts of Asia [16, 17]. A lot of these studies used UFP number concentrations as input for source apportionment [11, 13, 14], while others relied on UFP mass concentrations ($PM_{0.1}$) [10, 12, 15]. There is no conclusion which is a better metric for analyzing UFP sources, but $PM_{0.1}$ has

been reported to be well correlated with particle surface area which determines the active area that UFP interacts with human body [18]. According to the results of these studies, the majority of atmospheric UFPs are emitted directly from combustion processes, including motor vehicles, biomass combustion, food cooking, etc. Secondary aerosol formation and other sources may also contribute to small portions of total UFP mass depending on the sampling location. Since UFPs have sharper spatial gradient than larger particles [19], it's important to carry out site-specific source apportionment studies for UFPs. In the current study, San Francisco Bay Area and Los Angeles in California, US were chosen as target locations because they have the one of the worst air qualities in the country.

Common approaches used for source apportionment of airborne particles include chemical mass balance (CMB) models and factor analysis techniques, for example Positive Matrix Factorization (PMF). Both approaches assume that the ratio of chemicals emitted by a source are conserved during transport and dilution in the environment so that the ambient concentration pattern can be described as a linear combination of source contributions. CMB apportions the organic part of particulate mass to sources based on previously acquired source profiles, while PMF must rely on expert opinion to assign source names to each factor resolved by the statistical model. CMB has the advantage of separating different organic sources, including gasoline and diesel vehicles, biomass burning, food cooking, etc., but the high cost of measuring corresponding organic tracers would limit the time resolution of the source apportionment study. PMF need a long series of ambient measurements (typically > 60) as input data and incorporates inorganic components of PM, which creates the possibility to resolve sources identified by inorganic tracers. At the same time, PMF may generate blended organic sources due to lack of organic tracers on higher time resolution. These two methods complement each other in PM source apportionment studies. CMB

has been used to calculate source contributions to $PM_{0.1}$ in California at multiple sites during a 4-week intensive study [20] and PMF has been applied to resolve sources at a single site during a full annual cycle [12]. but no direct comparison of PMF and CMB was carried out in these past studies. A broader set of long-term measurements at multiple sites would provide additional information about the sources that contribute to $PM_{0.1}$ concentrations that may affect public health in California.

The purpose of this study is to describe PMF results from a year of $PM_{0.1}$ samples collected at two sites in Northern California and one site in Southern California. The details of the PMF solution are reviewed, major sources of UFPs are identified, the locations of sources relative to measurement sites are discussed, and the seasonal patterns of source contributions to UFP concentrations are analyzed. The PMF results are compared with CMB results generated from the same sampling campaign [10]. The findings provide new information regarding source contributions to UFP concentrations in California and insights into the strengths and weaknesses of both source apportionment methods.

3.2 Methods

3.2.1 Sample collection and chemical analysis

$PM_{0.1}$ samples were collected continuously over 3 - day intervals from August 2015 to July 2016 at two adjacent sites in San Francisco Bay Area - San Pablo (SP) and East Oakland (EO), and Los Angeles (LA), yielding approximately 120 samples at each location. The SP location is 3 km to the northwest of San Francisco Bay and is within 5 km of a major chemical refinery. The EO location is 5 km northeast of the Oakland International Airport and 15 km east of the Port of Oakland. Both the SP and EO measurements sites are surrounded by vehicular, industrial, commercial and residential sources. The sampling site at LA was located at the University of

Southern California campus, which is surrounded by major highways and downwind of the Los Angeles International Airport and the Port of Los Angeles.

$PM_{0.1}$ samples at all sites were collected using Micro Orifice Uniform Deposit Impactors (MOUDIs- [21]) on Teflon and aluminum foil impaction substrates. Thirty-four elements were solvent-extracted off Teflon substrates and analyzed by ICP-MS following the methods described by [22]. Organic carbon (OC) and elemental carbon (EC) concentrations were measured on samples collected with aluminum foil substrates using the NIOSH thermal optical method as described by [23]. The compounds that make up OC and EC were further separated into OC 1,2,3,4, and EC 1,2,3,4,5,6 based on their evolution at different temperature ranges under helium only for OC and 98% helium and 2% oxygen conditions for OC. More details of the sampling campaign and chemical analysis methods are described in [24].

Details of the CMB method carried out for the same sampling campaign can be found in [10]. What's worth noting is that the molecular markers capable of separating organic sources were measured in monthly composite samples but not in 3-day average samples due to prohibitive cost

3.2.2 Positive matrix factorization (PMF) analysis

EPA PMF 5.0 is a factor analysis model that quantifies factor(source) contributions within a multicomponent time series. PMF solves the chemical balance equation between measured species concentrations $x_{i,j}$ and derived factor(source) chemical profiles $f_{k,j}$, assuming some a-priori number of sources p. The amount of mass contributed by each factor(source) to concentrations in each individual sample is represented by $g_{i,k}$, as shown in Eq. 3.1, where e_{ij} is the residual for each species j in sample i. The factor(source) contributions $g_{i,k}$ and factor profiles $f_{k,j}$ are calculated by minimizing the objective function Q (Eq. 3.2), where μ_{ij} represents the uncertainty associated with

species *j* in sample *i*.

$$x_{ij} = \sum_{k=1}^{p} g_{ik} f_{kj} + e_{ij} \quad \text{(Eq. 3.1)}$$

$$Q = \sum_{i=1}^{n} \sum_{j=1}^{m} \left[\frac{x_{ij} - \sum_{k=1}^{p} g_{ik} f_{kj}}{u_{ij}} \right]^2 \quad \text{(Eq. 3.2)}$$

PMF differs from traditional factor analysis techniques by requiring that all factor contributions are positive but it does not require that all factor profiles are orthogonal. In the current study, the uncertainty for each species concentration in the PMF analysis was calculated based on the measurement method detection limit (MDL) and error fraction when the concentration was greater than the MDL (Eq. 3.3); if the concentration was less than the MDL, the uncertainty was calculated as a fixed fraction of the MDL (Eq. 3.4).

$$Q = \sum_{i=1}^{n} \sum_{j=1}^{m} \left[\frac{x_{ij} - \sum_{k=1}^{p} g_{ik} f_{kj}}{u_{ij}} \right]^2 \quad \text{(Eq. 3.3)}$$

$$Unc = \frac{5}{6} \times MDL \quad \text{(Eq. 3.4)}$$

The signal to noise ratio (S/N) was calculated to quantify the quality of the input data. Species with S/N > 1 were categorized to Strong species and species with 0.5 < S/N < 1 were categorized to Weak species. The uncertainty for Weak species was increased by a factor of 3 to reduce their influence on the model fit. Species with S/N < 0.5 were categorized to Bad and removed from the analysis [25].

A range of PMF solutions based on three to seven important sources (*p*) were examined in the current study. The optimal solution was determined considering the Q values, the results of model fit, and interpretability of the resulting factor profiles and time series [26]. Bootstrap and Displacement runs were performed to evaluate the stability of the solution. Rotation with different FPEAK strengths were run to find the optimal solution.

3.2.3 CPF plots

Conditional Probability Function (CPF) plots were constructed by coupling hourly wind data with factor concentration throughout the sampling period using Eq. 3.5.

$$CPF = \frac{m_{\Delta\theta}}{n_{\Delta\theta}} \quad \text{(Eq. 3.5)}$$

where $m_{\Delta\theta}$ stands for the number of wind readings in direction θ with factor concentration exceeding a specified threshold and $n_{\Delta\theta}$ is the total number of wind readings in the same direction θ. Multiple target thresholds were tested and the upper 20th percentile was found to best resolve the directionality for factors in the current study. Wind speeds lower than 2 m sec^{-1} were excluded from the analysis. All wind data used in the analysis was "vectorized".

3.3 Results and Discussion

3.3.1 Diagnostics

Table 3.1 summarizes the settings of the PMF base runs and results from error estimation including Displacement and Bootstrap. OC fractions, EC fraction, K, V, Br, Rb, Sn and Sb were categorized to "Strong" for all three sites because of their high S/N ratios and good fit by PMF. The species listed as "Weak" either had low S/N ratios or could not be simulated well (R^2<0.7) by PMF. This includes the most volatile OC fraction (OC1) which is prone to sampling bias due to partitioning between gas and condensed phase. The Weak species also include EC1, which consistently had R^2<0.8 in the PMF solution. The uncertainties for Weak species were thus enlarged in the PMF calculations but their existence in factor profiles could aid source identification.

Table 3.1. Summary of PMF parameters and error estimation results at San Pablo, East Oakland, and Los Angeles

Diagnostic	San Pablo	East Oakland	Los Angeles
Strong species	OC2-4, EC2-3, K, V, Br, Rb, Sn, and Sb	OC2-3, EC2-3, K, V, Br, Rb, Sn, and Sb	OC2-3, EC2-3, K, V, Br, Rb, Sn and Sb
Weak species	OC1, EC1, EC4, Li, Na, Mg, Ca, Cr, Mn, Co, Zn, Ga, As, Se, Sr, Mo, Ag, Cd, Tl, Pb, and U	OC1, OC4, EC1, EC4, Li, Na, Mg, Ca, Cr, Mn, Zn, Ga, As, Se, Sr, Mo, Ag, and Pb	OC1, OC4, EC1, EC4, Li, Na, Mg, Ca, Mn, Co, Zn, Ga, As, Se, Sr, Mo, Ag, Cd, and Pb
Number of factors	7	7	7
Q_{robust}	2178	2012	2438
Q_{true}	2238	2106	2512
Slope for total $PM_{0.1}$ mass	0.94	0.94	1.02
R^2 for total $PM_{0.1}$ mass	0.96	0.94	0.96
DISP drop of Q	0	0	-0.098
DISP swapping	0	0	0
Bootstrap mapping, for Min Corr R=0.8	100% for 5 factors, and 96%, 99%	100% for 5 factors, and 98% for the other 2 factors	100% for all factors

Q_{true} is the goodness-of-fit parameter calculated including all points input to the model, while Q_{robust} measures the goodness-of-fit calculated excluding points not fit by the model, which are defined as samples for which the uncertainty-scaled residual is greater than 4. The difference between these two parameters reflects the impact of data points with high scaled residuals. The small difference between Q_{true} and Q_{robust} for all three sites shows that most of the data points were predicted well by the model. Different numbers of factors were explored for all three sites, and the final solution was determined by assessing Q values, regression analysis for $PM_{0.1}$ total mass and the Strong species, and interpretability of the resolved sources. The seven-factor solution was selected for all three locations since they achieved the best model fit for important species and they

resolved factor profiles that were consistent with current knowledge about UFP source composition and weekly/seasonal activity patterns.

The coefficient of determination (R^2) measures the degree to which the predicted values match with the observed values. The R^2 values for the total $PM_{0.1}$ mass at SP, EO and LA were 0.96, 0.94 and 0.94, indicating that the resolved sources can effectively reproduce the measured concentrations. Displacement (DISP) evaluates the stability of the PMF solution by adjusting each value in the factor profile and computing the new Q-value. The Q-values didn't increase or only had a minimal increase after the Displacement and no factors swapped after the DISP recomputation, indicating that the PMF solutions were robust. Bootstrap can be used to estimate whether a small set of observations affects the PMF solution by randomly sampling blocks of observations until the BS data set is the same size as the original data set. One hundred bootstrap data sets were processed with PMF and the factors resolved by each bootstrap run would be mapped with base factors with which the bootstrap factor contribution has the highest and greater than R>0.8 correlation. The mapping of bootstrap runs for all three sites were all larger than 96% which indicates that the PMF solution was not overly influenced by a small portion of data points.

3.3.2 Source identification

Seven consistent $PM_{0.1}$ factors were resolved for SP, EO, and LA: Factor1-Gasoline+Motor Oil+Meat Cooking+Natural Gas+SOA, Factor 2-Diesel+Motor Oil, Factor 3-Wood Burning, Factor 4-Shipping, Factor 5-Sea Spray, Factor 6-Brake Wear and Factor 7-Sn. Factor source names were chosen based on the chemical composition of each factor (Figures 3.2-3.4), the contribution that each factor makes to total $PM_{0.1}$ mass (Figures 3.5-3.7), the direction of each factor relative to the sampling site (Figures 3.8-3.10), and the time series of the factor concentrations (Figures 3.11-3.12). Table 3.2 shows the signature ratios of chemicals that can be compared to published source

profiles to assist source identification.

Factors 1 and 2 contain the majority of measured $PM_{0.1}$ OC and EC mass meaning they dominate total $PM_{0.1}$ mass. Factor 2 contains the majority of EC and EC3(a sub-fraction of elemental carbon that is volatilized and oxidized at temperature range700-775°C) and the majority of total EC, while Factor 1 contains almost no EC3 and the majority of the total OC. The EC3 measured using NIOSH protocol in the current study is equivalent to the EC2 measured using the IMPROVE protocol [27], which were found to contribute to the majority of EC from diesel engines [28-30]. Therefore the factor contains the highest EC3 is very likely to be diesel emissions. Additionaly, a day-of-week analysis performed on the same dataset [24] shows that total $PM_{0.1}$ EC concentrations peak in the middle of the week because of the increased diesel vehicle activity. The weekly trend of Factor 2 follows this same pattern at all three sites (Figure 3.1). Based on this evidence, Factor 2 was assigned the name Diesel (including associated motor oil).

Factor 3 contains more than half of K and Rb, and significant amounts of OC1-4 and EC1-2. K and Rb were found to be enriched when measuring compostion of biomass burning smoke [31, 32]. K and Rb displayed similar size distribution and temporal pattern in an particulate matter sampling campaign in central California [33]. The weekly patterns of $PM_{0.1}$ K and Rb based on the same dataset also showed very good correlation [24], thus K and Rb can be used as tracers for biomass burning. Factor 3 has peak concentrations during the winter season, consistent with the pattern of residential wood combustion in California. This time pattern causes the wood burning factor to be unambiguously separated from all other PMF factors in the range of possible solutions, thus Factor 3 was recognized to be Wood Burning.

Factor 4 contains over 80% of the V measured in $PM_{0.1}$ samples. Vanadium is often present in

particles emitted from heavy fuel oil (HFO) combustion [34]. The source of Factor 4 is located in the direction of the San Francisco Bay and the Port of Oakland for the San Pablo and East Oakland locations. Based on this evidence, Factor 4 is assigned the name Shipping and other heavy fuel oil combustion.

Factor 5 contains 74%, 70% and 57% of Br and some K and Rb. The in K/Br and Rb/Br values in Factor 5 are close to those in sea water at site SP and EO (Table 3.2) and Factor 5 is from the direction of the ocean (Figure 3.8 and 3.9), thus Factor 5 can be identified as Sea Spray for these two sites. Site LA is more inland and the K/Br value is an order of magnitude smaller than that of sea water (Table 3.2), which indicates that Factor 5 at LA may be Sea Spray blended with other unknown sources.

Factor 6 contains over 70% of Sb. The major sources of Sb in the United States are brake wear and waste incineration [35]. Since waste incineration is sparse in California, the Sb source is most likely associated with brake wear. Sb_2S_3 is frequently added in brake pads and Sb can be oxidized under high temperatures during aggressive braking [36]. A number of studies have linked Sb with brake wear from motor vehicles [37, 38] and railway cars [39, 40], therefore this factor was identified as Brake Wear.

Factor 7 contains over 70% of Sn. Possible sources of ultrafine Sn in California include smelting and refining processes and oil combustion, or other industrial activities [41].

Factor 1 is the largest contributor to $PM_{0.1}$ mass at the two Northern California sites and the second largest contributor to $PM_{0.1}$ mass at the Los Angeles site. Factor 1 is mainly composed of OC1-4 and EC1-2. It is expected that Factor 1 should correspond to the major sources of $PM_{0.1}$ OC not already associated with the factors discussed above. The CMB study carried out based on the same

sampling campaign as current study [10] identified wood burning, meat cooking, gasoline engine exhaust, motor oil and diesel engine exhaust as major sources of $PM_{0.1}$ OC. Other sources possible organic sources include natural gas combustion and secondary organic aerosol (SOA) formation. Natural gas combustion was found to be significant in California by model simulation [19]. Secondary organic aerosols were also present in some ultrafine source apportionment studies based on particle mass [42, 43] or particle number [11, 44]. Although the contribution to total $PM_{0.1}$ from SOA varies drastically from study to study, we believe there is some portion of SOA in Factor. By process of elimination, Factor 1 in the current study was named to be a blend of Gasoline, Motor oil, Meat cooking, Natural Gas, and SOA. PMF was not capable of individually resolving $PM_{0.1}$ contributions from this lumped category because specific organic tracers were measured monthly instead of every 3 days because of the high cost.

PMF solutions using five and six factors were also analyzed, but these solutions did not resolve the diesel factor, which is a source of primary interest. Likewise, increasing the number of factors to eight caused a minor factor to be split from the Sn or Sb factor, further complicating the identification of sources. Overall, the seven factor PMF solution has better performance than other possible PMF solutions.

Table 3.2. Chemical signature comparison for identified sources at SP, EO, and LA.

Source type	Chemical signature	SP	EO	LA	Ranges reported
Gasoline + Motor Oil + Meat Cooking	EC/TC	0.48	0.72	0.61	0.50-0.80[45]
Diesel + Motor Oil	EC/TC	0.09	0.35	0.24	<0.40[45]
Wood burning	K/Rb	620	565	838	227-1957[46]
Shipping	OC/EC	0.84	1.63	2.01	0.4-5.8[47]
	$V*10^3/EC$	3.72	2.38	2.50	<2 for sea, >8 for land[47]
Sea Spray	K/Br	5.48	4.49	0.38	5.9701[48]
	Rb/Br	0.0053	0.0076	0.0030	0.0033[48]

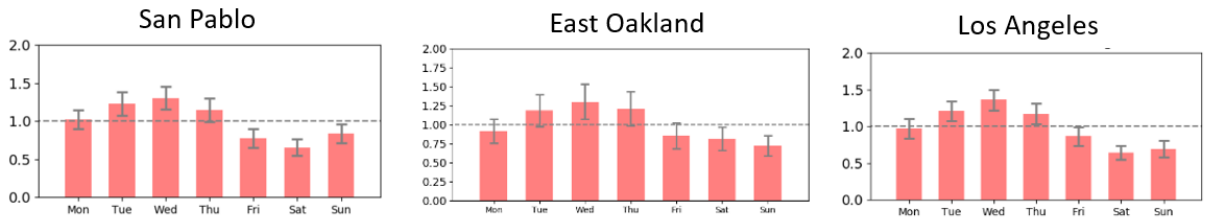

Figure 3.1. Annual averaged day-of-week concentration of Factor 2 (Diesel) for SP, EO and LA. Normalized to annual mean concentration.

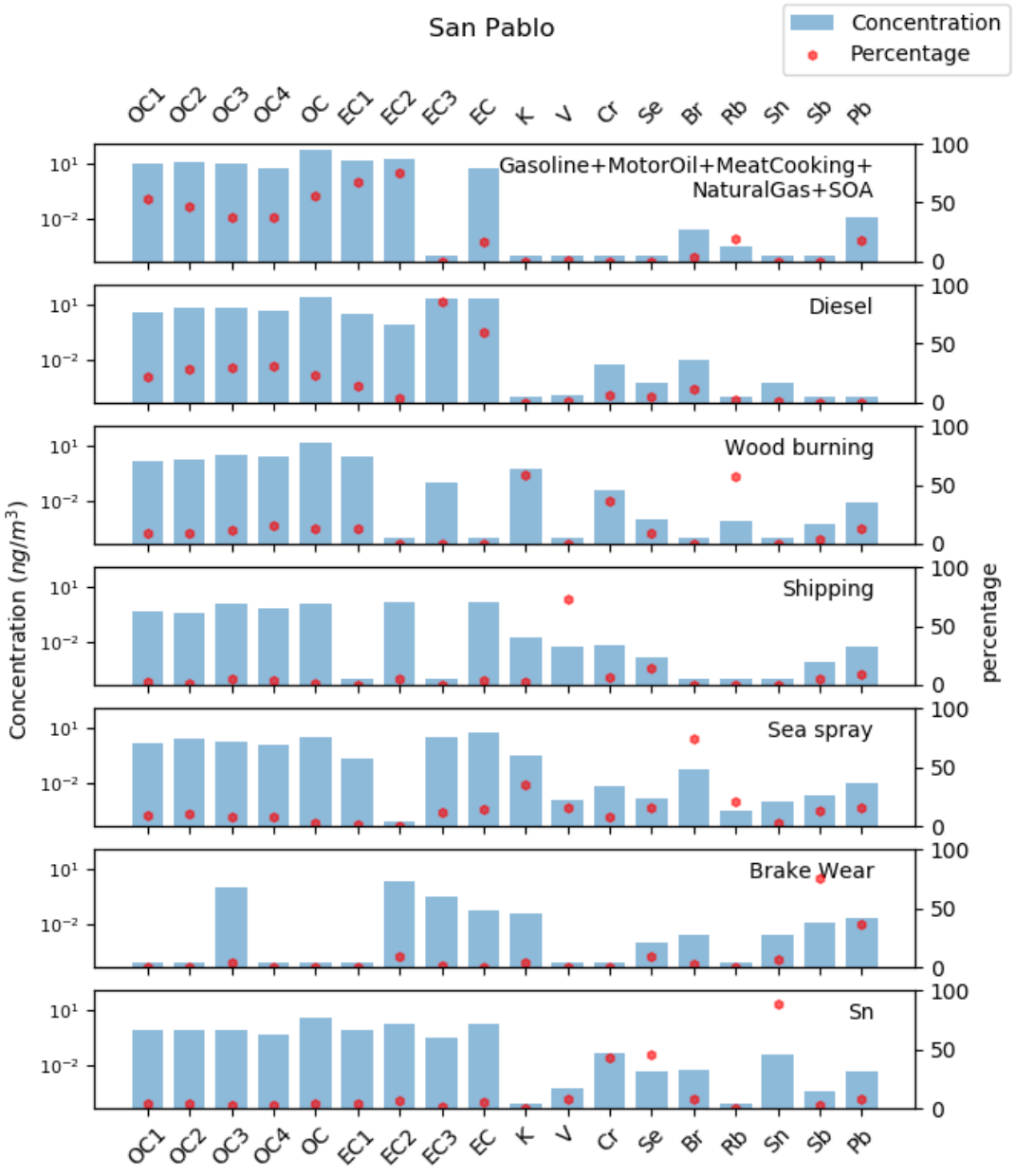

Figure 3.2. PMF species profile at San Pablo. Blue bars (left axis) represent concentration of species in each factor and red dots (right axis) represents the percentage of species mass in each factor. Note that OC1, EC1, Cr, and Pb are weak species with higher uncertainty in the concentration profile.

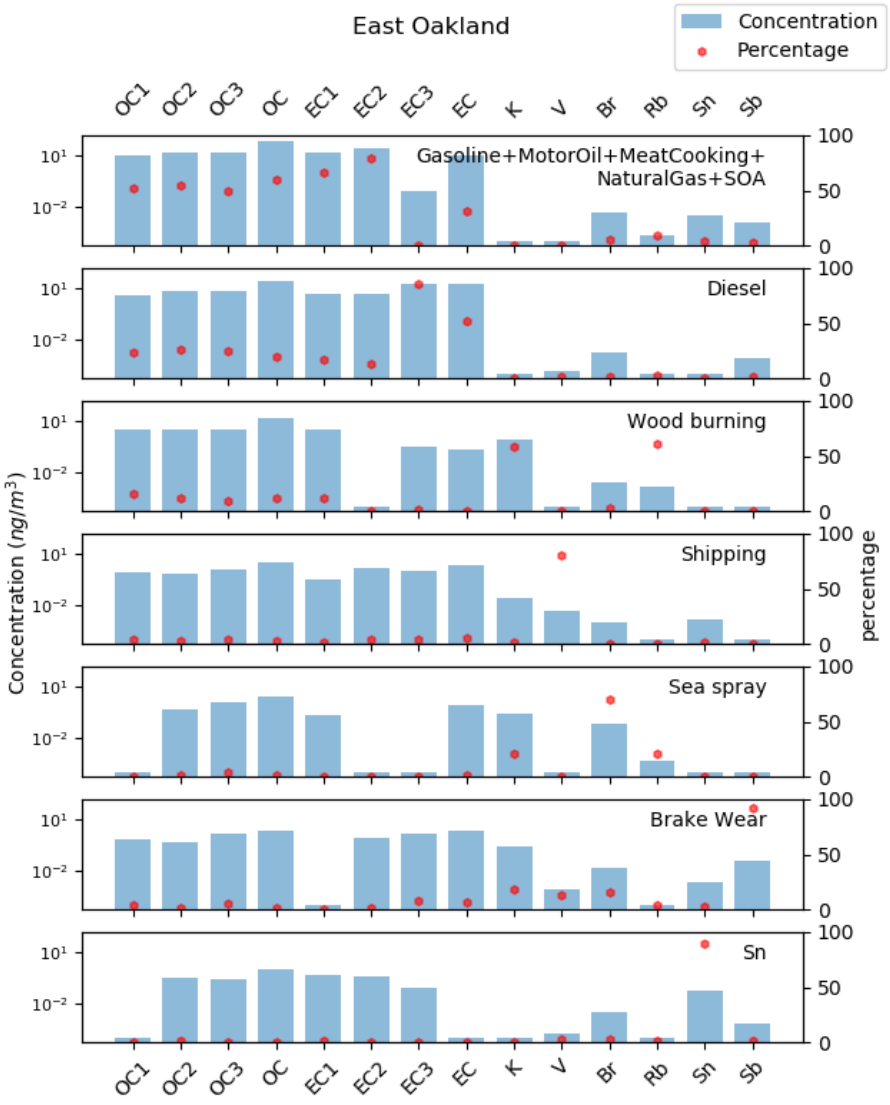

Figure 3.3. PMF species profile at East Oakland. Blue bars (left axis) represent concentration of species in each factor and red dots (right axis) represents the percentage of species mass in each factor. Note that OC1 and EC1 are weak species with higher uncertainty in the concentration profile.

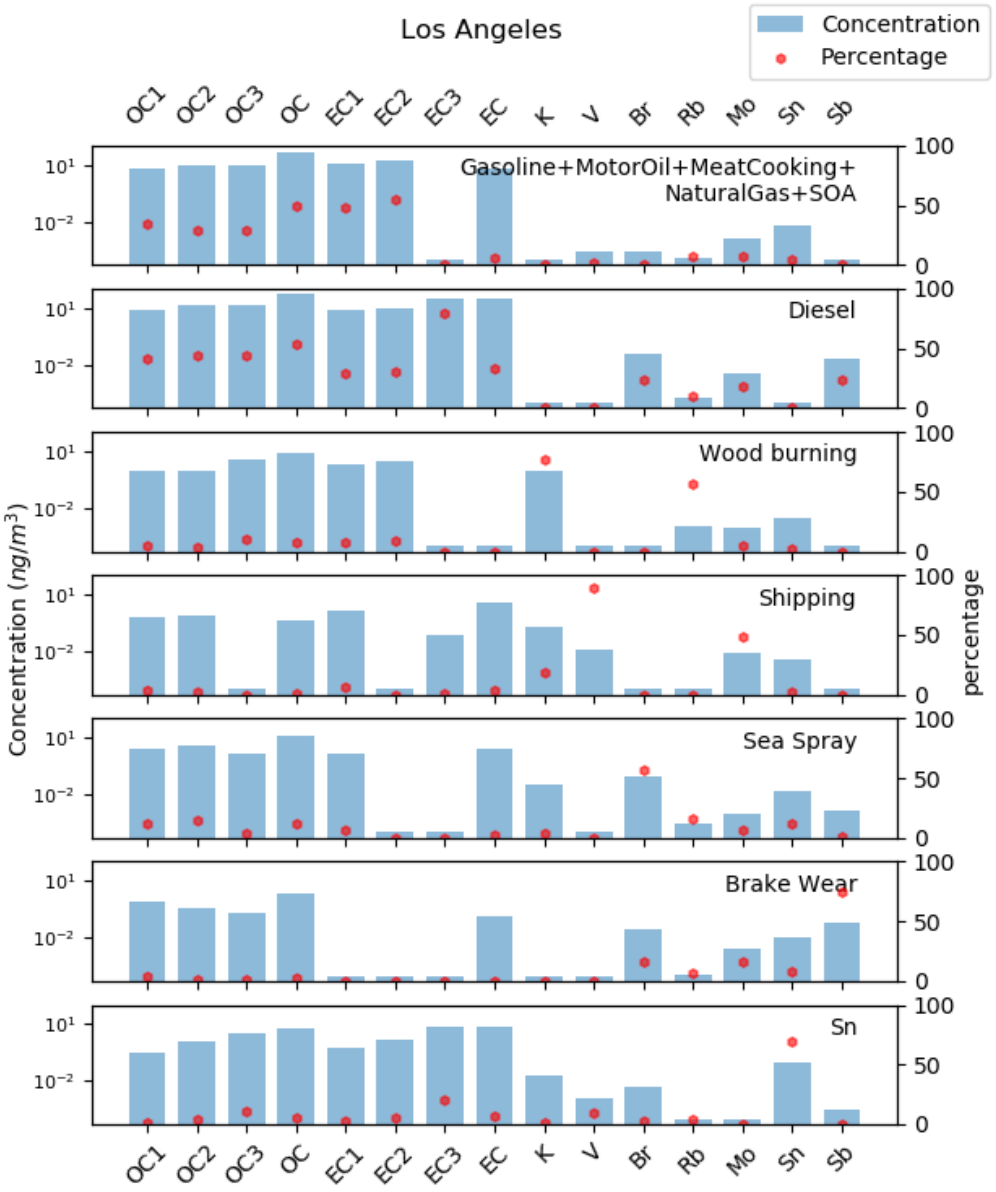

Figure 3.4. PMF species profile at Los Angeles. Blue bar s(left axis) represent concentration of species in each factor and red dots (right axis) represents the percentage of species mass in each factor. Note that OC1, EC1, and Mo are weak species with higher uncertainty in the concentration profile.

3.3.3 Source contributions to $PM_{0.1}$ mass

Figures 3.5-3.7 show $PM_{0.1}$ mass fractions at the three sampling sites. San Pablo and East Oakland display similar distribution, with Gasoline+Motor Oil+Meat Cooking+Natural Gas+SOA, Diesel,

and Wood Burning as the three largest sources of $PM_{0.1}$. Diesel exceeds the mixed sources of Gasoline+Motor Oil+Meat Cooking+Natural Gas+SOA at LA to be the largest source. The contribution from Wood Burning shrinks at LA because Southern California relies less on wood burning for residential heating.

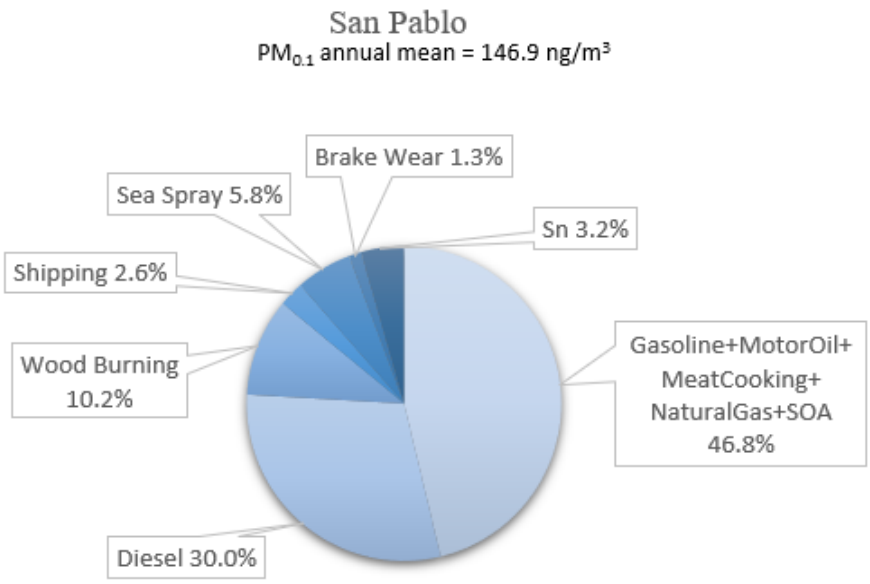

Figure 3.5. Source contributions to $PM_{0.1}$ mass at San Pablo.

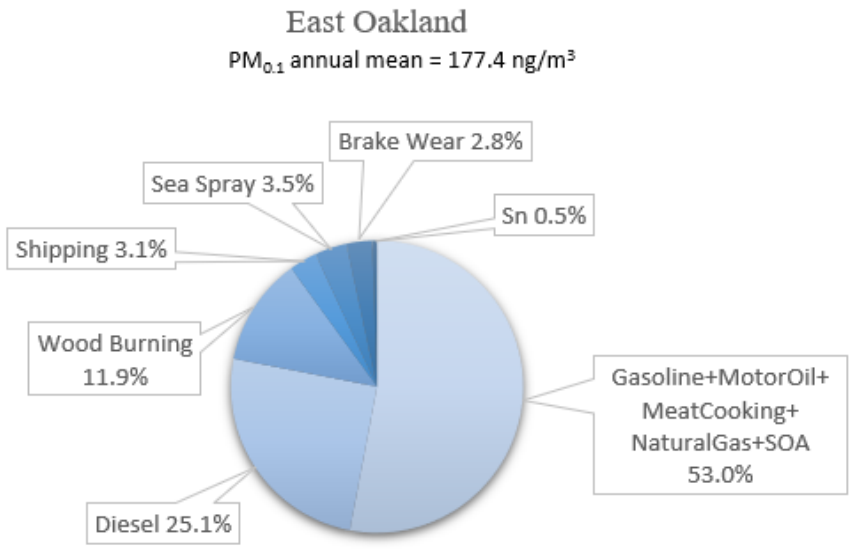

Figure 3.6. Source contributions to $PM_{0.1}$ mass at East Oakland.

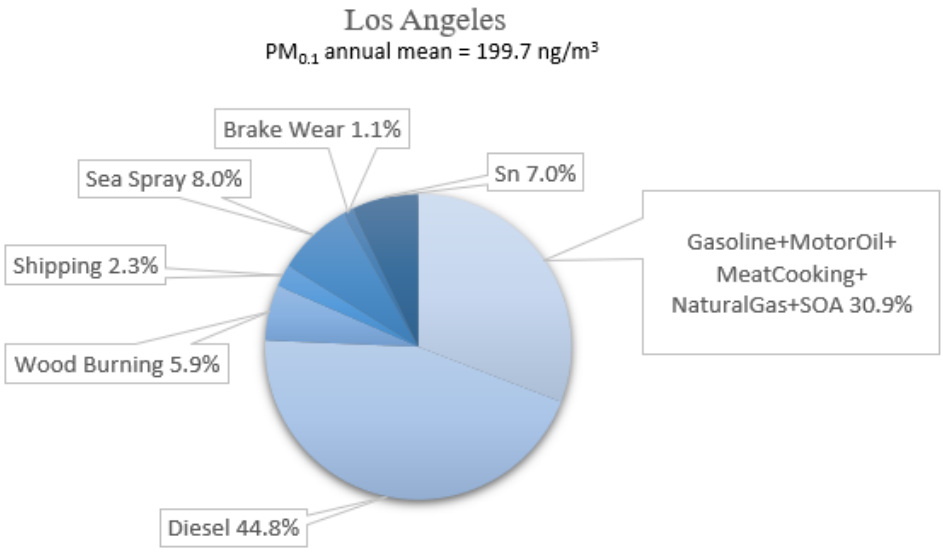

Factor 3.7. Source contributions to $PM_{0.1}$ mass at Los Angeles.

3.3.4 Source location conditional probability function (CPF)

Source Conditional Probability Function (CPF) plots show the most probable direction of sources relative to the measurement sites. As described in the previous section, Shipping and other heavy fuel oil combustion and Sea Spray at SP and EO are located in the direction of the ocean, which corroborates their source identification. The Wood Burning and Gasoline+Motor Oil+Meat Cooking+Natural Gas+SOA sources at SP and EO are from the northeast, east and southeast, which is consistent with the location of commercial and residential areas. The CPF plot for Diesel Engines + Motor Oil at SP shows slightly more contribution from the east than the southwest. This can be explained by the fact that SP is surrounded by interstate highway 80 to the east and interstate highway 580 to the southwest, but the I80 highway has higher traffic volume and is closer to the sampling site. Site EO has I880 to the west and I580 to the east, consistent with the CPF plot of Diesel source that has higher probabilities on the west and east. The Sb – Brake Wear source at EO is mainly from the southwest, which aligns with the location of a railway corridor just 1 mile away from the sampling location along the southwest. A railway station is also located to the south of SP sampling site, which is consistent with the directionality of the Brake Wear CPF plot at this location.

The CPF plots at LA have little directionality because the wind speed at the sampling location is very low which makes it difficult to resolve source directions.

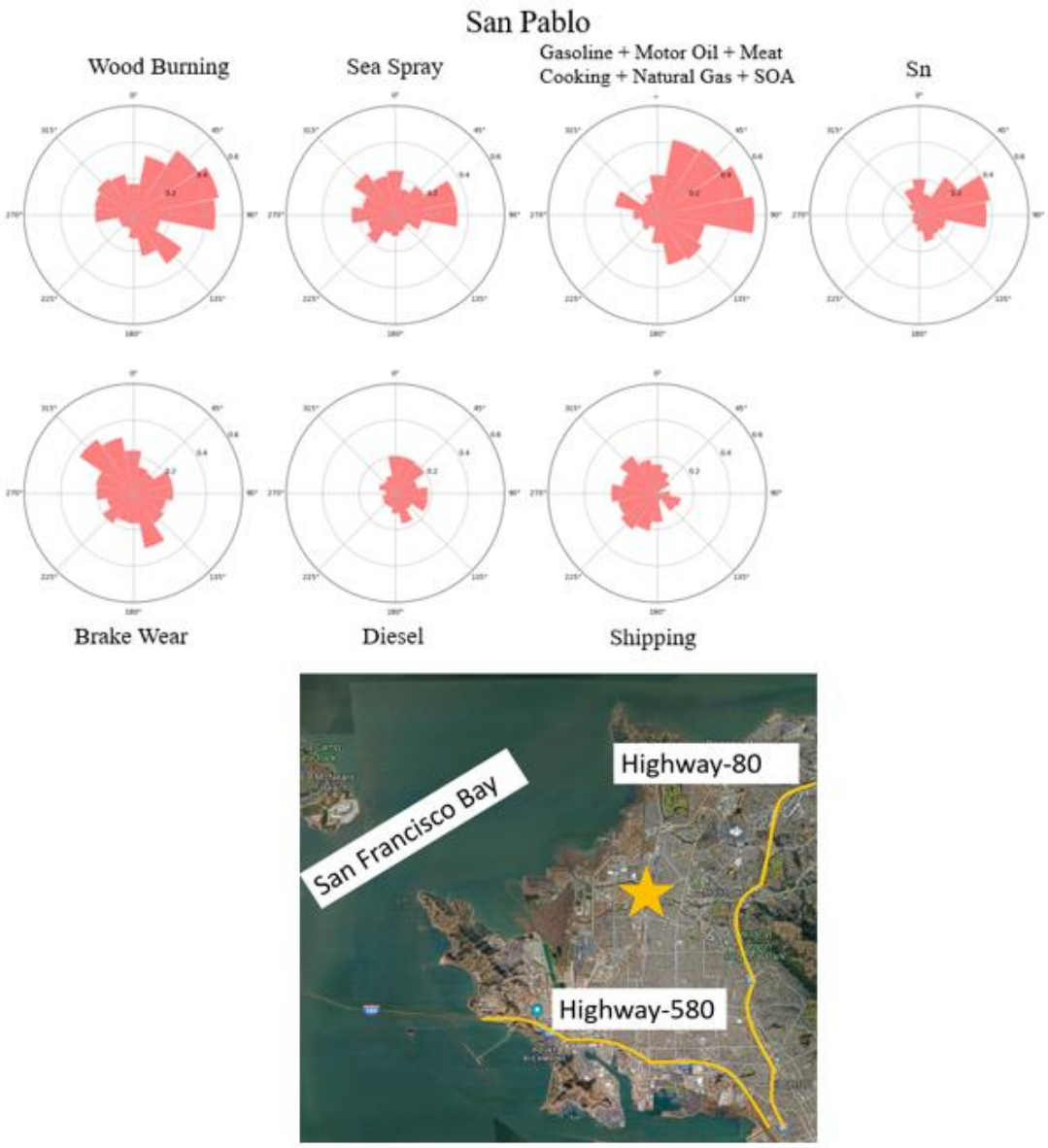

Figure 3.8. CPF plots and map of sampling location for San Pablo.

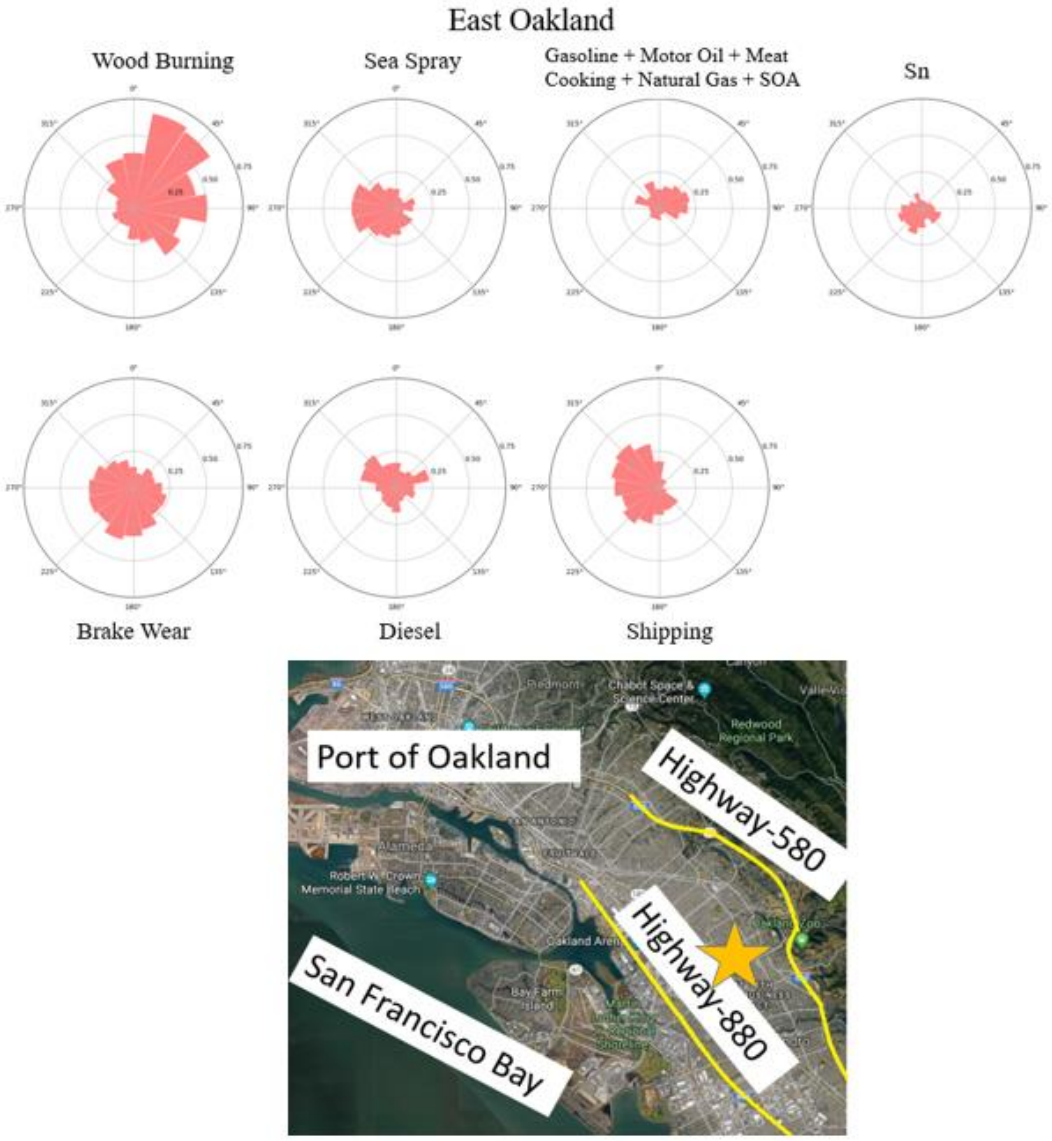

Figure 3.9. CPF plots and map of sampling location for East Oakland.

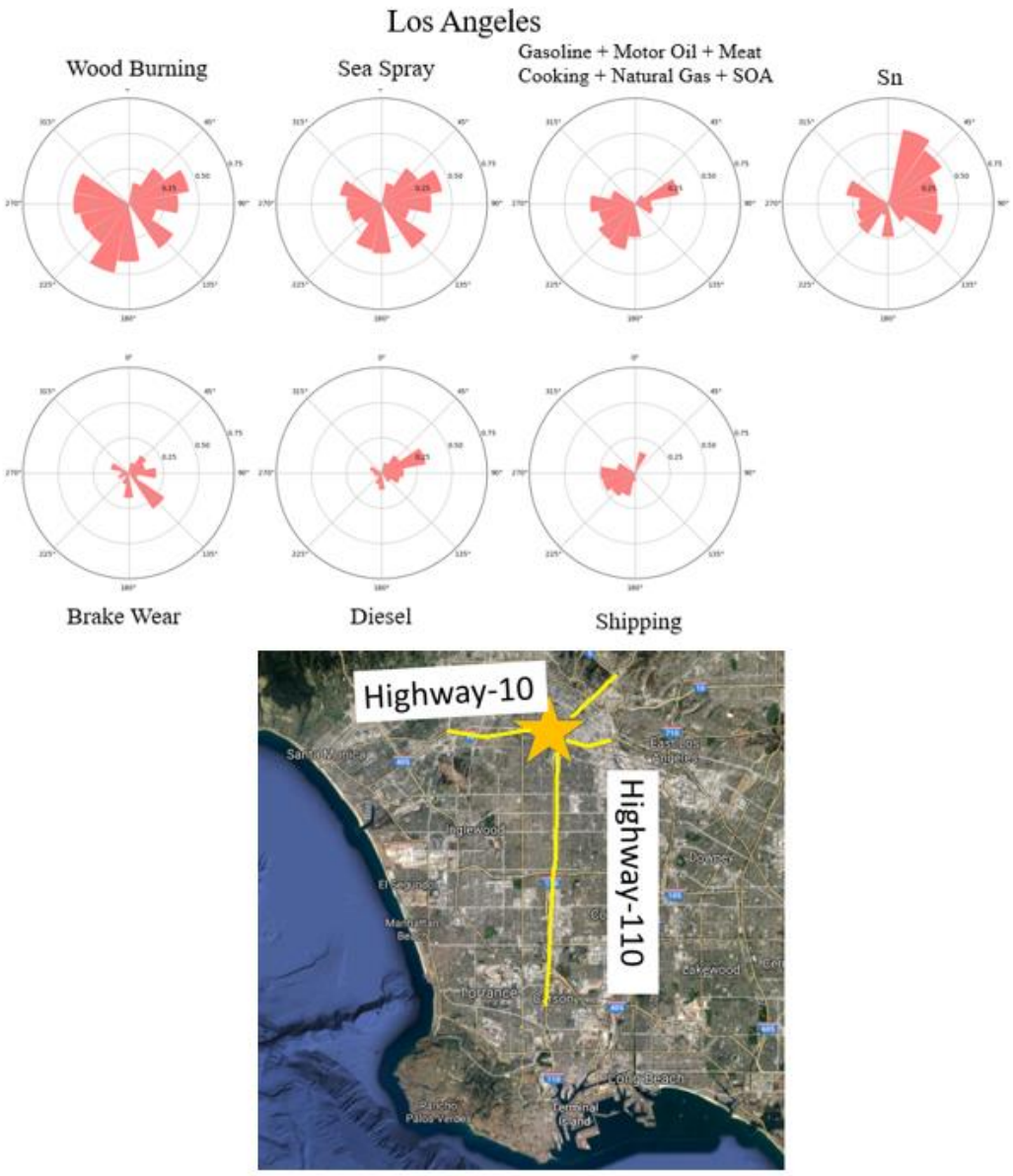

Figure 3.10. CPF plots and map of sampling location for Los Angeles.

3.3.5 Time series

Figures 3.11 through 3.13 show the time series of source factor contributions to $PM_{0.1}$ concentrations over the annual sampling period with 3-day resolution. The source Gasoline+Motor Oil+Meat Cooking+Natural Gas+SOA generally increases in fall/winter season at all three sites, most likely due to reduced atmospheric mixing in the colder season and the increased partitioning

of semi organic species to the particle phase as a result of lower temperatures. Wood burning $PM_{0.1}$ concentrations also increased during winter due to increased source activity and reduced atmospheric mixing. Wood burning $PM_{0.1}$ peaks during the Thanksgiving holiday in late November due to the effects of increased residential wood combustion. Diesel engine + motor oil contributions to $PM_{0.1}$ are relatively constant throughout the annual cycle at all three sites. The Sea Spray contributions are higher in the warm season at SP and EO, coinciding with greater wind speed during summer. This effect is not observed at Los Angeles, possibly because the sampling site is located farther from the coast giving the ultrafine particles time to coagulate with larger particles. The Shipping and other heavy fuel oil combustion, Brake Wear and Sn sources have no clear seasonal trend. Sn at SP and EO exhibits a pattern consistent with a point source with plumes intermittently washing over the sampling site.

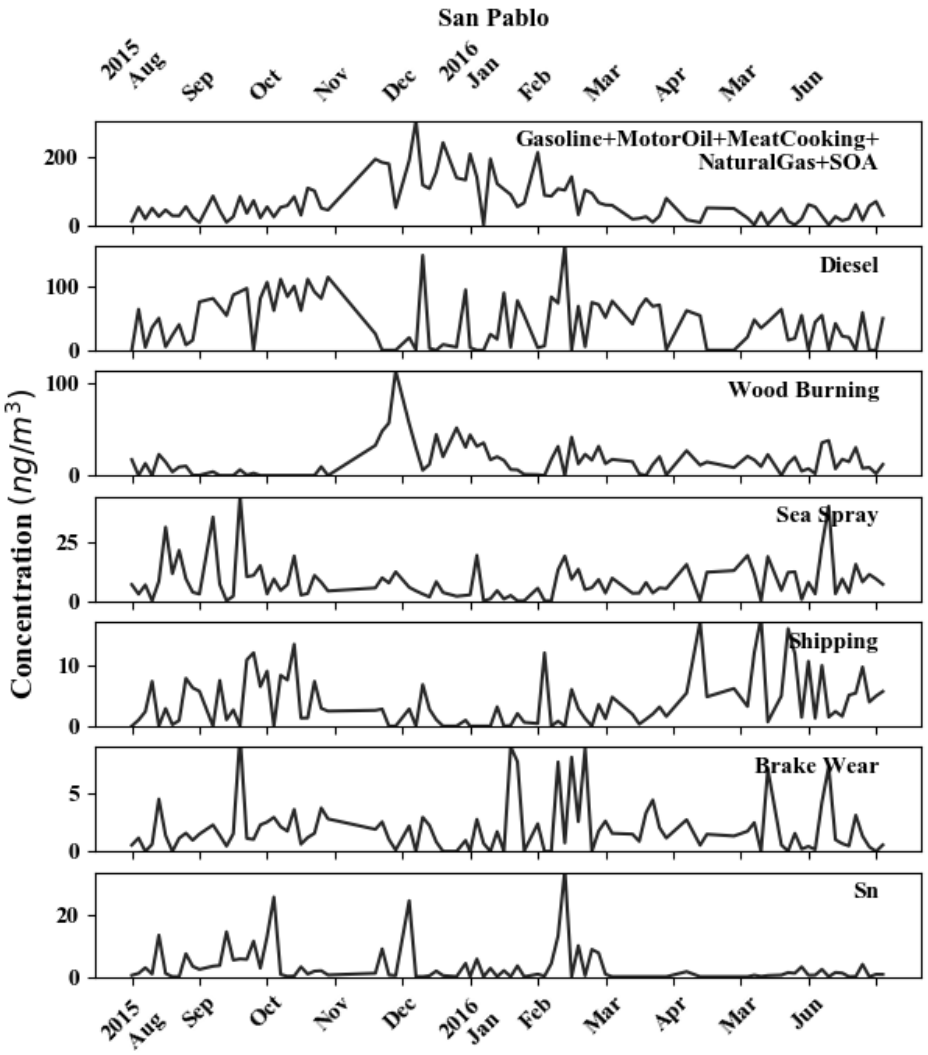

Figure 3.11. Time series of resolved $PM_{0.1}$ factors at San Pablo.

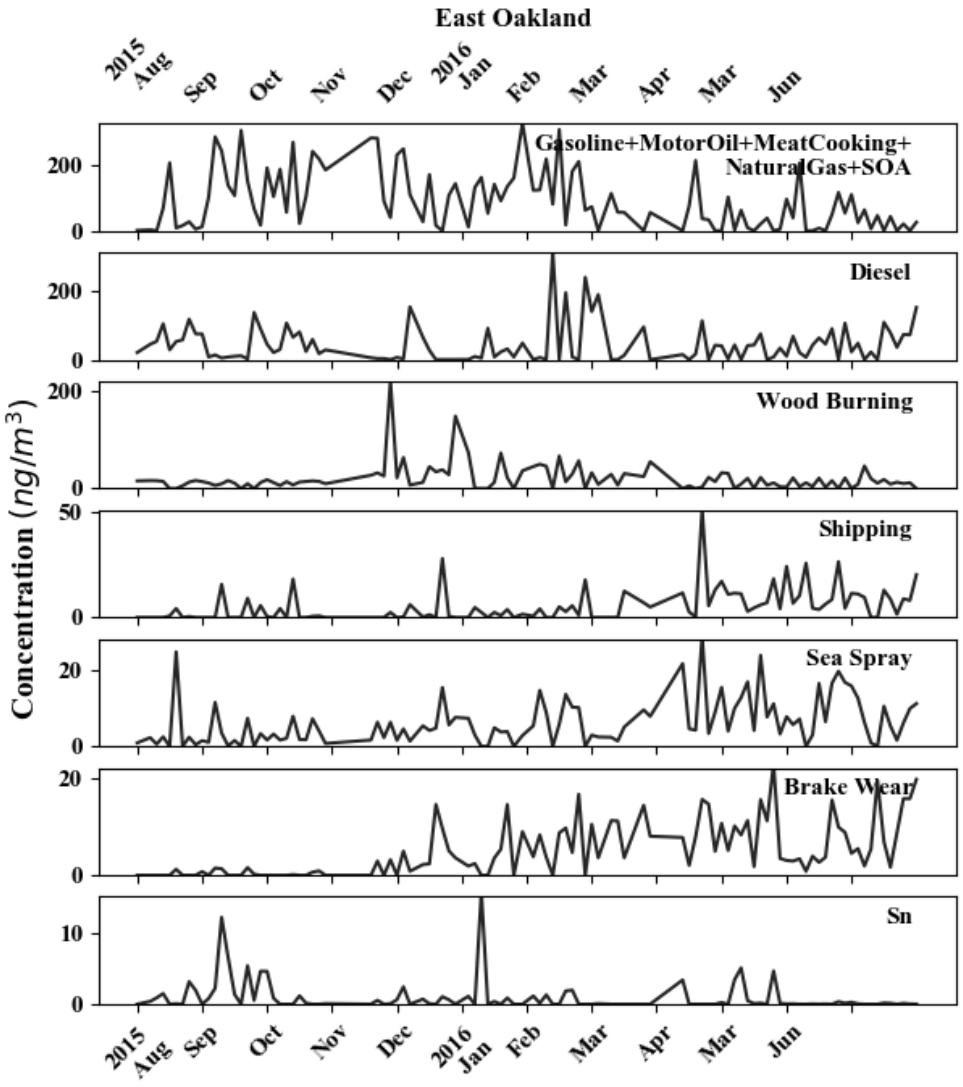

Figure 3.12. Time series of resolved $PM_{0.1}$ factors at East Oakland.

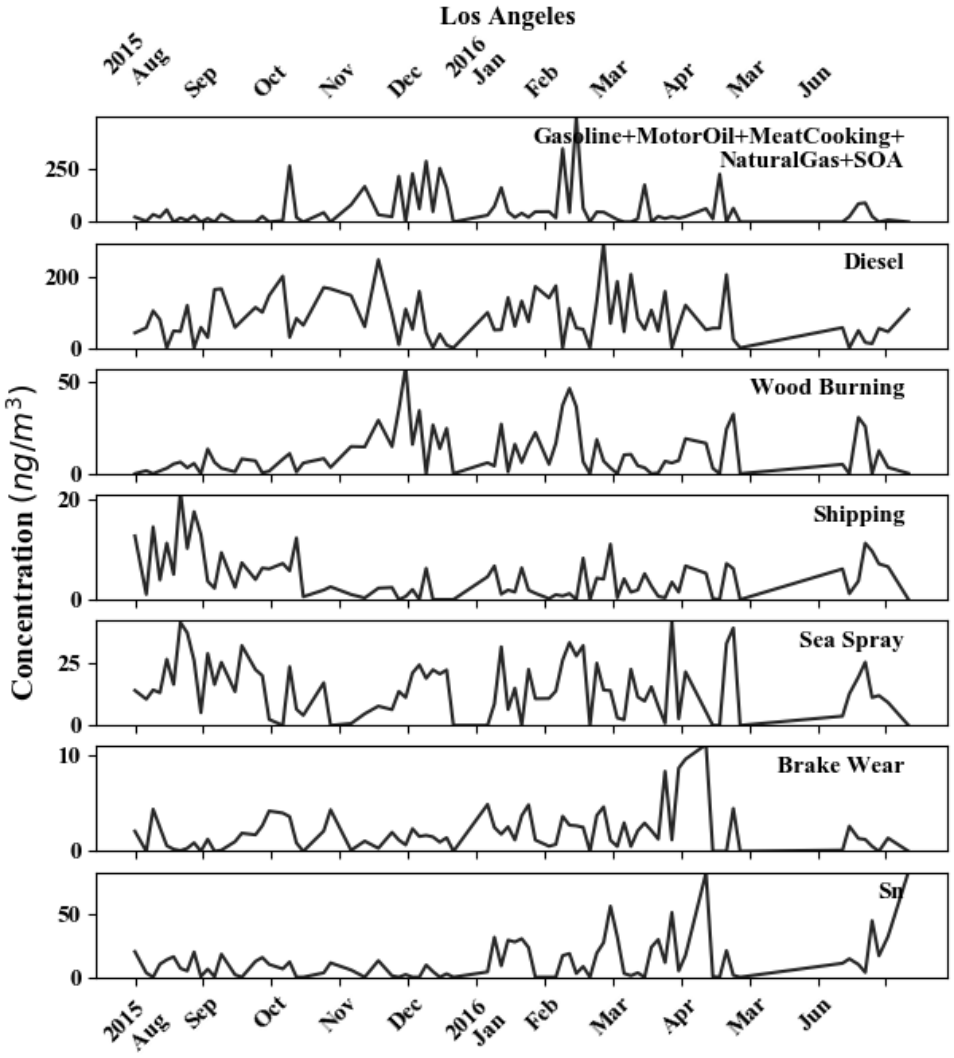

Figure 3.13. Time series of resolved $PM_{0.1}$ factors at Los Angeles.

3.3.6 Comparison with CMB results

Figures 3.14 through 3.16 compare monthly $PM_{0.1}$ concentrations from Wood burning, Diesel Engines + Motor Oil, and Gasoline+Motor Oil+Meat Cooking+Natural Gas+SOA predicted by the PMF calculations in the current study and the CMB calculations from [10]. PMF and CMB source predictions generally follow similar seasonal trends at all three sites, which builds confidence that both PMF and CMB can correctly resolve $PM_{0.1}$ sources. The PMF Gasoline+Meat Cooking+Natural Gas+SOA source contributions are generally higher than the CMB Gasoline+Motor Oil+Meat Cooking source contributions during the colder months, possibly because the CMB results do not include the Natural Gas source contributions. The PMF-Wood burning is higher than the CMB-Wood burning, especially in warmer seasons. This may be due to the chemical reaction of the Levoglucosan tracer used in CMB analysis [49]. K was found to better associated with wildfire-emitted OC than levoglucosan because levoglucosan could transform under high temperature in a more complete combustive process, like severe wildfires [50]. This difference may be especially important for predicting the contribution to $PM_{0.1}$ mass from wildfires during the late summer and early fall when oxidant concentrations are high. Despite the differences in PMF vs. CMB wood burning in summer, both models predict that the highest $PM_{0.1}$ concentrations associated with wood burning occur during the late fall and winter seasons due to residential wood combustion.

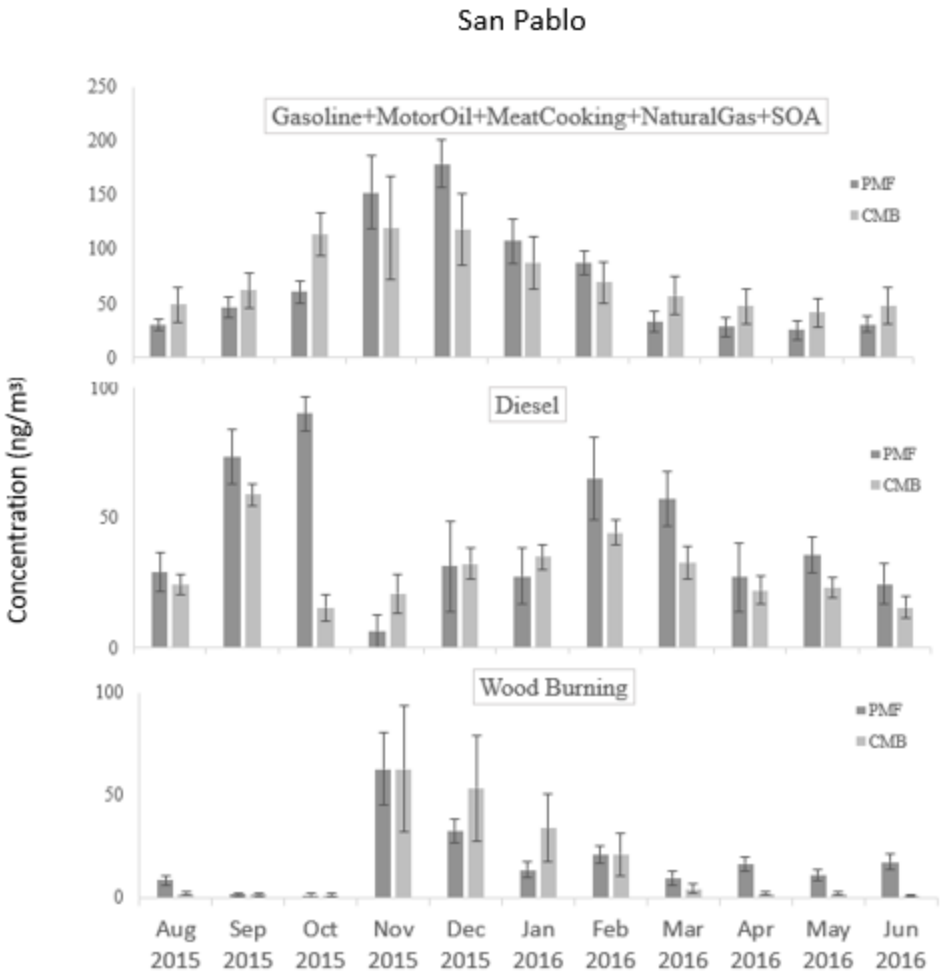

Figure 3.14. Comparison of monthly source contributions to $PM_{0.1}$ predicted by PMF and CMB for San Pablo.

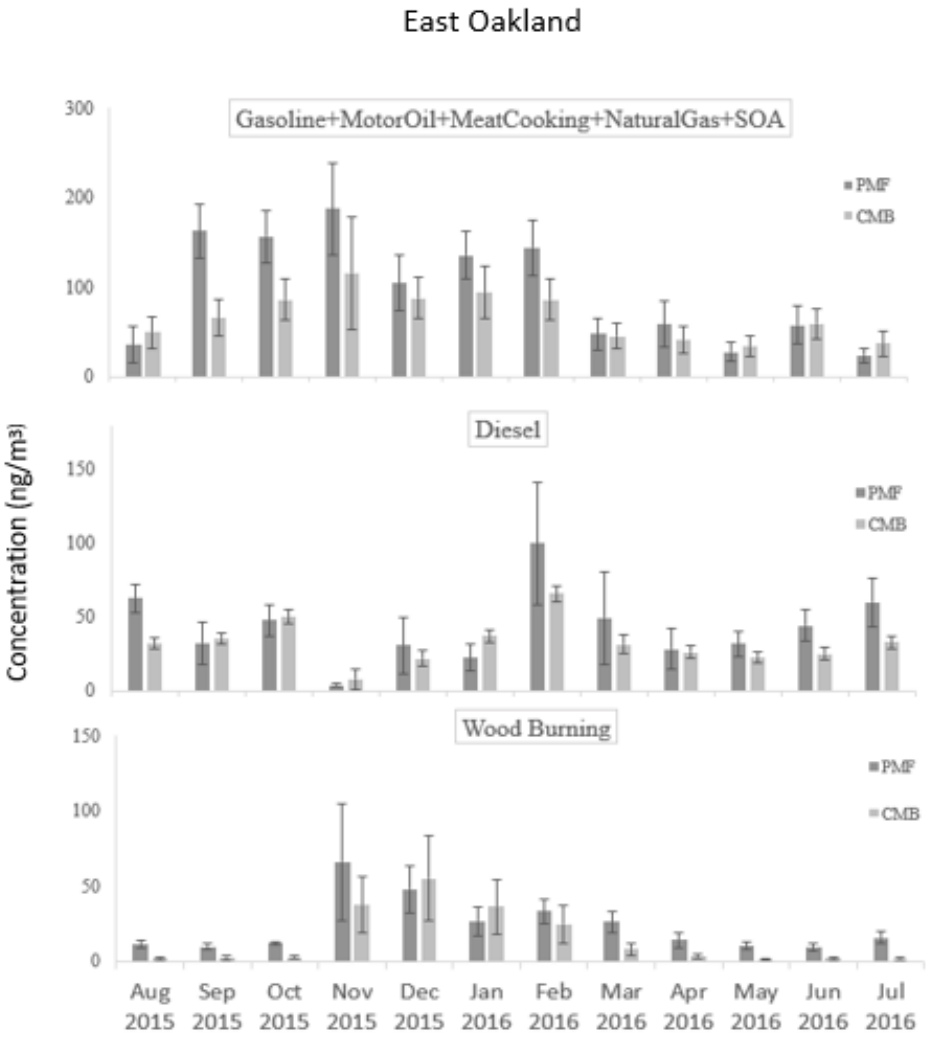

Figure 3.15. Comparison of monthly source contributions to $PM_{0.1}$ predicted by PMF and CMB for East Oakland.

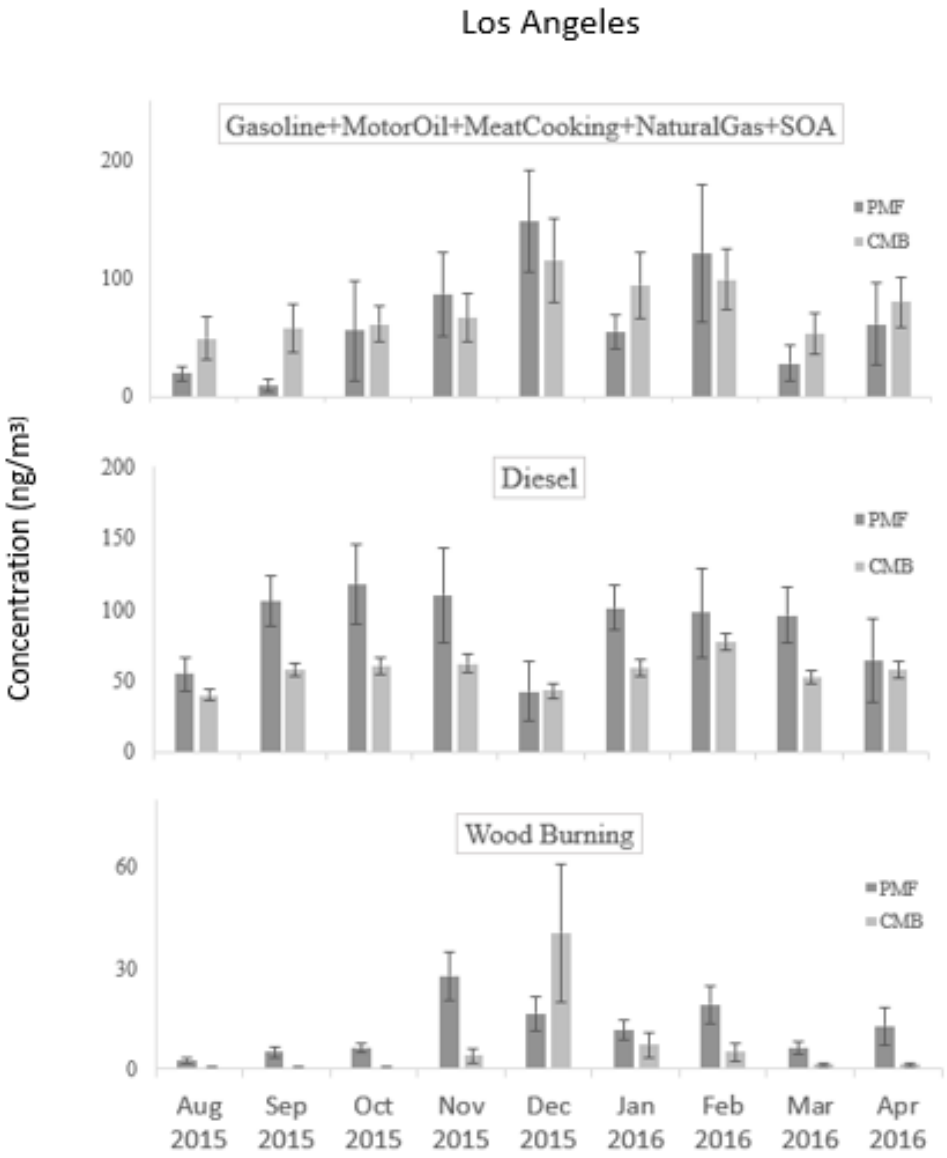

Figure 3.16. Comparison of monthly source contributions to $PM_{0.1}$ predicted by PMF and CMB for Los Angeles.

3.4 Discussion

In the current study, the averaged $PM_{0.1}$ mass at three locations in California ranged from 146.9 to 199.7 ng/m^3 in the year 2015 summer – 2016 summer. A study reported $PM_{0.1}$ to be 171 ng/m^3 at a site near SP and EO in Northern California in 2010 [12], which was comparable to the $PM_{0.1}$ level in the current study. There are few studies that determined entire composition of $PM_{0.1}$ mass consisting of OC, EC, ionic species (sulfate, nitrate, ammonium) and metals [51]. One example was that a study carried out in Southern California in 1996-1997 found that inorganic ions and metals each accounts for ~10-20% of total $PM_{0.1}$ that was ~ 800 ng/m^3 [52]. Assuming this fraction stays constant over 20 years, the current $PM_{0.1}$ mass measured should be ~80-90 % of the actual ambient $PM_{0.1}$ concentrations. $PM_{0.1}$ mass varies drastically globally - it was reported to be ~3,000 ng/m^3 in Italy in 2016 [15], ~7,000 ng/m^3 in China 2012 [53], and ~ 1,000 ng/m^3 in Japan 2009 [54]. These comparisons show that UFP levels vary considerably worldwide and further stresses the necessity to characterize UFP on local basis.

To the best knowledge of authors, it's the first time that ultrafine Shipping and Brake Wear sources were resolved by PMF, which was made possible by accurate measurement of V and Sb on ultrafine level. Diesel source identified by a sub-fraction of EC(EC3), Brake Wear identified by Sb, and Wood Burning identified by Rb were not seen in previous literature, either. Measuring elements in $PM_{0.1}$ is much more difficult than in $PM_{2.5}$ because the extremely low concentrations of commonly seen elements, such as Na, Cl, Cu, Fe and Mn, would be interfered by background noises. This makes these elements incapable of acting as tracers in $PM_{0.1}$ source apportionment as in $PM_{2.5}$. The current study provides alternative tracers for ultrafine source apportionment, which may be useful for future studies.

The current study shows that PMF is capable of resolving organic sources of $PM_{0.1}$ with three-day

time resolution without the use of expensive molecular marker analysis, but the source-resolution of the analysis is limited. PMF was not able to separate gasoline engines, meat cooking, natural gas combustion and SOA since specific markers are not available for these formation pathways. Comparing $PM_{0.1}$ source apportionment results with those of $PM_{2.5}$ in a previous study in San Francisco Bay Area [55], desiel exhaust contributes 25-30% to $PM_{0.1}$ total mass and 9.4% to $PM_{2.5}$. Gasoline+Motor Oil+Meat Cooking+Natural Gas+SOA contributes to 46-53% of $PM_{0.1}$ while secondary sulfate, secondary nitrate, gasoline vehicle each accounts for 13.1%, 20%, amd 14.8% of $PM_{2.5}$, respectively. Considering the finding that secondary ionic species only accounts for 10-20% of $PM_{0.1}$ [52], SOA fraction in $PM_{0.1}$ is less than that in $PM_{2.5}$. $PM_{2.5}$ also contains aged sea salt and road salt sources that don't exist in $PM_{0.1}$ resolved sources. A comparison with $PM_{2.5}$ source apportionment study in LA [56] yields similar results. These comparisons reveals that $PM_{0.1}$ contains less aged aerosol and more fresh emissions than $PM_{2.5,}$ which is probably because, owing to Kelvin Effect, higher surface curvature in smaller particles leads to enhanced evaporation of semi-volatile components (such as hydrocarbons and ammonium nitrate) in UFPs [51].

The increased time resolution inherent in the PMF analysis provides information that can be analyzed to infer source characteristics. Figure 3.16 illustrates the frequency histogram of source contributions to $PM_{0.1}$ concentrations at San Pablo, East Oakland, and Los Angeles during the one-year study period spanning the years 2015 and 2016. Pollutant concentrations in the environment often follow a log-normal probability distribution and so it's not surprising that many of the $PM_{0.1}$ source contributions illustrated in Figure 3.16 have a single mode and approximately symmetric shapes. The asymmetry in the Gasoline+Motoroil+Meat Cooking+Natural Gas+SOA histogram may reflect the contribution from multiple sources to this factor. The shape of each histogram displayed in Figure 3.16 reflects variability in the emissions strength of nearby sources, wind

direction, and atmospheric dilution rates. Concentrations from most sources with approximately constant emissions rates span approximately two orders of magnitude (see for example diesel engines). The concentration of the unidentified Sn source spans three or more orders of magnitude, suggesting that the strength of the Sn source varies considerably over the annual cycle or that this may be a point source that only affects concentrations at the receptor site periodically.

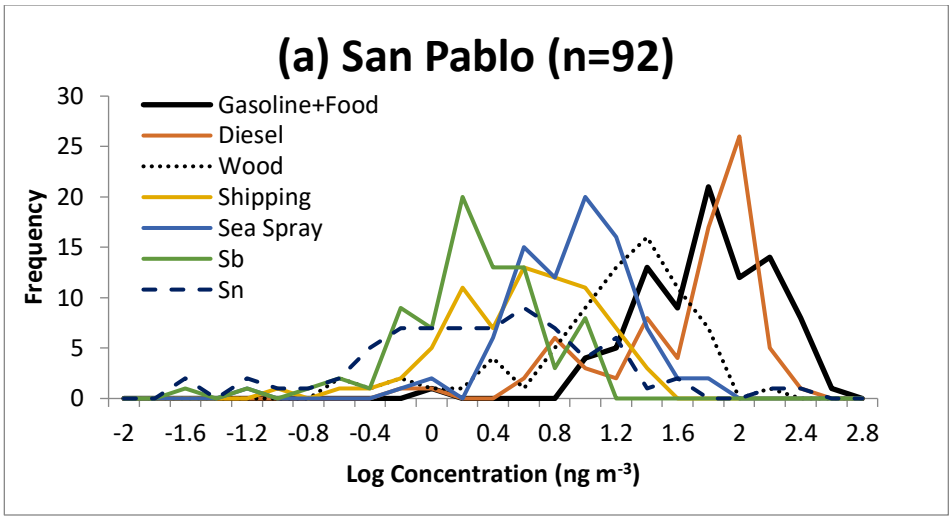

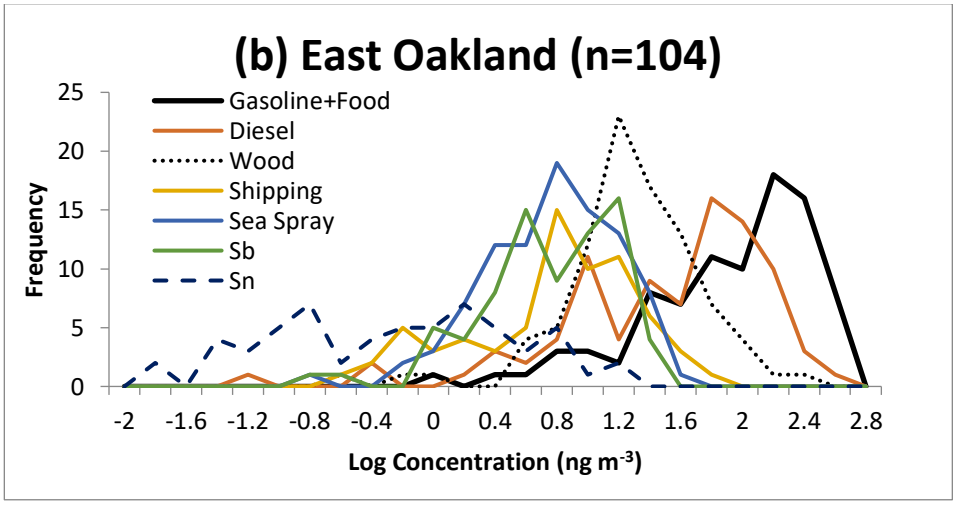

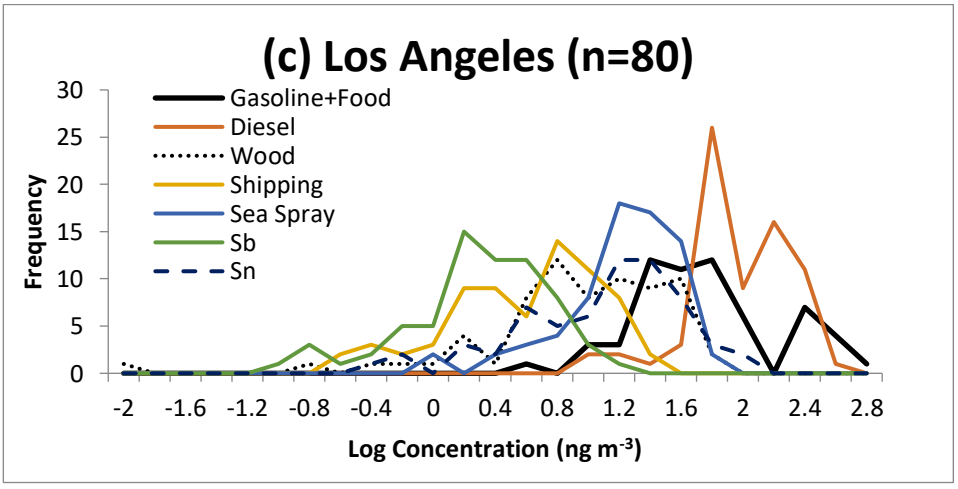

Figure 3.16. Frequency histograms of source contributions to $PM_{0.1}$ concentrations at San Pablo, East Oakland, and Los Angeles during the one-year study period. Each tabulated frequency corresponds to the number of three-day average samples that fall into the indicated concentration bin.

3.5 Conclusions

Three-day average samples of $PM_{0.1}$ collected over a full year at San Pablo, East Oakland, and Los Angeles were analyzed using Positive Matrix Factorization to identify source contributions at each location. Seven $PM_{0.1}$ sources were identified: Factor1-Gasoline+Motor Oil+Meat Cooking+Natural Gas+SOA, Factor 2- Diesel+Motor Oil, Factor 3-Wood Burning, Factor 4-Shipping and other heavy fuel oil combustion, Factor 5-Sea Spray, Factor 6-Sb Brake Wear, and Factor 7-Sn. Gasoline+Motor Oil+Meat Cooking+Natural Gas+SOA, Diesel+Motor Oil, and Wood Burning are the highest contributors to $PM_{0.1}$ mass. Wood Burning contributions to $PM_{0.1}$ were highest in the winter season when residential wood combustion was active. The monthly-averaged $PM_{0.1}$ source apportionment results calculated by PMF in the current study are consistent with the $PM_{0.1}$ source apportionment results calculated using CMB, showing the robustness of the PMF method. EC3, K and Rb, V, Br, and Sb were used as tracers for Factor 2-6 respectively. It's the first time that Shipping and Brake Wear were resolved by PMF for $PM_{0.1}$. The higher time resolution inherent with in PMF method may help infer source characteristics.

3.6 Acknowledgements:

This research was supported by the California Air Resources Board under contract 14-314. The statements and conclusions in this manuscript are those of the authors and not necessarily those of the California Air Resources Board. The authors would like to thank Alam Hasson and Annabelle Lolinco at the California State University at Fresno for help with sample collection.

3.7 References

1. Ostro, B., et al., *Associations of mortality with long-term exposures to fine and ultrafine particles, species and sources: results from the California Teachers Study Cohort.* Environ Health Persp., 2015. **123**(6): p. 549-56.

2. Laurent, O., et al., *A Statewide Nested Case-Control Study of Preterm Birth and Air Pollution by Source and Composition: California, 2001-2008.* Environmental Health Perspectives, 2016.
3. Laurent, O., et al., *Low birth weight and air pollution in California: Which sources and components drive the risk?* Environment International, 2016. **92-93**: p. 471-477.
4. Li, N., et al., *Ultrafine particulate pollutants induce oxidative stress and mitochondrial damage.* Environmental Health Perspectives, 2003. **111**(4): p. 455-460.
5. Nel, A., et al., *Toxic potential of materials at the nanolevel* Science, 2006. **311**(5761): p. 622-627.
6. Geiser, M., et al., *Ultrafine particles cross cellular membranes by nonphagocytic mechanisms in lungs and in cultured cells.* Environmental health perspectives, 2005. **113**(11): p. 1555.
7. Elder, A. and G. Oberdörster, *Translocation and effects of ultrafine particles outside of the lung.* Clinics in occupational and environmental medicine, 2005. **5**(4): p. 785-796.
8. Ham, W.A. and M.J. Kleeman, *Size-resolved source apportionment of carbonaceous particulate matter in urban and rural sites in central California.* Atmospheric Environment, 2011. **45**(24): p. 3988-3995.
9. Hasheminassab, S., et al., *Source apportionment and organic compound characterization of ambient ultrafine particulate matter (PM) in the Los Angeles Basin.* Atmospheric environment, 2013. **79**: p. 529-539.
10. Xue, J., et al., *Seasonal and Annual Source Appointment of Carbonaceous Ultrafine Particulate Matter (PM0. 1) in Polluted California Cities.* Environmental science & technology, 2018. **53**(1): p. 39-49.
11. Sowlat, M.H., S. Hasheminassab, and C. Sioutas, *Source apportionment of ambient particle number concentrations in central Los Angeles using positive matrix factorization (PMF).* Atmospheric Chemistry and Physics, 2016. **16**(8): p. 4849-4866.
12. Kuwayama, T., C.R. Ruehl, and M.J. Kleeman, *Daily trends and source apportionment of ultrafine particulate mass (PM0.1) over an annual cycle in a typical California city.* Environ Sci Technol, 2013. **47**(24): p. 13957-66.
13. Squizzato, S., et al., *Long-Term Changes of Source Apportioned Particle Number Concentrations in a Metropolitan Area of the Northeastern United States.* Atmosphere, 2019. **10**(1): p. 27.
14. del Águila, A., et al., *Sources and physicochemical characteristics of submicron aerosols during three intensive campaigns in Granada (Spain).* Atmospheric Research, 2018. **213**: p. 398-410.
15. Bernardoni, V., et al., *Size-segregated aerosol in a hot-spot pollution urban area: Chemical composition and three-way source apportionment.* Environmental pollution, 2017. **231**: p. 601-611.
16. Wang, S., et al., *Size-fractionated particulate elements in an inland city of China: Deposition flux in human respiratory, health risks, source apportionment, and dry deposition.* Environmental pollution, 2019. **247**: p. 515-523.
17. Tan, J.H., et al., *Source apportionment of size segregated fine/ultrafine particle by PMF in Beijing.* Atmospheric Research, 2014. **139**: p. 90-100.
18. Baldauf, R.W., et al., *Ultrafine Particle Metrics and Research Considerations: Review of the 2015 UFP Workshop.* International journal of environmental research and public health, 2016. **13**(11): p. 1054.

19. Venecek, M.A., X. Yu, and M.J. Kleeman, *Predicted ultrafine particulate matter source contribution across the continental United States during summertime air pollution events.* Atmospheric Chemistry and Physics, 2019. **19**(14): p. 9399-9412.
20. Kleeman, M.J., et al., *Source Apportionment of Fine (PM1.8) and Ultrafine (PM0.1) Airborne Particulate Matter during a Severe Winter Pollution Episode.* Environmental Science & Technology, 2009. **43**(2): p. 272-279.
21. Marple, V.A., K.L. Rubow, and S.M. Behm, *A microorifice uniform deposit impactor (MOUDI): Description, calibration, and use.* Aerosol Science and Technology, 1991. **14**(4): p. 434-446.
22. Herner, J.D., P.G. Green, and M.J. Kleeman, *Measuring the trace elemental composition of size-resolved airborne particles.* Environmental science & technology, 2006. **40**(6): p. 1925-1933.
23. Herner, J.D., et al., *Size and composition distribution of airborne particulate matter in northern California: I-particulate mass, carbon, and water-soluble ions.* Journal of the Air & Waste Management Association, 2005. **55**(1): p. 30-51.
24. Xue, W., et al., *Day-of-week patterns for ultrafine particulate matter components at four sites in California.* Atmospheric Environment, 2019: p. 117088.
25. Norris, G., et al., *EPA Positive Matrix Factorization (PMF) 5.0 fundamentals and User Guide Prepared for the US Environmental Protection Agency Office of Research and Development, Washington, DC.* Inc., Petaluma, 2014.
26. Reff, A., S.I. Eberly, and P.V. Bhave, *Receptor modeling of ambient particulate matter data using positive matrix factorization: review of existing methods.* Journal of the Air & Waste Management Association, 2007. **57**(2): p. 146-154.
27. Pavlovic, J., J. Kinsey, and M. Hays, *The influence of temperature calibration on the OC–EC results from a dual-optics thermal carbon analyzer.* Atmospheric Measurement Techniques, 2014. **7**(9): p. 2829-2838.
28. Zhu, C.-S., et al., *Characterization of carbon fractions for atmospheric fine particles and nanoparticles in a highway tunnel.* Atmospheric Environment, 2010. **44**(23): p. 2668-2673.
29. Cao, J., et al., *Characterization of roadside fine particulate carbon and its eight fractions in Hong Kong.* Aerosol Air Qual. Res, 2006. **6**(2): p. 106-122.
30. Liu, W., et al., *Enhanced source identification of southeast aerosols using temperature-resolved carbon fractions and gas phase components.* Atmospheric Environment, 2006. **40**: p. 445-466.
31. Kleeman, M.J., J.J. Schauer, and G.R. Cass, *Size and composition distribution of fine particulate matter emitted from wood burning, meat charbroiling, and cigarettes.* Environmental Science & Technology, 1999. **33**(20): p. 3516-3523.
32. Pereira, E., et al., *Airborne measurements of aerosols from burning biomass in Brazil related to the TRACE A experiment.* Journal of Geophysical Research: Atmospheres, 1996. **101**(D19): p. 23983-23992.
33. Ham, W.A., et al., *Size Distribution of Health-Relevant Trace Elements in Airborne Particulate Matter During a Severe Winter Stagnation Event: Implications for Epidemiology and Inhalation Exposure Studies.* Aerosol Science and Technology, 2010. **44**(9): p. 753-765.
34. Querol, X., et al., *Source origin of trace elements in PM from regional background, urban and industrial sites of Spain.* Atmospheric Environment, 2007. **41**(34): p. 7219-7231.

35. Tian, H., et al., *A comprehensive global inventory of atmospheric antimony emissions from anthropogenic activities, 1995–2010.* Environmental science & technology, 2014. **48**(17): p. 10235-10241.
36. Sathickbasha, K., et al., *The dual role of metal sulfides as lubricant and abrasive: an interface study in friction composite.* Materials Research Express, 2019.
37. Querol, X., et al., *PM speciation and sources in Mexico during the MILAGRO-2006 Campaign.* Atmospheric Chemistry and Physics, 2008. **8**(1): p. 111-128.
38. Johansson, C., M. Norman, and L. Burman, *Road traffic emission factors for heavy metals.* Atmospheric Environment, 2009. **43**(31): p. 4681-4688.
39. Abbasi, S., et al., *A study of airborne wear particles generated from organic railway brake pads and brake discs.* Wear, 2011. **273**(1): p. 93-99.
40. Namgung, H.-G., et al., *Generation of nanoparticles from friction between railway brake disks and pads.* Environmental science & technology, 2016. **50**(7): p. 3453-3461.
41. Roper, W., *Toxicological profile for tin.* US department of health and human services, agency for toxic substances and disease registry, 1992.
42. Shirmohammadi, F., et al., *Fine and ultrafine particulate organic carbon in the Los Angeles basin: Trends in sources and composition.* Sci Total Environ, 2016. **541**: p. 1083-1096.
43. Gugamsetty, B., et al., *Source Characterization and Apportionment of PM10, PM2.5 and PM0.1 by Using Positive Matrix Factorization.* Aerosol and Air Quality Research, 2012. **12**(4): p. 476-491.
44. Al-Dabbous, A.N. and P. Kumar, *Source apportionment of airborne nanoparticles in a Middle Eastern city using positive matrix factorization.* Environmental Science-Processes & Impacts, 2015. **17**(4): p. 802-812.
45. Schauer, J.J., *Evaluation of elemental carbon as a marker for diesel particulate matter.* Journal of Exposure Science and Environmental Epidemiology, 2003. **13**(6): p. 443.
46. Fine, P.M., G.R. Cass, and B.R. Simoneit, *Chemical characterization of fine particle emissions from the wood stove combustion of prevalent United States tree species.* Environmental Engineering Science, 2004. **21**(6): p. 705-721.
47. Viana, M., et al., *Chemical tracers of particulate emissions from commercial shipping.* Environmental science & technology, 2009. **43**(19): p. 7472-7477.
48. https://web.stanford.edu/group/Urchin/mineral.html.
49. Hoffmann, D., et al., *Atmospheric stability of levoglucosan: a detailed laboratory and modeling study.* Environmental science & technology, 2009. **44**(2): p. 694-699.
50. Pio, C., et al., *Chemical composition of atmospheric aerosols during the 2003 summer intense forest fire period.* Atmospheric Environment, 2008. **42**(32): p. 7530-7543.
51. AQEG(UK), A.Q.E.G., *Ultrafine Particles (UFP) in the UK.* 2018.
52. Cass, G.R., et al., *The chemical composition of atmospheric ultrafine particles.* Philosophical Transactions of the Royal Society of London A: Mathematical, Physical and Engineering Sciences, 2000. **358**(1775): p. 2581-2592.
53. Lü, S., et al., *Size distribution of chemical elements and their source apportionment in ambient coarse, fine, and ultrafine particles in Shanghai urban summer atmosphere.* Journal of Environmental Sciences, 2012. **24**(5): p. 882-890.
54. Kim, K.H., et al., *Seasonal variation of carbonaceous and ionic components in ultrafine and fine particles in an urban area of Japan.* Atmospheric environment, 2011. **45**(8): p. 1581-1590.

55. Wang, Y. and P.K. Hopke, *A ten–year source apportionment study of ambient fine particulate matter in San Jose, California.* Atmospheric Pollution Research, 2013. **4**(4): p. 398-404.
56. Hasheminassab, S., et al., *Long-term source apportionment of ambient fine particulate matter (PM2. 5) in the Los Angeles Basin: A focus on emissions reduction from vehicular sources.* Environmental pollution, 2014. **193**: p. 54-64.

4.0 Comparison of size-resolved PM elements measured using aluminum foil and Teflon impaction substrates: implications for ultrafine particle source apportionment and future sampling networks

Wei Xue[a], Jian Xue[a], and Michael J. Kleeman[a,]*

[a] Department of Civil and Environmental Engineering, University of California – Davis, Davis, California, USA

*corresponding author: mjkleeman@ucdavis.edu

4.1 Introduction

Inhaled airborne particulate matter (PM) threatens human health through mechanisms including respiratory and cardiovascular stress and diseases [1, 2]. PM composed of particles with diameter smaller than 0.1 μm, or utlrafine particulate matter (UFPM; $PM_{0.1}$), is potentially more toxic than larger PM size fractions because the smaller particles have the ability to deposit deep into lungs, cross cell membranes, and enter the bloodstream [3, 4]. $PM_{0.1}$ is typically composed of freshly emitted particles whereas particles in the accumulation mode exhibit greater evidence of atmospheric processing that can mask the source identity. Numerous sampling networks have been implemented across the globe to analyze the chemical composition of $PM_{2.5}$ to support source apportionment calculations and develop mitigation measures [5-8]. The deployment of $PM_{0.1}$ networks has been limited by the high expense of equipment, supplies, and labor needed for sample collection and analysis [9, 10].

$PM_{0.1}$ samples are typically collected using cascade impactors that impinge the aerosol flow onto collection substrates using successively faster jets that collect successively smaller particles. Multiple impactors have been employed for $PM_{0.1}$ collection including the Micro-Orifice Uniform Deposit Impactor (MOUDI) [11], Personal Cascade Impactor Sampler (PCIS) [12], the Harvard

Impactor [13], and the Rotating Drum Impactor (RDI) [14]. Most of these devices require that samples be collected on multiple types of impaction substrates to support a full range of chemical analysis for carbonaceous compounds, inorganic compounds, and elements. As an example, Xue et al. [10, 15, 16] operated a $PM_{0.1}$ sampling network for a full year at four locations in California using a MOUDI loaded with aluminum foil substrates (carbonaceous analysis) in parallel with a MOUDI loaded with Teflon substrates (inorganic analysis and elemental analysis). Operating two impactors at each sampling site increases equipment and supply costs, most notably for Teflon substrates that are 10x more expensive than foil substrates.

Herner *et al.* developed a relatively safe and efficient technique to extract and measure elements on Teflon substrate [17], which has proved to be effective for both larger particles, and also for $PM_{0.1}$ [10, 16, 18, 19]. Here we explore the feasibility of modifying this method to extract particles from foil substrates followed by elemental analysis so that each $PM_{0.1}$ sampling site needs to employ only a single MOUDI loaded with foil substrates to measure both carbonaceous content and elements. The original and modified elemental extraction and analysis methods are compared for particles in diameter range 0.1 – 1.8 μm. The regression analysis comparing the two methods in diameter range 0.1-0.18 μm is used to simulate a $PM_{0.1}$ dataset collected on foil substrates. $PM_{0.1}$ source apportionment studies are conducted using element concentrations that incorporate the uncertainty introduced by the use of foil substrates. The results are then compared to traditional $PM_{0.1}$ source apportionment results generated using parallel impactors loaded with foil and Teflon substrates. The accuracy and cost savings of the new method are presented for a typical $PM_{0.1}$ sampling network collecting samples every three days for a full year.

4.2 Method

4.2.1 PM sampling network

An ultrafine particle mass ($PM_{0.1}$) sampling network was operated over the time period August 2015 – July 2016 at three cities in California –Los Angeles, East Oakland and San Pablo. $PM_{0.1}$ samples were also collected in Fresno, California during the months of Jan, Feb, Apr, Jun and Jul of 2016. Locations of sites are shown in Figure 4.1. All the measurement sites were located at urban areas surrounded by traffic, commercial and residential neighborhood. Samples were collected at each site using two identical Mirco-orifice Uniform Deposit Impactors (MOUDIs) model 110R (MSP Corporation, Shoreview, MN, USA); one MOUDI was loaded with uncoated Teflon membranes filters (Teflo R2PJ047; Pall Corp., Port Washington, NY, USA) and the other was loaded with uncoated and pre-baked aluminum foil impaction substrates (Foil 0100-96-0573A-X; MSP Corp., Shoreview, MN, USA). MOUDIs were operated at a standard flow rate of 30 L/min with AIHL-design cyclones installed upstream to remove any particles with diameter greather than 1.8 μm since these particles have a greater probability of bouncing off uncoated impaction substrates. $PM_{0.1}$ samples were collected over three days on the final MOUDI stage that collects particles in the diameter range 0.056 – 0.1 μm. Substrates on stages 5 though 9 were changed monthly. Further details of the sampling network are discussed by [10, 15, 16].

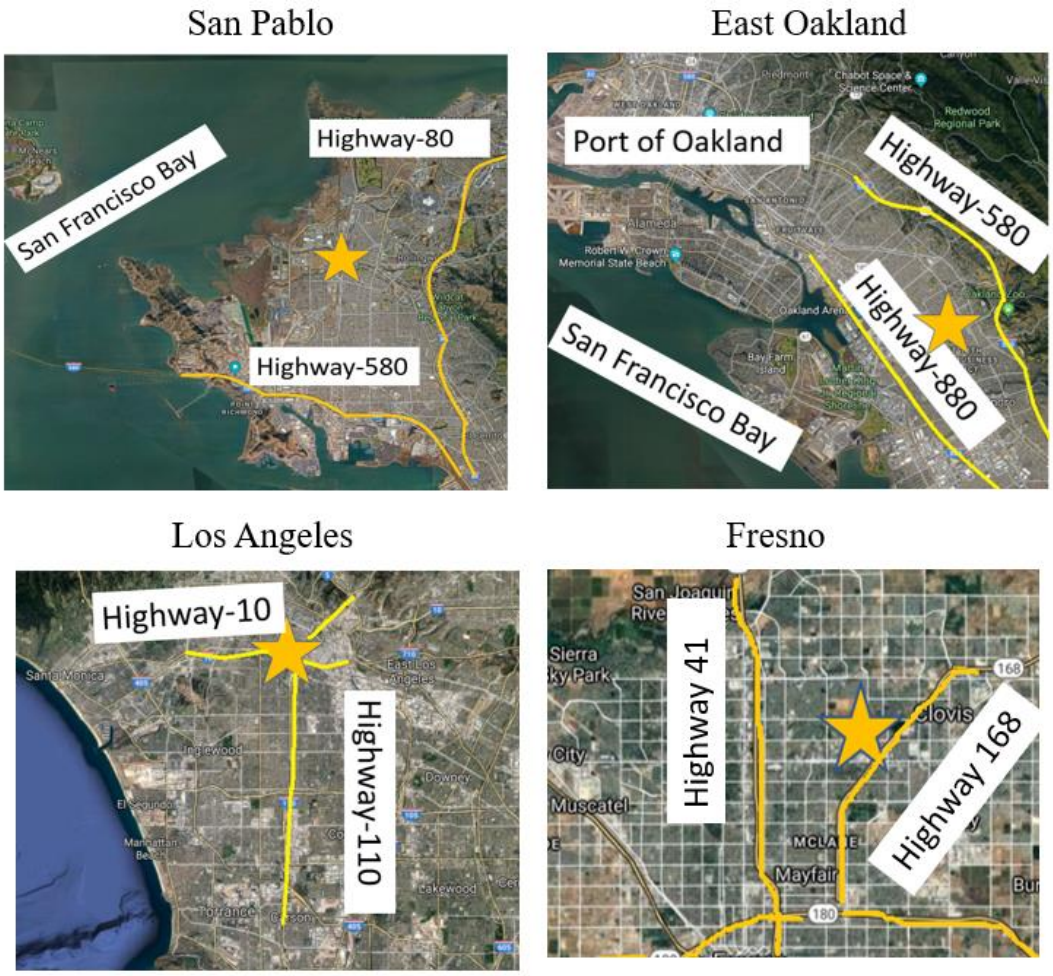

Figure 4.1. Maps of four sampling locations: San Pablo, East Oakland, Los Angeles, and Fresno.

4.2.2 Modified sample processing method

A 1.5 cm^2 portion of the $PM_{0.1}$ samples collected on aluminum foil substrates were analyzed for OC/EC content using a Sunset Laboratory EC/OC analyzer (10180 SW Nimbus Avenue, Suite J/5, Tigard, OR 97223-4341) following the National Institute for Occupational Safety and Health (NIOSH) protocol [20]. The remainder of the $PM_{0.1}$ foil samples were analyzed for molecular markers as part of a chemical mass balance (CMB) study [15]. $PM_{0.1}$ samples collected on Teflon filters were cut in half, extracted in a mixture of 25% 1N nitric acid and 75% acetone, concentrated under nitrogen evaporation, and analyzed for elements using Inductively Coupled Plasma Mass

Spectrometry (ICP-MS) [17]. $PM_{0.1}$ OC/EC concentratioand elemental concentrations have been analyzed for their weekly trends [16] and source contributions [10, 15] in Chapters 2 and 3 of this dissertation.

The current study aims to explore the feasibility of analyzing $PM_{0.1}$ elements from foil substrates so that a single MOUDI can be used at each location of the $PM_{0.1}$ sampling network. The extraction protocol for elements collected on foil substrates was modified into two steps to minimize prolonged contact between aluminum foil and nitric acid. In the modified protocol, foil substrates were first sonicated in 22.5 mL of pure acetone for 30 min. An additional 7.5 mL of 1N HNO_3 was then added to the mixture for a further 5 min of sonication. The extracted material was then decanted into storage vials pending ICP-MS analysis following the standard protocol [17]. This modified extraction procedure dissolves the organic matter in particles using acetone and keeps the elements in acidified solution without substantially disolving the foil collection substrate. Some minor amount of foil substrate was decanted into the final storage vials but this material did not appear to interfere with the ICP-MS analysis. The modified protocol was applied to monthly-average foil samples collected on stage 5 through 9, i.e. particulate matter in size ranges of 1 – 1.8 μm, 0.56 – 1 μm, 0.32 – 0.56 μm, 0.18 – 0.32 μm and 0.1 – 0.18 μm. The original protocol [17] was applied to Teflon samples collected on stage 5 through 9 as a comparison to the modified procedure.

4.2.3 Chemical analysis and size distribution

Thirty-six elements were quantified with ICP-MS - Li, Na, Mg, Al, Si, P, S, Cl, K, Ca, Ti, V, Cr, Mn, Fe, Co, Ni, Cu, Zn, Ga, As, Se, Br, Rb, Sr, Mo, Ag, Cd, Sn, Sb, Cs, Ba, Tl, Pb, Bi, and U. More than 30 Teflon blanks and foil blanks were treated along with samples. Method detection limits were calculated as the sum of blank average and 3 times of standard deviation of the blanks.

ICP-MS analysis precision was assessed by replicate analysis of 10% of total samples. All final values were blank subtracted and converted to air concentration in ng/m^3. A regression analysis was performed with 89 pairs of Teflon vs. foil from stage 5 through 9. Elements with Pearson's r value greater than 0.7 were chosen for further analysis.

A total of 19 groups covering the particle diameter range 0.10 – 1.8 μm, with each group containing one set of stage 5-9, were acquired for both Teflon and foil with a few missing due to handling errors. The averaged particle size distributions and size distribution by size and season are plotted and analyzed.

4.2.4 Foil PM0.1 simulation

Since $PM_{0.1}$ foil samples collected on MOUDI stage 10 were not available for elemental analysis in the current study, the regression of monthly foil vs Teflon on MOUDI stage 9 (particles in size range 0.1-0.18 μm; "quasi-ultrafine" particles) were used to represent the relationship of foil vs Teflon on stage 10 (ultrafine particles). Elements with R^2 greater than 0.6 in the stage 9 regression were selected for further analysis. Datasets describing simulated 3-day average foil $PM_{0.1}$ concentrations were generated based on measured 3-day average Teflon $PM_{0.1}$ concentrations using equation 4.1, where slopes and intercepts were derived from the stage 9 foil vs. Teflon regression. Since the predicted foil $PM_{0.1}$ element concentrations have inherent uncertainty that will influence the results of downstream source apportionment calcualtions, Monte Carlo simulations were used to estimate the effects of this uncertainty on the source apportionment results predicted by the Postive Matrix Factorization (PMF). Errors of predicted values were calculated by multiplying standard error term by randomly generated T-distribution deviates (Eq. 4.2 and Eq. 4.3). Thirty 3-day $PM_{0.1}$ foil datasets with random errors were generated using this approach for three sites: Los Angeles, East Oakland and San Pablo. The number of samples

collected at site Fresno was insufficient for a source apportionment study. These data were combined with measured $PM_{0.1}$ OC/EC data to form a complete dataset ready to use with PMF.

$$\text{predicted foil } PM_{0.1} = \text{measured Teflon } PM_{0.1} * \text{slope} + \text{intercept} + \text{random error} \quad \text{(Eq. 4.1)}$$

$$\text{random error} = \text{standard error} * \text{random } t_{\text{n-2}} \quad \text{(Eq. 4.2)}$$

where $t_{\text{n-2}}$ is randomly generated deviated from T-distribution with degree of freedom of n-2, and n is the number of (x,y) pairs for regression.

$$\text{standard error} = \sigma\sqrt{1 + \frac{1}{n} + \frac{(x_0 - \bar{x})^2}{S_{xx}}} \quad \text{(Eq. 4.3)}$$

$$\text{where } \sigma = \frac{SS_T - slope \cdot S_{xy}}{n-2}$$

$$SS_T = \sum_{i=0}^{n} y_i^2 - \text{n} \cdot \bar{y}^2$$

$$S_{xx} = \sum_{i=1}^{n} x_i^2 - \frac{(\sum_{i=0}^{n} x_i)^2}{n}$$

$$S_{xy} = \sum_{i=1}^{n} x_i y_i - \frac{(\sum_{i=1}^{n} x_i)(\sum_{i=1}^{n} y_i)}{n}$$

where x and y are measured Teflon and foil values, repectively.

4.2.5 Positive matrix factorization comparison

EPA PMF 5.0 is a factor analysis model that attributes the measured species mass $x_{i,j}$ to factor profiles $f_{k,j}$, assuming factor profiles are constant through time. The amount of mass contributed by each factor (source) to concentrations in each individual sample is represented by $g_{i,k}$, as shown in Eq.4.4, where p is pre-determined number of factors and e_{ij} is the residual for each species j in

sample *i*. The factor(source) contributions $g_{i,k}$ and factor profiles $f_{k,j}$ are calculated by minimizing the objective function Q (Eq.4.5), where μ_{ij} represents the uncertainty associated with species *j* in sample *i*.

$$x_{ij} = \sum_{k=1}^{p} g_{ik} f_{kj} + e_{ij} \quad \text{(Eq.4.4)}$$

$$Q = \sum_{i=1}^{n} \sum_{j=1}^{m} \left[\frac{x_{ij} - \sum_{k=1}^{p} g_{ik} f_{kj}}{u_{ij}} \right]^2 \quad \text{(Eq.4.5)}$$

In the current study, the uncertainty for each species concentration in the PMF analysis was calculated based on the measurement method detection limit (MDL) and error fraction when the concentration was greater than the MDL (Eq.4.6); if the concentration was less than the MDL, the uncertainty was calculated as a fixed fraction of the MDL (Eq.4.7).

$$\text{Unc} = \sqrt{(\text{Error Fraction} \times \text{concentrations})^2 + (0.5 \times MDL)^2} \quad \text{(Eq.4.6)}$$

$$Unc = \frac{5}{6} \times MDL \quad \text{(Eq.4.7)}$$

The signal to noise ratio (S/N) was calculated to quantify the quality of the input data. Species with S/N > 1 were categorized to Strong species and species with 0.5 < S/N < 1 were categorized to Weak species. The uncertainty for Weak species was increased by a factor of 3 to reduce their influence on the model fit. Species with S/N < 0.5 were categorized to Bad and removed from the analysis [21].

A range of PMF solutions based on five to nine important sources (*p*) were examined in the current study. The optimal solution was determined considering Q values, the results of model fit, and interpretability of the resulting factor profiles and time series [22]. Bootstrap and displacement

runs were performed to evaluate the stability of the solution. Rotation with different Fpeak strengths of +0.1, -0.1, +0.2, and -0.2 were run, because Fpeak values out of this range would lead to greater than 5% of Q value increase compared to base model. A standard of at least 40/50 of bootstrap remapping for r-value = 0.8 was established to select a robust solution. Any base model solution or rotation solution that passes this standard was saved. Results of the PMF runs with 30 foil $PM_{0.1}$ datasets were summarized and compared with the those from Teflon $PM_{0.1}$ at East Oakland from study Xue *et al*. 2020[10].

4.3 Results and Discussion

4.3.1 Stage 5 through 9 regression and size distribution

More than 30 Teflon and foil blanks were treated with traditional and modified extraction protocols, respectively, and analyzed by ICP-MS. Table 4.1 shows the averaged concentrations of measured elements on the blank samples and the corresponding MDLs. The averaged concentration and MDL of element Al is three orders of magnitude higher on Al foil blanks than on Teflon blanks, which is expected due to the partial dissolution of foil subtrates during the extraction procedure. Among the other 35 measured elements, 23 have blank concentrations and MDLs that are on the same order of magnitude for foil and Teflon substrates. Ti, Mn, Fe, Sn, Tl, Pb, and U have blank levels or MDLs that are an order of magnitude higher on foil than Teflon, and P, Cl, Ni, As, Se, Cd and Cs have blank concentrations or MDLs that are an order of magnitude higher on Teflon than foil. The fact that most of the elements exhibit similar blank concentrations and MDLs on both types of substrates increases confidence that the new extraction protocol using foil substrates may be feasible.

Table 4.1. Averaged elements concentrations and 3 times of standard deviation of more than 30 method blanks of foil and Teflon substrates. MDL = blank average + 3*std dev of blanks. All values in unit ng/filter

Element	blank avg		3*std dev of blank		MDL	
	foil	Teflon	foil	Teflon	foil	Teflon
Li	4.51E-01	7.15E-01	4.31E-01	1.29E-01	8.82E-01	8.45E-01
Na	3.60E+01	1.92E+02	2.64E+02	1.69E+03	3.00E+02	1.88E+03
Mg	2.77E+01	8.38E+00	4.69E+01	1.93E+01	7.46E+01	2.77E+01
Al	9.64E+04	4.86E+01	4.49E+05	2.84E+02	5.46E+05	3.32E+02
Si	6.11E+03	1.17E+04	4.97E+03	2.78E+04	1.11E+04	3.95E+04
P	1.20E+01	6.21E+02	8.03E+01	2.35E+02	9.23E+01	8.57E+02
S	1.13E+03	2.66E+03	2.57E+03	8.71E+02	3.70E+03	3.54E+03
Cl	7.14E+01	3.34E+03	4.63E+02	2.40E+03	5.35E+02	5.74E+03
K	2.77E+01	6.67E+01	1.86E+02	1.14E+02	2.13E+02	1.81E+02
Ca	2.70E+02	9.85E+01	1.68E+02	1.37E+02	4.38E+02	2.35E+02
Ti	6.29E+00	4.77E-01	2.93E+01	4.46E-01	3.56E+01	9.23E-01
V	1.49E+00	3.20E-01	1.23E+00	2.86E-01	2.71E+00	6.05E-01
Cr	1.30E+01	2.62E+01	1.30E+01	3.28E+01	2.61E+01	5.90E+01
Mn	1.84E+00	3.82E-01	2.58E+01	1.68E+00	2.76E+01	2.07E+00
Fe	2.16E+02	5.13E+01	4.53E+03	2.66E+02	4.75E+03	3.18E+02
Co	1.11E-01	1.03E-01	1.42E+00	3.78E-01	1.53E+00	4.82E-01
Ni	5.00E+00	2.69E+01	1.84E+01	1.06E+03	2.34E+01	1.09E+03
Cu	3.21E+01	6.96E+01	5.59E+01	1.18E+02	8.80E+01	1.88E+02
Zn	1.87E+01	5.50E+01	4.74E+01	8.81E+01	6.61E+01	1.43E+02
Ga	3.48E-01	1.55E-01	2.54E+00	3.15E-01	2.89E+00	4.70E-01
As	1.73E-02	1.85E-01	8.83E-02	4.62E-01	1.06E-01	6.47E-01
Se	0.00E+00	1.86E-01	6.34E-02	6.54E-01	6.34E-02	8.40E-01
Br	2.95E+00	1.46E+00	8.66E+00	9.72E-01	1.16E+01	2.44E+00
Rb	2.88E-02	9.50E-02	2.66E-01	8.63E-02	2.95E-01	1.81E-01
Sr	2.74E-01	2.27E-01	4.19E-01	9.61E-01	6.93E-01	1.19E+00
Mo	0.00E+00	6.41E-01	6.05E-01	4.98E-01	6.05E-01	1.14E+00
Ag	4.64E-01	1.48E-01	1.52E+00	4.72E-01	1.98E+00	6.20E-01
Cd	3.45E-02	1.88E-01	6.29E-02	6.87E-01	9.75E-02	8.75E-01
Sn	1.94E+00	4.52E-02	4.04E+00	1.83E+00	5.98E+00	1.87E+00
Sb	6.71E-02	8.85E-02	5.24E-01	1.96E-01	5.91E-01	2.84E-01
Cs	1.38E-02	1.28E-02	9.86E-03	7.43E-01	2.36E-02	7.56E-01
Ba	0.00E+00	0.00E+00	0.00E+00	4.69E+00	0.00E+00	4.69E+00
Tl	2.48E+00	1.55E-02	6.17E+00	1.30E+00	8.66E+00	1.32E+00
Pb	2.80E+01	1.84E+00	7.48E+01	1.05E+01	1.03E+02	1.23E+01
Bi	9.08E+01	2.14E+02	1.99E+02	8.64E+02	2.90E+02	1.08E+03
U	2.97E-01	6.92E-03	2.30E+00	1.56E+00	2.60E+00	1.56E+00

Figure 4.2 shows the regression analysis results for 89 pairs of foil vs. Teflon elemental concentrations on MOUDI stages 5-9. Eighteen elements (Li, Na, Mg, K, Ti, V, Ga, As, Se, Br,

Rb, Sr, Mo, Cd, Sn, Sb, Ba and Pb) had Pearson's r value greater than 0.7 .The good correlation for these elements builds confidence in the new method for the size range 0.1-1.8 μm, thus these samples were chosen to further test the foil method on $PM_{0.1}$. Most of Cd data points fall close to zeros in the plot because there were a few data points with high concentrations. These data points should represent some intermittent emission of Cd and so they were not treated as outliers. Analysis of low values of Cd also showed good agreement between foil vs Teflon.

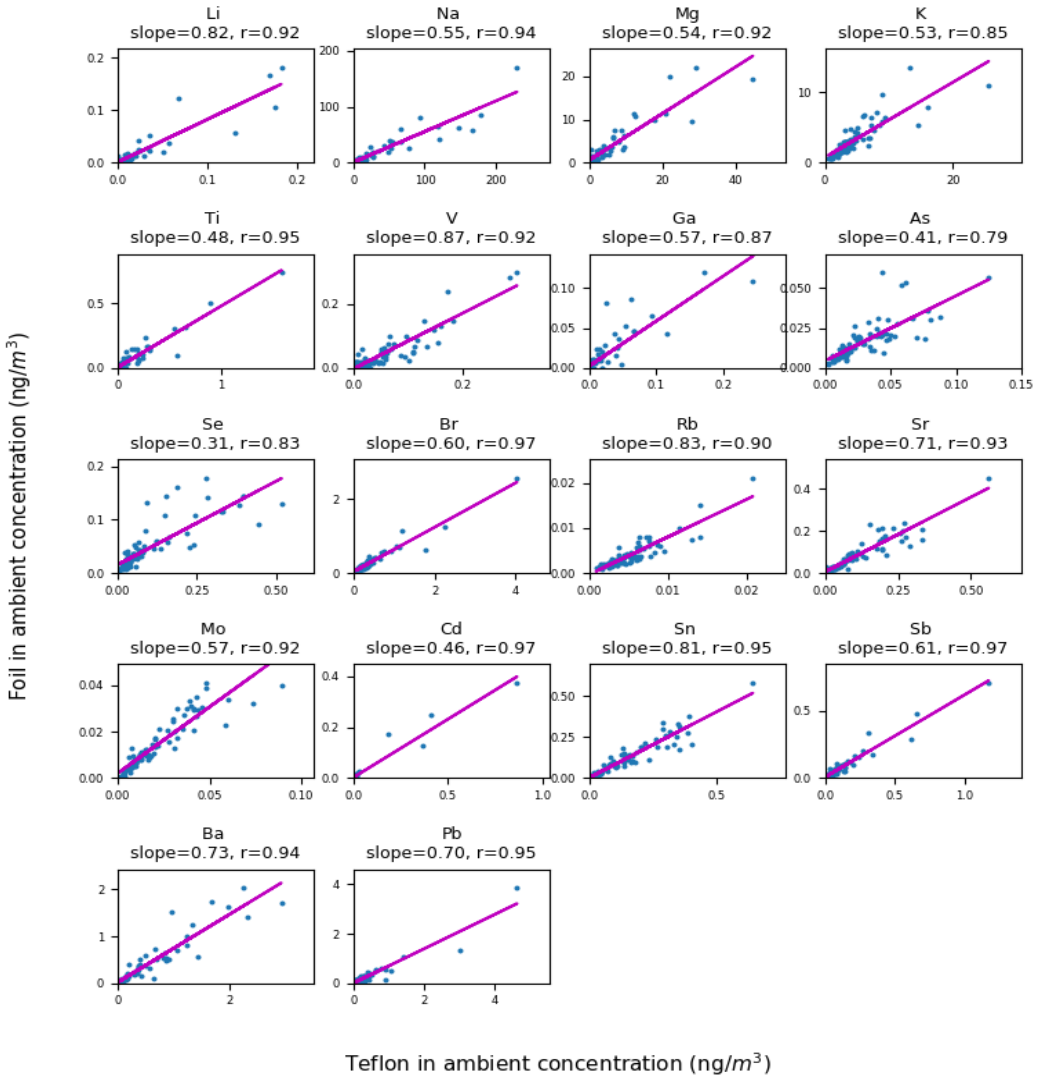

Figure 4.2. Teflon vs. foil air concentration comparison in size range 0.1-1.8 µm, corresponding to stage 5 through 9 of MOUDI. A total of 89 pairs of samples analyzed.

The slopes of the regression lines shown in Figure 4.2 range from 0.31 to 0.87, indicating that the foil substrates collected lower elemental concentrations than the Teflon substrates. This trend may be related to particle collecting efficiency on different substrate materials. In the current study, Teflon and foil substrates were loaded on two co-located MOUDIs on stages 5 through 10. Particles smaller than 0.056 µm or larger particles that bounce off upstream impaction substrates are collected on an after-filter below stage 10. The elements collected on the after-filter

downstream of foil substrates were 4.3 to 62.6 times higher than the Teflon after-filter during a test experiment, with an average enahancement of 16.7. The increased concentration of elements on the after filter downstream of the foil MOUDI suggests that a greater fraction of particles bounce off the foil MOUDI impaction stages 5 through 10 compared to the Teflon MOUDI. Particle bounce on cascade impaction stages has been reported in multiple previous studies, with mitigation strategies usually involving substrate coating by grease/oil [23, 24]. The current study did not coat substrates to minimize potential interference in the downstream chemical analysis. A previous study found that a greater fraction of particles with diameter between 0.1 -2.5 μm bounced off uncoated foil substrates than uncoated Teflon substrates[25]. Bounce was more likely to happen on uncoated foil substrates as relative humidity (RH) decreased compared to uncoated Teflon substrates; uncoated foil and Teflon could sample $PM_{0.1}$ concentrations accurately at RH greater than 75% and 65%, respectively [25]. This result is consistent with the trend of enhanced element concentrations on the after-filter and reduced elements measured on foil substrates in the current study.

Another explanation for slope < 1 is extraction efficiency of the modified protocol. Sonication with HNO_3 + acetone mixture was reduced from 30 min to 5 min to prevent excessive breakage of foil samples, which may interfere with ICP-MS operation. However, sample contact with HNO_3 in resting state was usually ~ 30 min to allow for experimental operations, which should guarantee full interaction between particles and acid, thus the reduced extraction efficiency should be a minor factor.

Figure 4.3 shows size distributions of selected elements averaged across all sites and seasons. Figures 4.4-4.11 show averaged size distributions of selected elements in warm and cold seasons at individual sites. Sodium (Na) and magnesium (Mg) exhibit consistent size distributions that

peak in the size range 1-1.8 μm (or larger) across all sites and seasons, which is consistent with the notion that crustal dust and sea salt account for the majority of atmosphere Na and Mg [26, 27]. Annual-average size distributions for potassium (K) and rubidium (Rb) do not have a clear lognormal size distributions shape because of seasonal variation. K and Rb samples collected in winter show a clear peak between 0.18 and 0.32 μm, representing emissions from biomass burning in cold weather [10, 18, 28]. Summer distributions for K and Rb peak in the size range 1-1.8 μm (or larger), resembling the size distribution for Na and Mg that originate from crustal sources such as sea salt and road dust. Other elements, including selenium (Se), bromine (Br), molybdenum (Mo), tin (Sn), antimony (Sb) and lead (Pb), also display different size distributions in summer and winter, indicating change of dominant sources in different seasons. For example, the mode in 0.18-0.32 μm for Br and Pb in winter months could be related to biomass burning [29, 30]. Vanadium (V) shows a peak in the size range 0.18-0.32 μm at site San Pablo and East Oakland which is very likely the contribution from marine vessel fuel combustion [31]. Barium (Ba) and titanium (Ti) constantly peak at 1-1.8 μm (or larger), consistent with findings that brake wear dust contains Ba and Ti [32, 33].

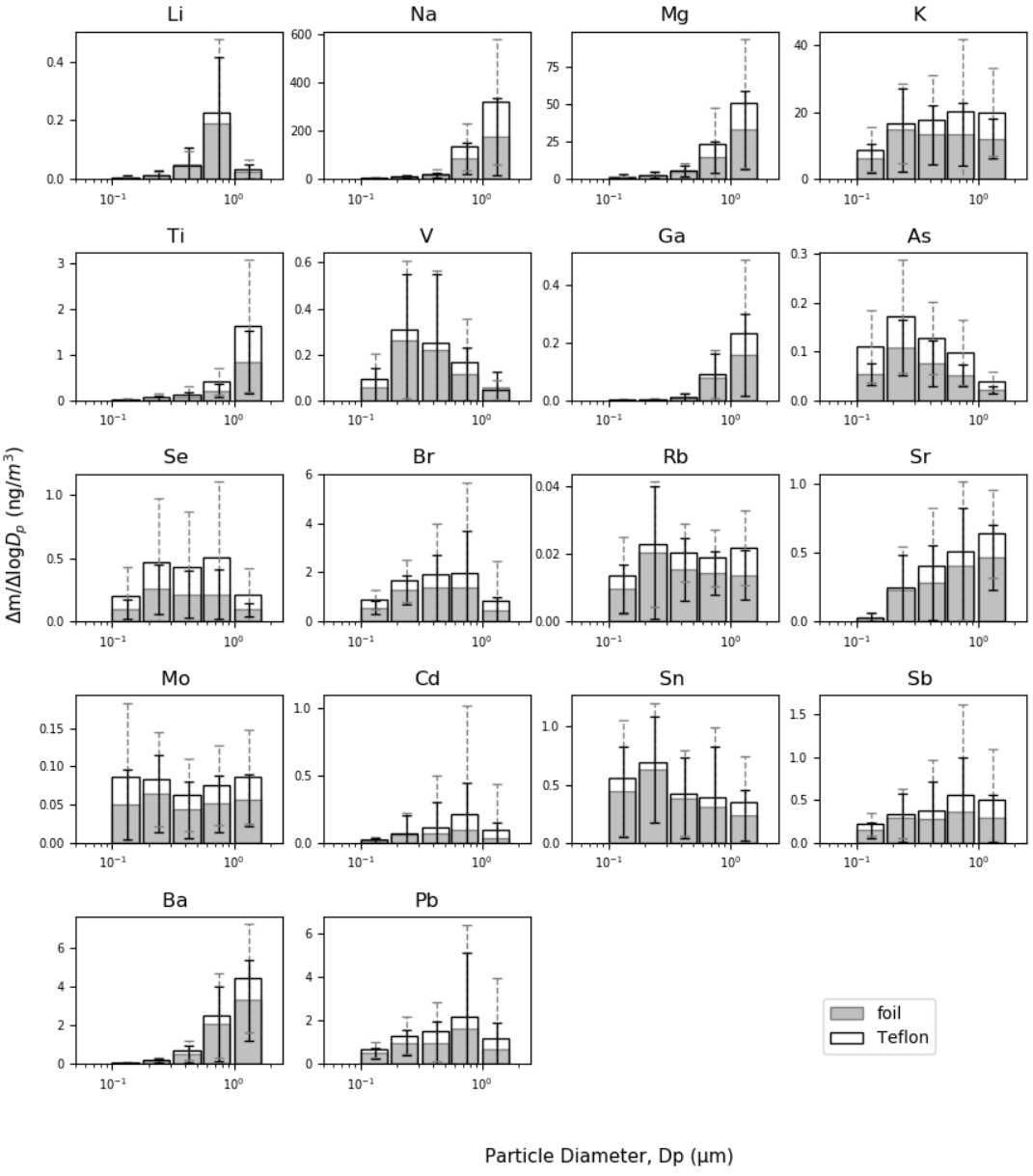

Figure 4.3. Averaged Teflon vs. foil size distribution in size range 0.1-1.8 μm, corresponding to stage 5 through 9 of MOUDI. Solid error bar represents standard deviation of foil, and dashed error bar represents standard deviation of Teflon.

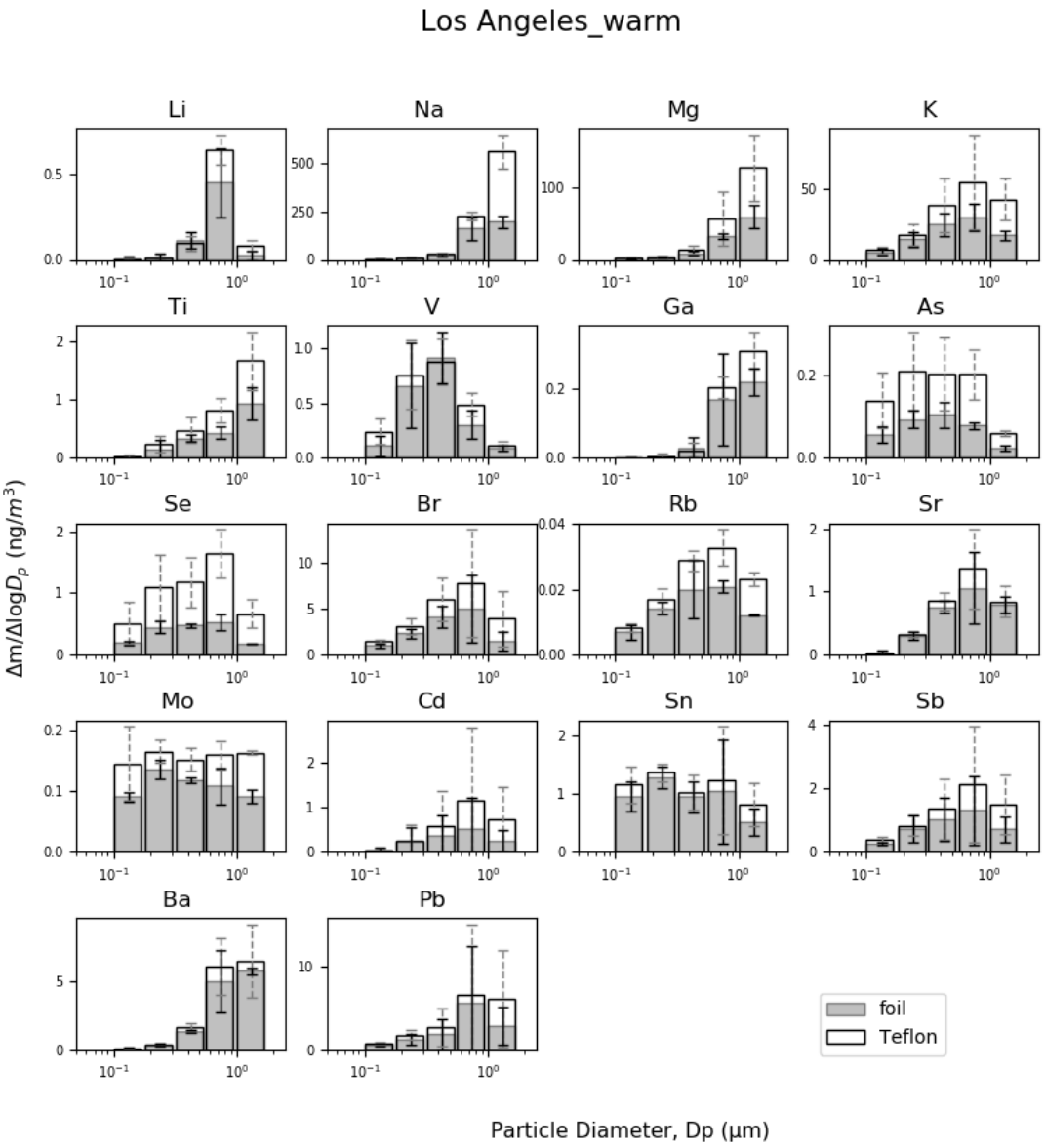

Figure 4.4. Averaged Teflon vs. foil size distribution in size range 0.1-1.8 μm in warm season (Jul and Aug, 2015) at Los Angeles, corresponding to stage 5 through 9 of MOUDI. Solid error bar represents standard deviation of foil, and dashed error bar represents standard deviation of Teflon.

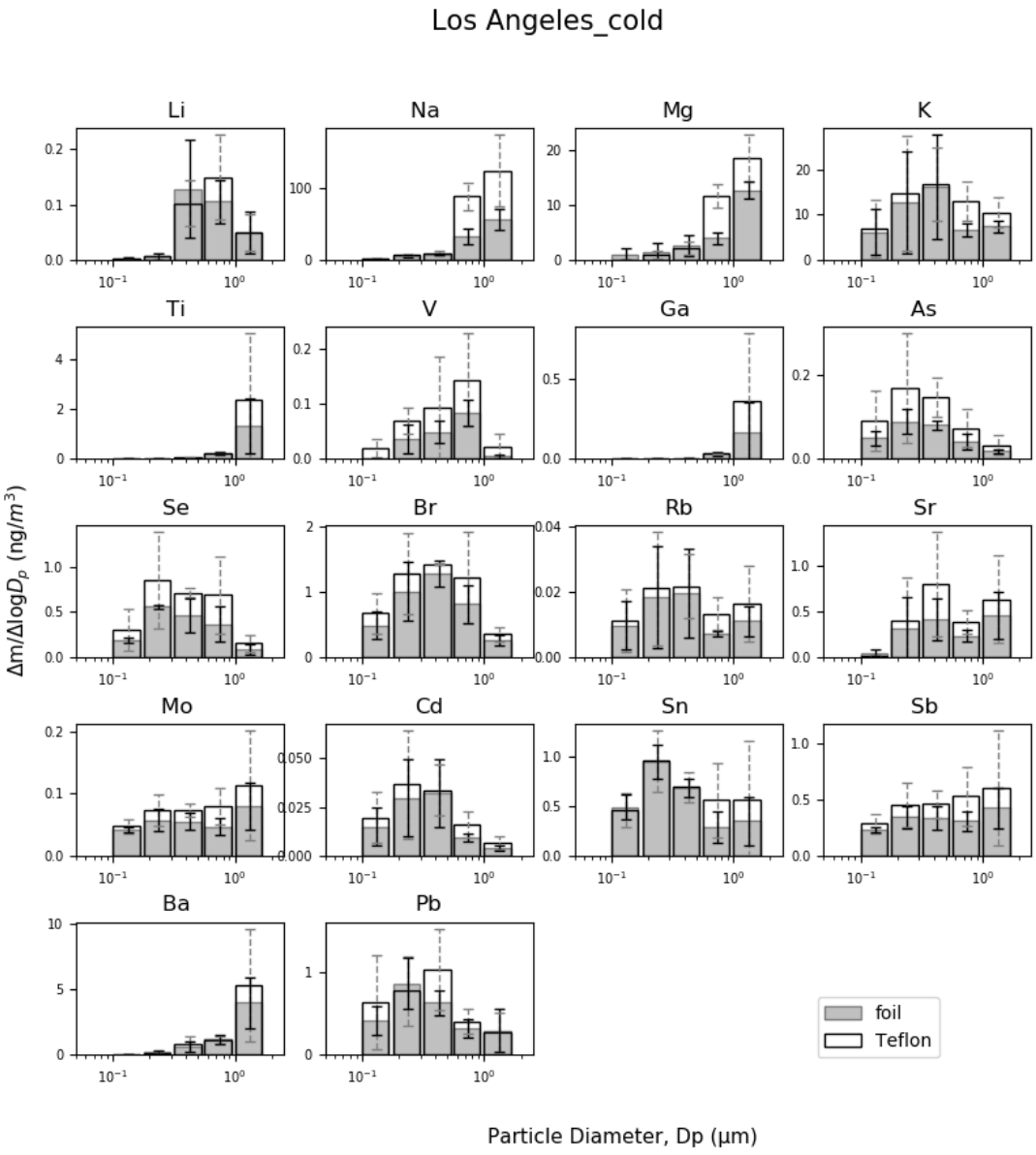

Figure 4.5. Averaged Teflon vs. foil size distribution in size range 0.1-1.8 μm in cold season (Oct and Nov, 2015) at Los Angeles, corresponding to stage 5 through 9 of MOUDI. Solid error bar represents standard deviation of foil, and dashed error bar represents standard deviation of Teflon.

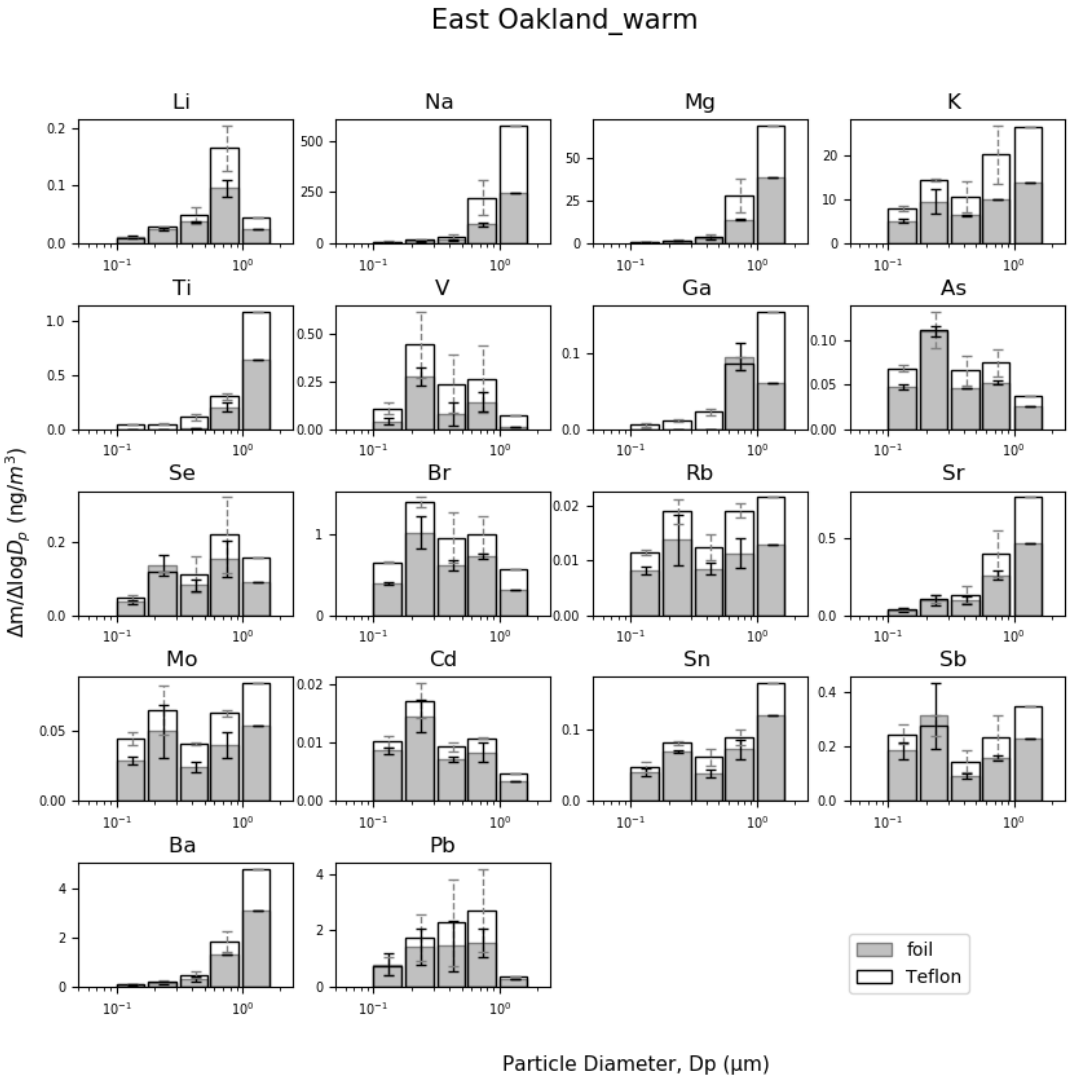

Figure 4.6. Averaged Teflon vs. foil size distribution in size range 0.1-1.8 μm in warm season (May and Jun, 2016) at East Oakland, corresponding to stage 5 through 9 of MOUDI. Solid error bar represents standard deviation of foil, and dashed error bar represents standard deviation of Teflon.

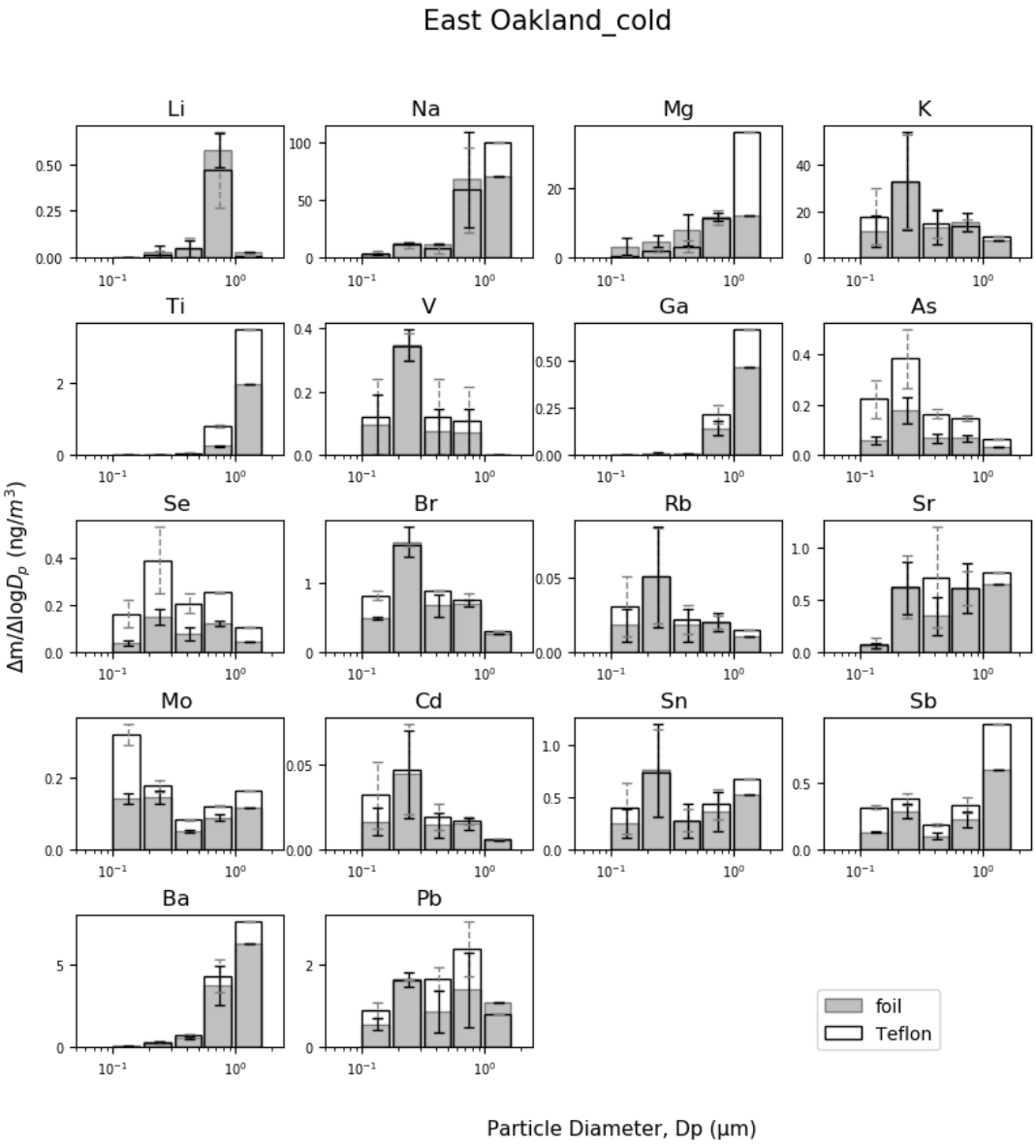

Figure 4.7. Averaged Teflon vs. foil size distribution in size range 0.1-1.8 μm in cold season (Oct and Nov, 2015) at East Oakland, corresponding to stage 5 through 9 of MOUDI. Solid error bar represents standard deviation of foil, and dashed error bar represents standard deviation of Teflon.

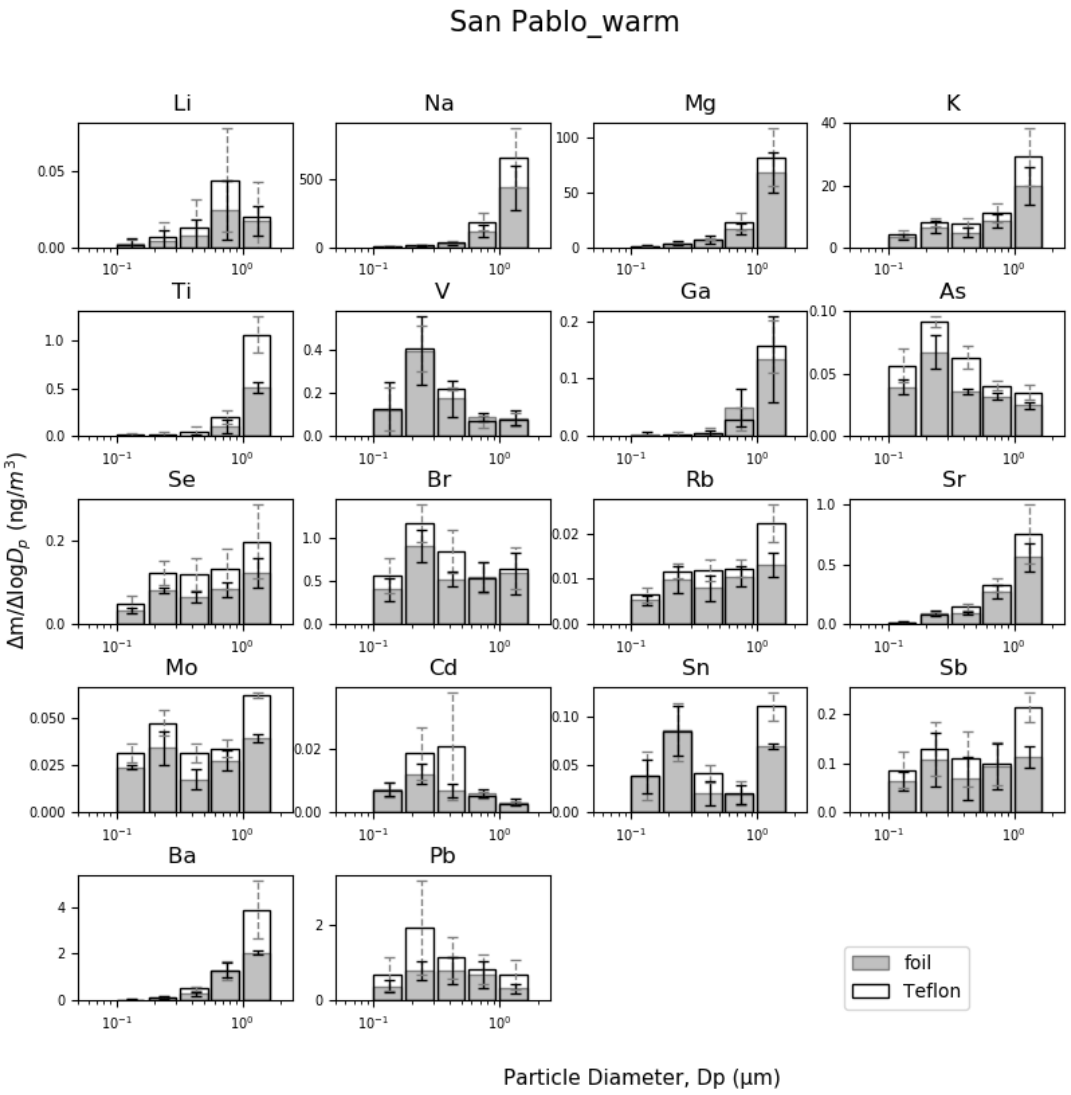

Figure 4.8. Averaged Teflon vs. foil size distribution in size range 0.1-1.8 μm in warm season (May and Jun, 2016),at San Pablo corresponding to stage 5 through 9 of MOUDI. Solid error bar represents standard deviation of foil, and dashed error bar represents standard deviation of Teflon.

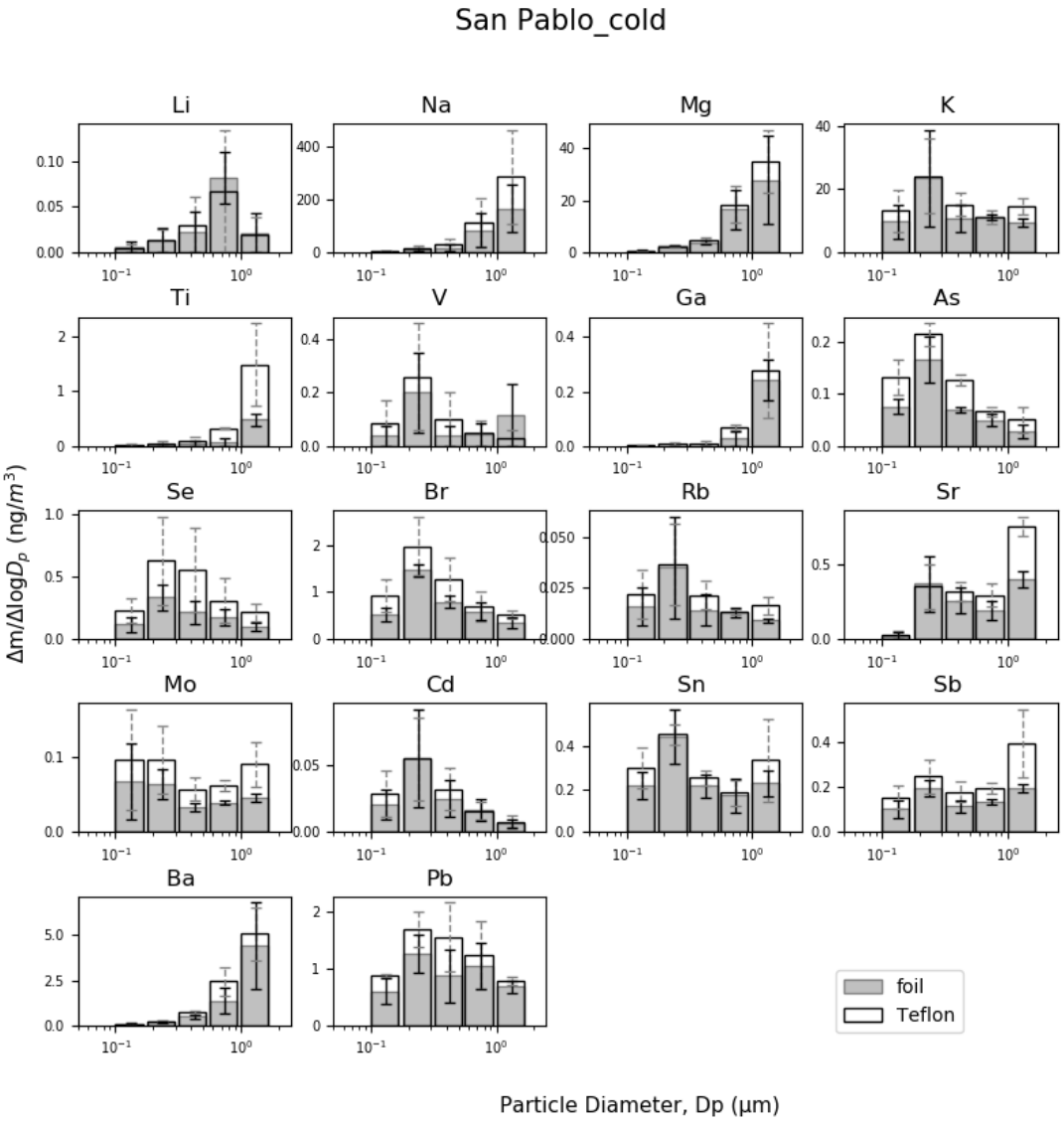

Figure 4.9. Averaged Teflon vs. foil size distribution in size range 0.1-1.8 μm in cold season (Oct and Nov, 2015) at San Pablo, corresponding to stage 5 through 9 of MOUDI. Solid error bar represents standard deviation of foil, and dashed error bar represents standard deviation of Teflon.

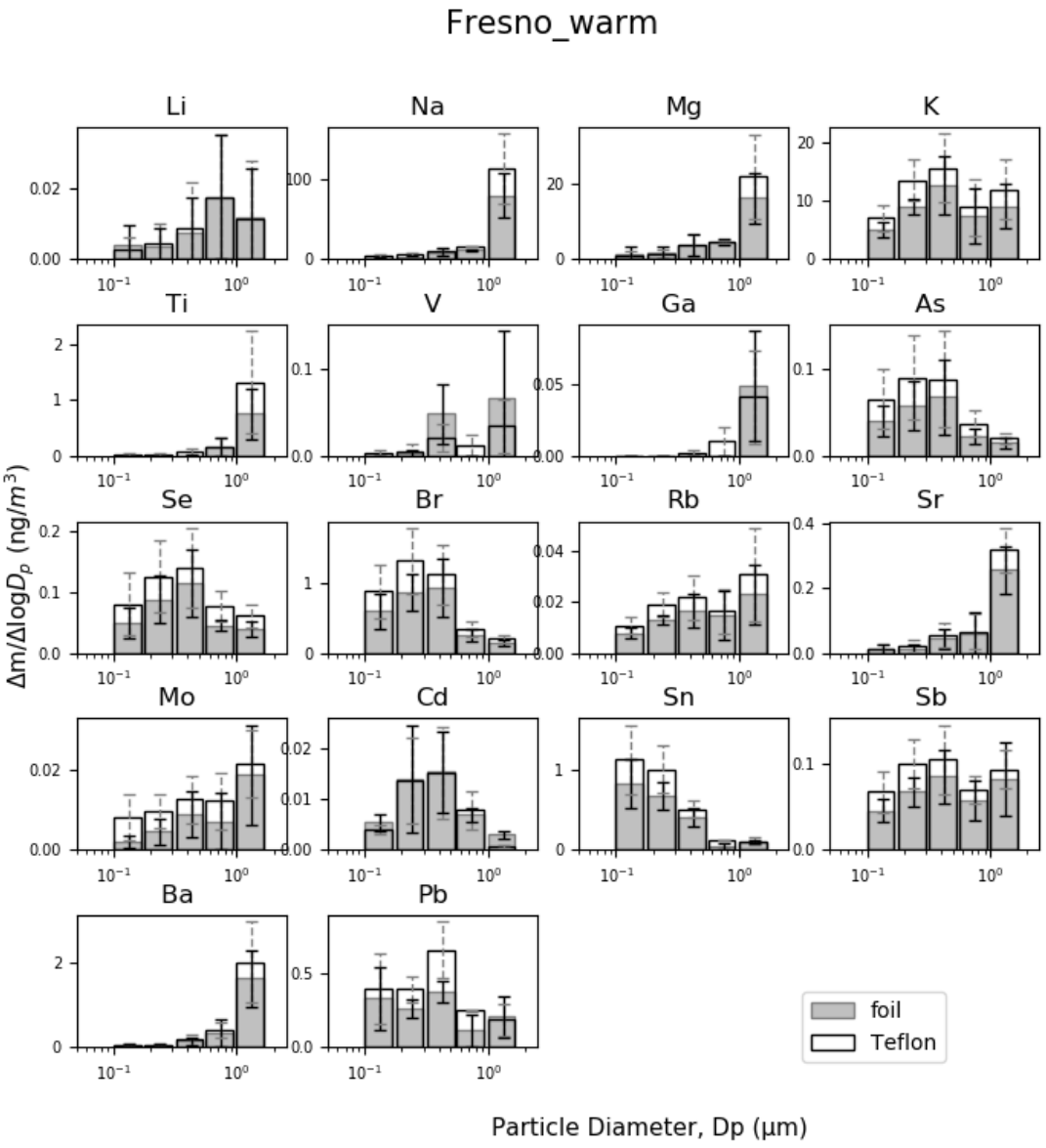

Figure 4.10. Averaged Teflon vs. foil size distribution in size range 0.1-1.8 μm in warm season (Apr and Jun, 2016) at Fresno, corresponding to stage 5 through 9 of MOUDI. Solid error bar represents standard deviation of foil, and dashed error bar represents standard deviation of Teflon.

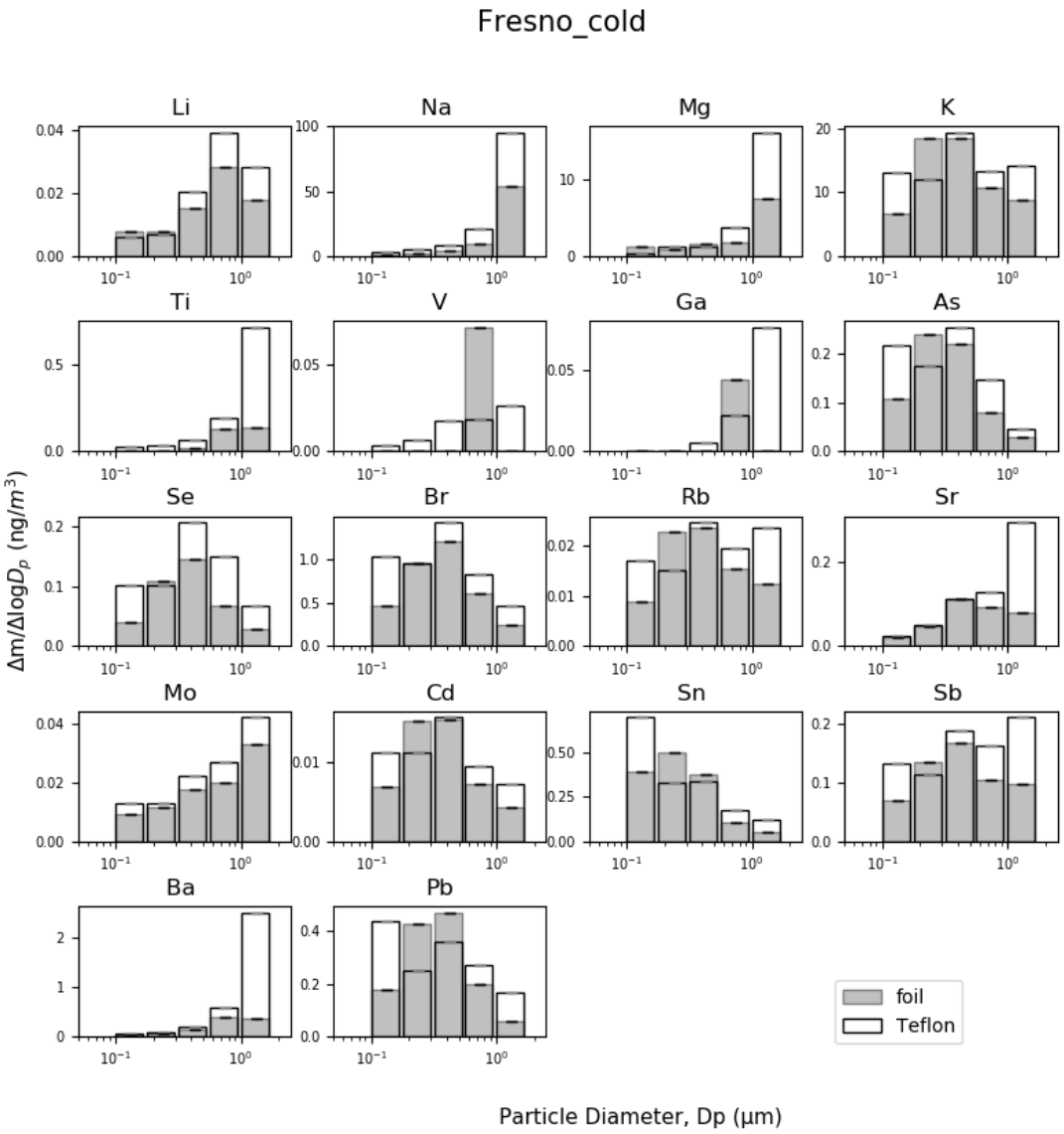

Figure 4.11. Averaged Teflon vs. foil size distribution in size range 0.1-1.8 μm in cold season at Fresno (Feb, 2016), corresponding to stage 5 through 9 of MOUDI. Solid error bar represents standard deviation of foil, and dashed error bar represents standard deviation of Teflon.

4.3.2 Stage 9 regression and $PM_{0.1}$ simulation

Regression analysis was carried out between element concentrations measured on MOUDI stage 9 Teflon and foil samples corresponding to particles with diameters between 0.1 μm to 0.18 μm. These "quasi-ultrafine" samples were selected for analysis because the MOUDI stage 10 foil samples were not available in the current study. Figure 4.12 shows the scatter plots for measured stage 9 foil vs Teflon and Table 4.2 shows the slope, intercept, and R^2 from regression analysis. Elements Li, K, V, Br, Rb, Mo, Cd, Sn, Sb, and Ba were selected to be used in PMF analysis because of their reasonably good R^2 values (>0.6).

The regression relationships summarized in Table 4.2 were used to simulate thirty sets of MOUDI stage 10 foil results for the 10 chosen elements (Li, K, V, Br, Rb, Mo, Cd, Sn, Sb, and Ba) during the study time period. Each set of simulated MOUDI stage 10 foil results used the corresponding MOUDI stage 10 Teflon measurement as the independent variable. MOUDI stage 10 foil concentrations were predicted using the regression equation summarized in Equations 4.1-4.3 combined with a random error term based on the standard errors in that regression equation.

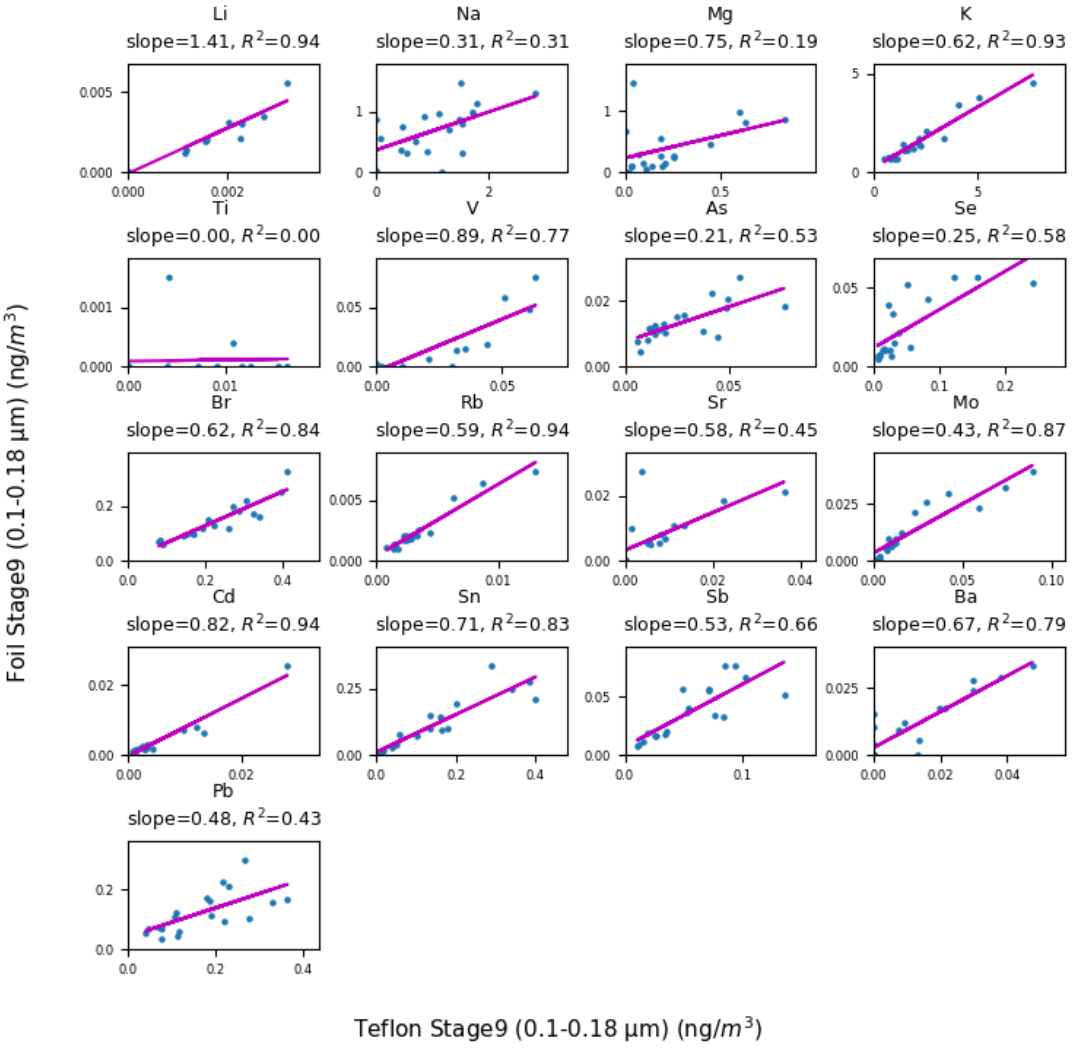

Figure 4.12. Regression of monthly stage 9 (0.1 – 0.18 µm) Teflon vs. foil.

Table 4.2. Regression results for foil vs Teflon based on monthly stage 9 filter sampling. Foil is the dependent variable and Teflon is the independent variable. The slope for elements with R squared greater than 0.6 are marked bold and selected for further PMF runs with simulated $PM_{0.1}$ dataset.

Elements	slope	intercept	R^2
Li	**1.41**	**-7.25E-05**	**0.94**
Na	0.31	3.69E-01	0.31
Mg	0.75	2.31E-01	0.19

K	**0.62**	**2.17E-01**	**0.93**
Ti	0	9.00E-05	0
V	**0.89**	**-4.19E-03**	**0.77**
As	0.21	7.60E-03	0.53
Se	0.25	1.17E-02	0.58
Br	**0.62**	**4.46E-03**	**0.84**
Rb	**0.59**	**4.13E-04**	**0.94**
Sr	0.58	3.26E-03	0.45
Mo	**0.43**	**3.38E-03**	**0.87**
Cd	**0.82**	**-2.25E-04**	**0.94**
Sn	**0.71**	**1.19E-02**	**0.83**
Sb	**0.53**	**7.30E-03**	**0.66**
Ba	**0.67**	**2.74E-03**	**0.79**
Pb	0.48	4.31E-02	0.43

4.3.3 PMF results comparison

Simulated foil $PM_{0.1}$ datasets were combined with measured foil $PM_{0.1}$ OC and EC data to form a complete dataset for PMF. Thirty datasets including random errors for the elements were analyzed with PMF. The base model and rotation solutions that have Bootstrap results greater than 40/50 were summarized for comparison.

PMF input settings and main diagnostics for three sites are shown in Table 4.3-4.5. Since all 30 solutions at each location have very similar diagnostic values, only one solution is listed as an example. The settings and diagnostics are also listed for the reference Teflon PMF solution which contains $PM_{0.1}$ OC/EC data from foil samples and elements data from Teflon samples [10]. This reference solution will hereafter be referred to as "foil+Teflon". The Strong Species elements in the foil+Teflon PMF solution (K, V, Br, Rb, Sn, and Sb) are all preserved in the foil PMF runs, because these elements show good correlation for foil vs Teflon in both stage 5 through 9 measured data and in stage 9 measured data. These Strong Species will also serve as tracers for source identification. Qtrue measures the goodness-of-fit parameter for all data points in the PMF model,

while Qrobust measures the goodness-of-fit excluding data points not fit by the model. Qrobust and Qtrue values for foil PMF are lower than those for foil+Teflon PMF because there are fewer elements in Weak Species, leading to less total difference between predicted and measured values. The small difference between Qrobust and Qtrue reflects the fact that most of the data points are well-predicted by both solutions. The R^2 values of 0.93-0.95 for $PM_{0.1}$ mass in foil PMF solution indicates that the resolved sources can effectively reproduce the measured concentrations. The equally good results for foil and foil+Teflon in Displacement and Bootstrap tests show that foil solutions are as robust and stable as foil+Teflon solutions at all three sites.

Table 4.3. Input and diagnostics of PMF runs foil PM0.1 dataset and Teflon PM0.1 dataset at site Los Angeles. Foil PM0.1 dataset contains OC and EC data measured on foil samples and elements data simulated for foil samples. Foil results are from simulated dataset #9, Fpeak = 0.1. Teflon $PM_{0.1}$ dataset contains OC and EC measured on foil samples and elements measured on Teflon samples.

Input and Diagnostic	Foil	Teflon
strong species	OC2-3, EC2-3, K, V, Br, Rb, Sn, and Sb	OC2-3, EC2-3, K, V, Br, Rb, Sn and Sb
weak species	OC1, OC4, EC1, EC4, EC6, Li, Sr, Mo, Cd	OC1, OC4, EC1, EC4, Li, Na, Mg, Ca, Mn, Co, Zn, Ga, As, Se, Sr, Mo, Ag, Cd, and Pb
number of factors	7	7
Qrobust	1109	2438
Qtrue	1110	2512
Slope for total $PM_{0.1}$ mass	0.98	1.02
R^2 for total $PM_{0.1}$ mass	0.94	0.96
DISP drop of Q	0	-0.098
DISP swapping	0	0
Bootstrap mapping, for Min Corr R=0.8	50/50 for all factors	100% for all factors

Table 4.4. Input and diagnostics of PMF runs foil PM0.1 dataset and Teflon PM0.1 dataset at site East Oakland. Foil PM0.1 dataset contains OC and EC data measured on foil samples and elements data simulated for foil samples. Foil results are from simulated dataset #26, Fpeak = -0.1. Teflon $PM_{0.1}$ dataset contains OC and EC measured on foil samples and elements measured on Teflon samples.

Input and Diagnostic	Foil	Teflon
strong species	OC2-3, EC2-3, K, V, Br, Rb, Sn, and Sb	OC2-3, EC2-3, K, V, Br, Rb, Sn, and Sb
weak species	OC1, OC4, EC1, EC4, EC6, Li, Sr, Mo, Cd	OC1, OC4, EC1, EC4, Li, Na, Mg, Ca, Cr, Mn, Zn, Ga, As, Se, Sr, Mo, Ag, and Pb
number of factors	7	7
Qrobust	1679	2012
Qtrue	1710	2106
Slope for total $PM_{0.1}$ mass	0.91	0.94
R^2 for total $PM_{0.1}$ mass	0.93	0.94
DISP drop of Q	0	0
DISP swapping	0	0
Bootstrap mapping, for Min Corr R=0.8	50/50 for 6 factors, 48/50 for the other factor	50/50 for 5 factors, and 49/50 for the other 2 factors

Table 4.5. Input and diagnostics of PMF runs foil PM0.1 dataset and Teflon PM0.1 dataset at site San Pablo. Foil $PM_{0.1}$ dataset contains OC and EC data measured on foil samples and elements data simulated for foil samples. Foil results are from simulated dataset #26, Fpeak = -0.1. Teflon PM0.1 dataset contains OC and EC measured on foil samples and elements measured on Teflon samples.

Input and Diagnostic	Foil	Teflon
strong species	OC2-4, EC2-3, K, V, Br, Rb, Sn, and Sb	OC2-4, EC2-3, K, V, Br, Rb, Sn, and Sb
weak species	OC1, EC1, EC4, EC6, Li, Sr, Mo, Cd	OC1, EC1, EC4, Li, Na, Mg, Ca, Cr, Mn, Co, Zn, Ga, As, Se, Sr, Mo, Ag, Cd, Tl, Pb, and U
number of factors	7	7
Qrobust	1288	2178

Qtrue	1295	2238
Slope for total $PM_{0.1}$ mass	0.89	0.94
R^2 for total $PM_{0.1}$ mass	0.95	0.96
DISP drop of Q	0	0
DISP swapping	0	0
Bootstrap mapping, for Min Corr R=0.8	50/50 for all factors	100% for 5 factors, and 96%, 99%

Seven factors were resolved for all the 30 foil solutions and foil+Teflon solutions at the three sites: Factor1-Gasoline+Motor Oil+Meat Cooking+Natural Gas+SOA, Factor 2-Diesel+Motor Oil, Factor 3-Wood Burning, Factor 4-Shipping, Factor 5-Sea Spray, Factor 6-Brake Wear and Factor 7-Sn. Figures 4.13-4.17 and Figures 4.18-4.22 show the chemical composition and time series for resolved factors of various foil and foil+Teflon PMF results at site East Oakland as an example. Signature species are identical for all results, and hence the detailed source identification process is similar to that described previously for the foil+Teflon results [10]. Briefly, Factors 1 and 2 contain the majority of $PM_{0.1}$ OC and EC mass, so they should include most of the organic sources. Factor 2 has the highest fraction of EC and EC3 (a sub-fraction of elemental carbon that is volatilized and oxidized at temperature range700-775°C) that was found to be the major component in EC emitted by diesel engines [34-37]. Factor 2 was therefore determined to be Diesel and associated Motor Oil. Factor 3 was recognized as Wood Burning because it contains the majority of K and Rb, which are frequently found in biomass burning emission [28, 38]. Factor 4 has more than 80% of the V in its species profile. Since V is often emitted from heavy oil combustion in marine vessels [31], this factor was named Shipping. In Factor 5, K/Br and Rb/Br values are close to those in sea water, thus Factor 5 was identified as Sea Spray. Factor 6 was named Brake Wear because it contains 70% of Sb, which is added in brake pads and often found in brake wear particles from motor vehicles [39, 40] and railway cars [41, 42]. Factor 7 contains

the majority of the Sn, which may represent smelting and refining processes and oil combustion [43]. Because this factor contributes to less than 3% of the $PM_{0.1}$ mass and no specific source could be identified, it was not given a specific source name. Factor 1 is the largest contributor to $PM_{0.1}$ mass. Based on previous studies on sources of $PM_{0.1}$ [15, 44-46] and process of elimination, Factor 1 was determined to be a blended source of Gasoline, Motor Oil, Meat Cooking, Natural Gas, and SOA; these sources could not be distinguished because molecular markers were not measured in the current study.

Rotation is a useful tool to explore rotational ambiguity in the solution by allowing a minimal increase of Q (dQ<5%), with Fpeak representing the strength of rotation imposed. A positive Fpeak value sharpens the species profile and smears the factor contribution; a negative Fpeak value smear the species profile and sharpens the factor contribution [21]. Two solution types, named R1 and R2, emerged from both foil and foil+Teflon rotation runs; R1 were usually generated from positive Fpeak values 0.1 or 0.2, and R2 from negative Fpeak values -0.1 or -0.2. The main difference between R1 and R2 lies in percentage contribution of Factor 1 - Gasoline+Motor Oil+Meat Cooking+Natural Gas+SOA and Factor 2– Diesel+Motor Oil to $PM_{0.1}$ mass. Factor 1 contributions are always higher than Factor 2 contributions in R1 solutions, with a reduced or reversed trend in R2 solutions.

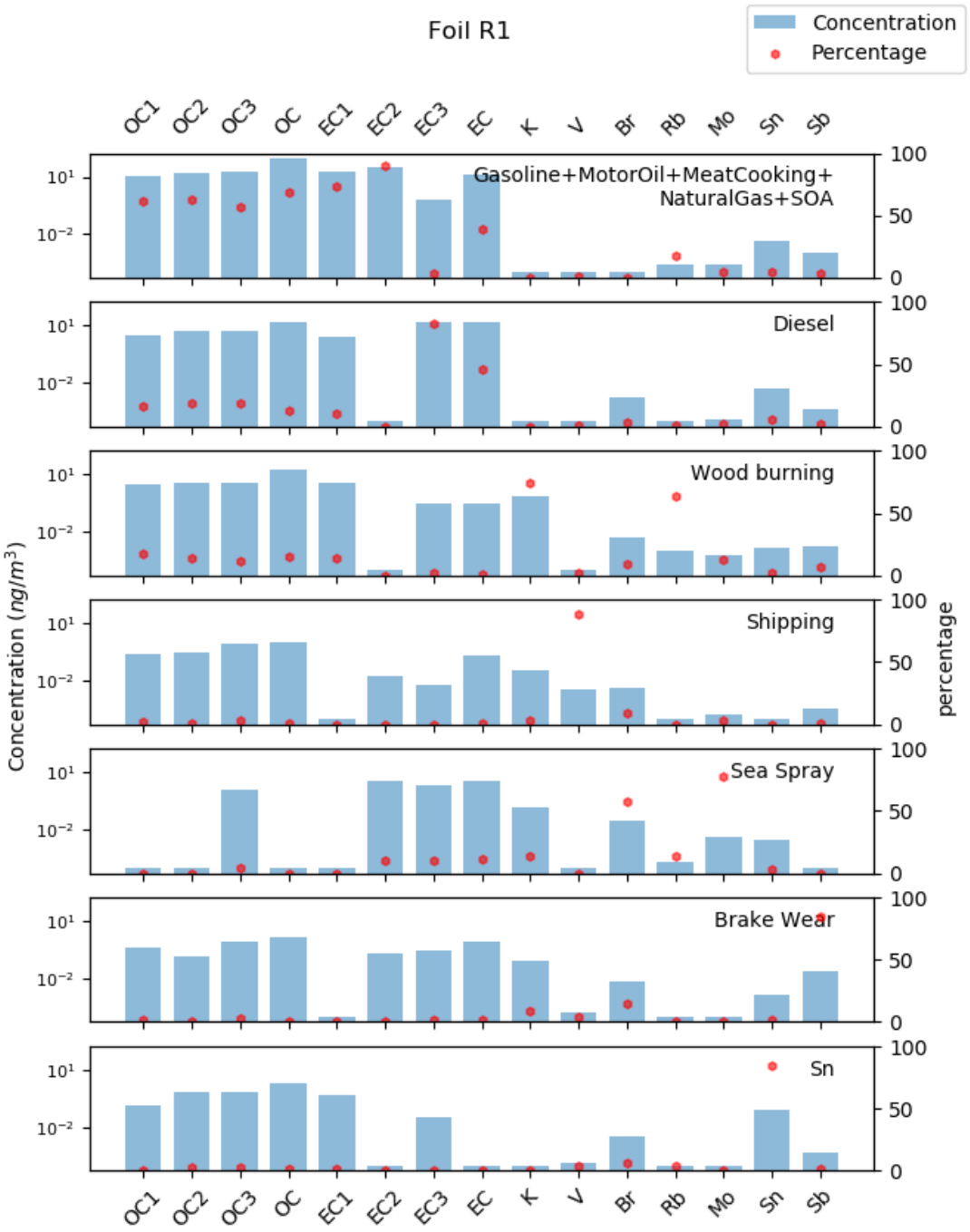

Figure 4.13. Species profile for R1 results of foil PMF run #26 at site EO. Blue bars (left axis) represent concentration of species in each factor and red dots (right axis) represents the percentage of species mass in each factor. Note that OC1, EC1 and Mo are weak species with higher uncertainty in the concentration profile.

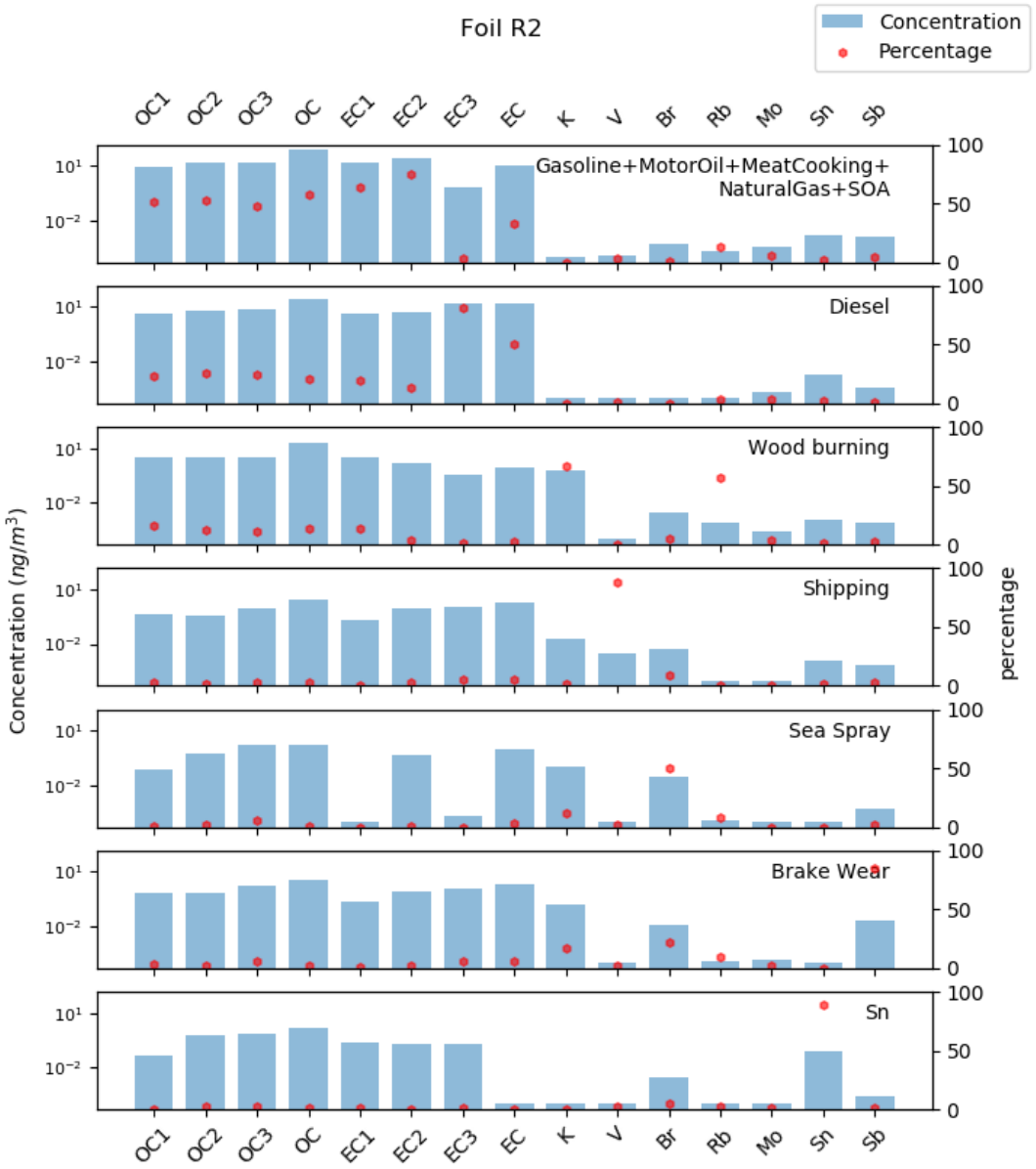

Figure 4.14. Species profile for R2 results of foil PMF run #26 at site EO. Blue bars (left axis) represent concentration of species in each factor and red dots (right axis) represents the percentage of species mass in each factor. Note that OC1, EC1 and Mo are weak species with higher uncertainty in the concentration profile.

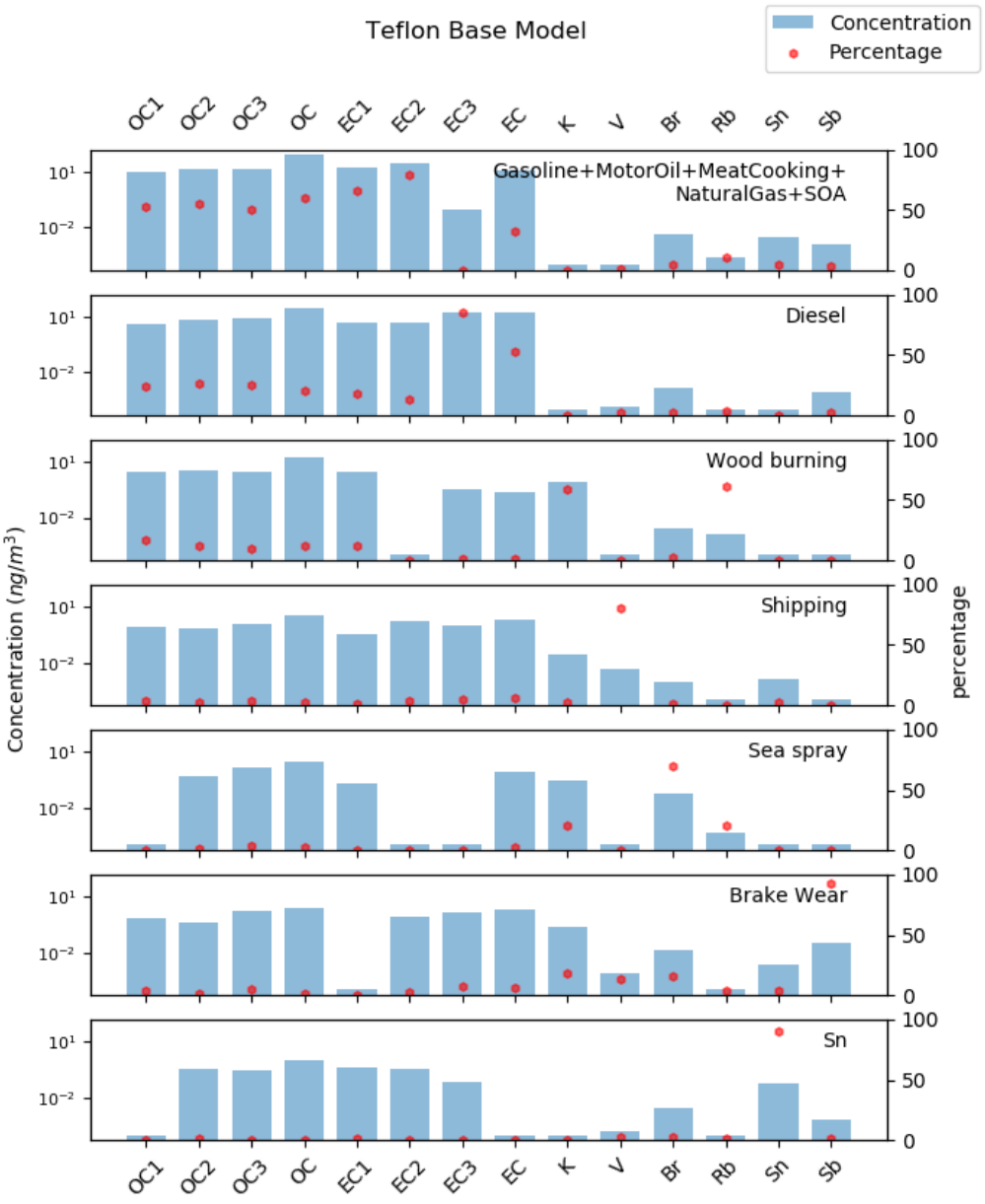

Figure 4.15. Species profile for Teflon base model results at site EO. Blue bars (left axis) represent concentration of species in each factor and red dots (right axis) represents the percentage of species mass in each factor. Note that OC1 and EC1 are weak species with higher uncertainty in the concentration profile.

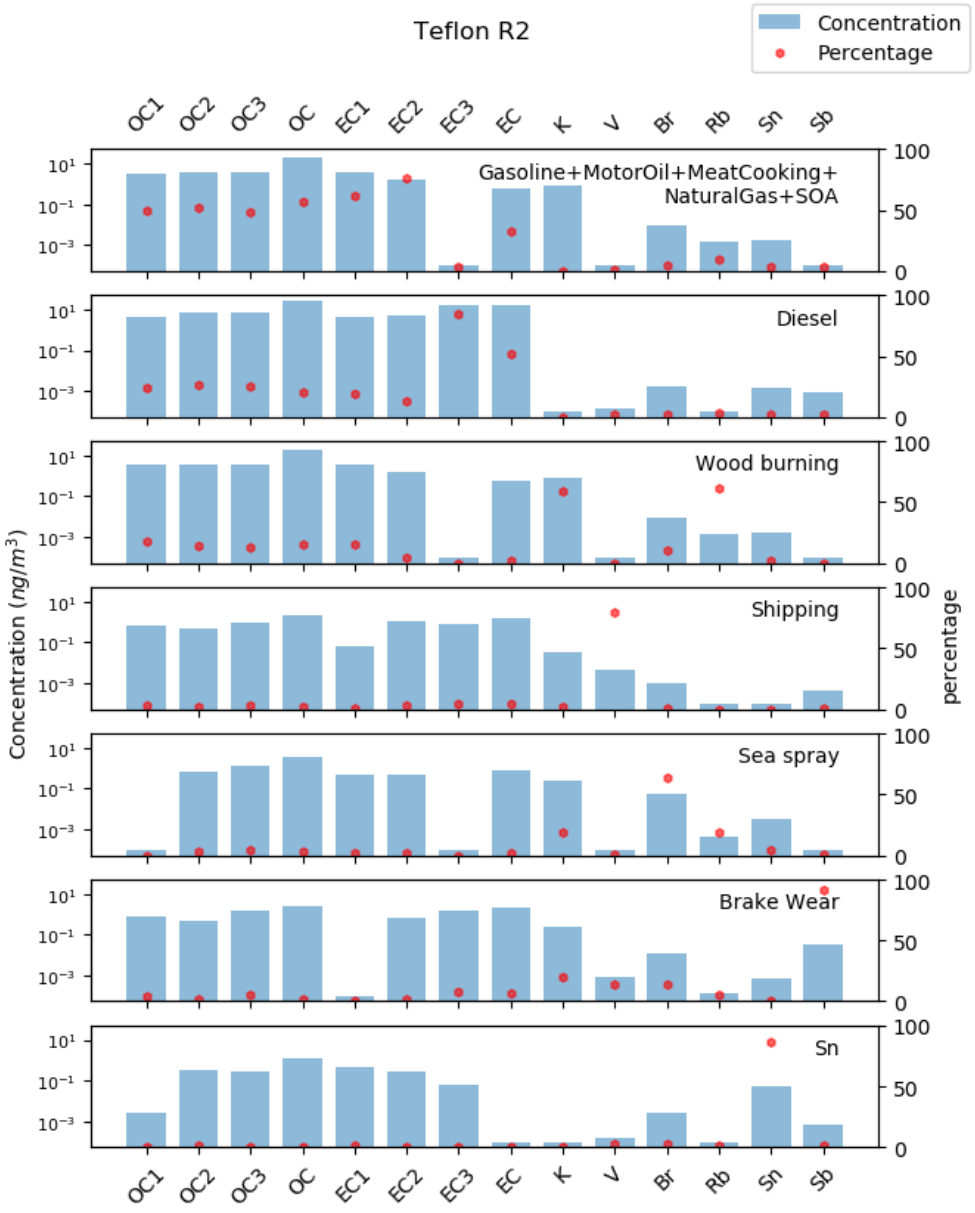

Figure 4.16. Species profile for Teflon R2 results at site EO. Blue bars (left axis) represent concentration of species in each factor and red dots (right axis) represents the percentage of species mass in each factor. Note that OC1 and EC1 are weak species with higher uncertainty in the concentration profile.

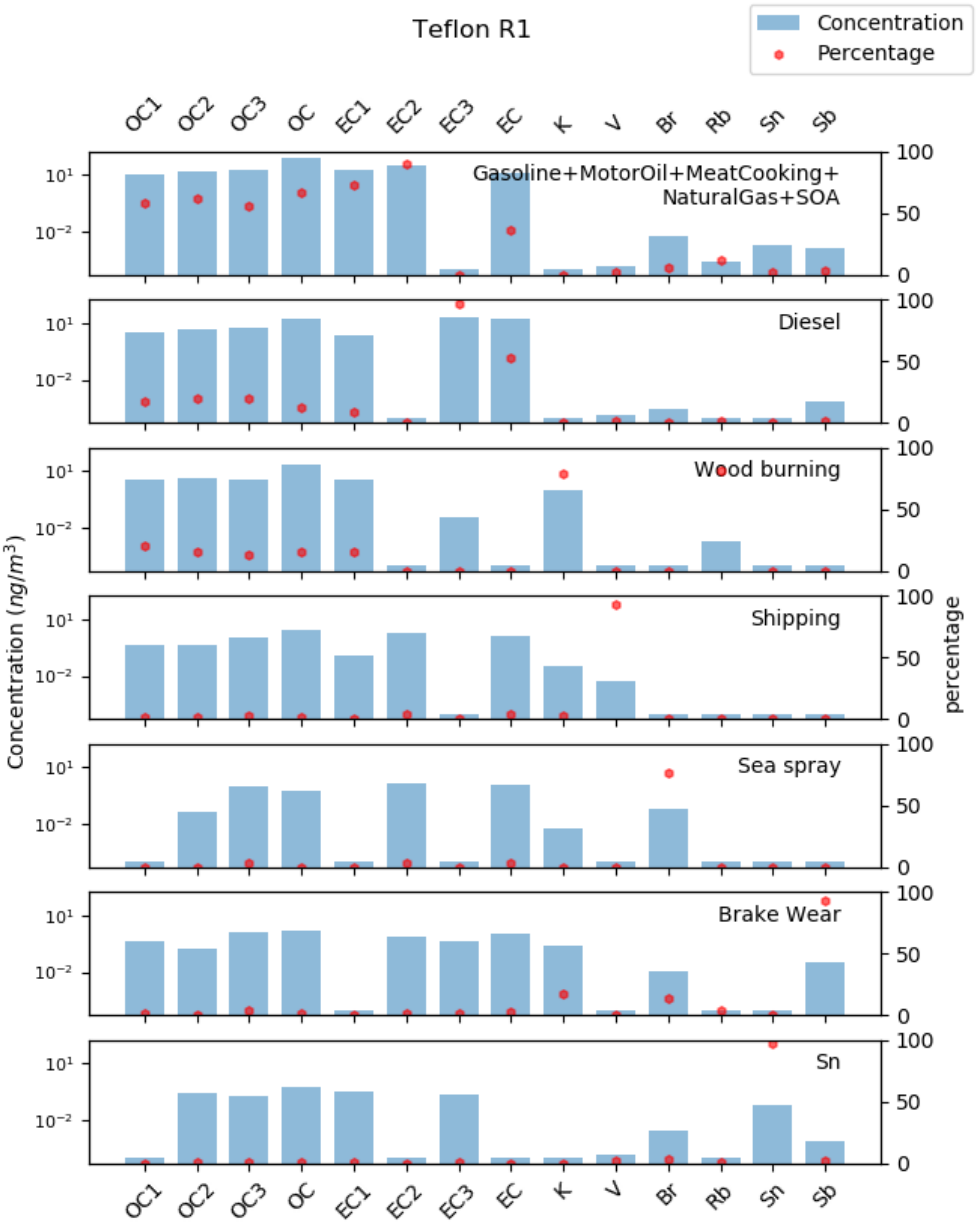

Figure 4.17. Species profile for Teflon R1 results at site EO. Blue bars (left axis) represent concentration of species in each factor and red dots (right axis) represents the percentage of species mass in each factor. Note that OC1 and EC1 are weak species with higher uncertainty in the concentration profile.

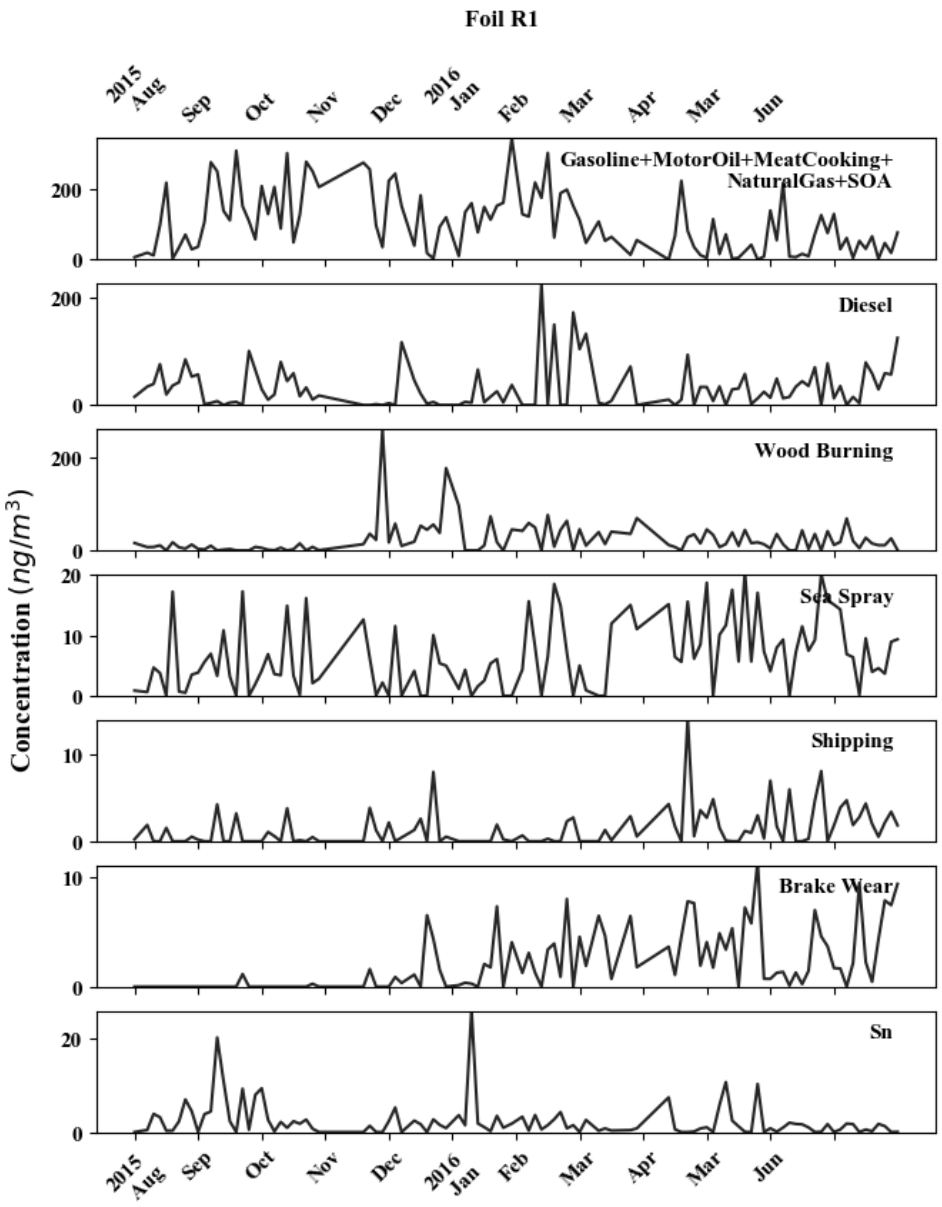

Figure 4.18. Time series for sources of foil R1 results at site EO.

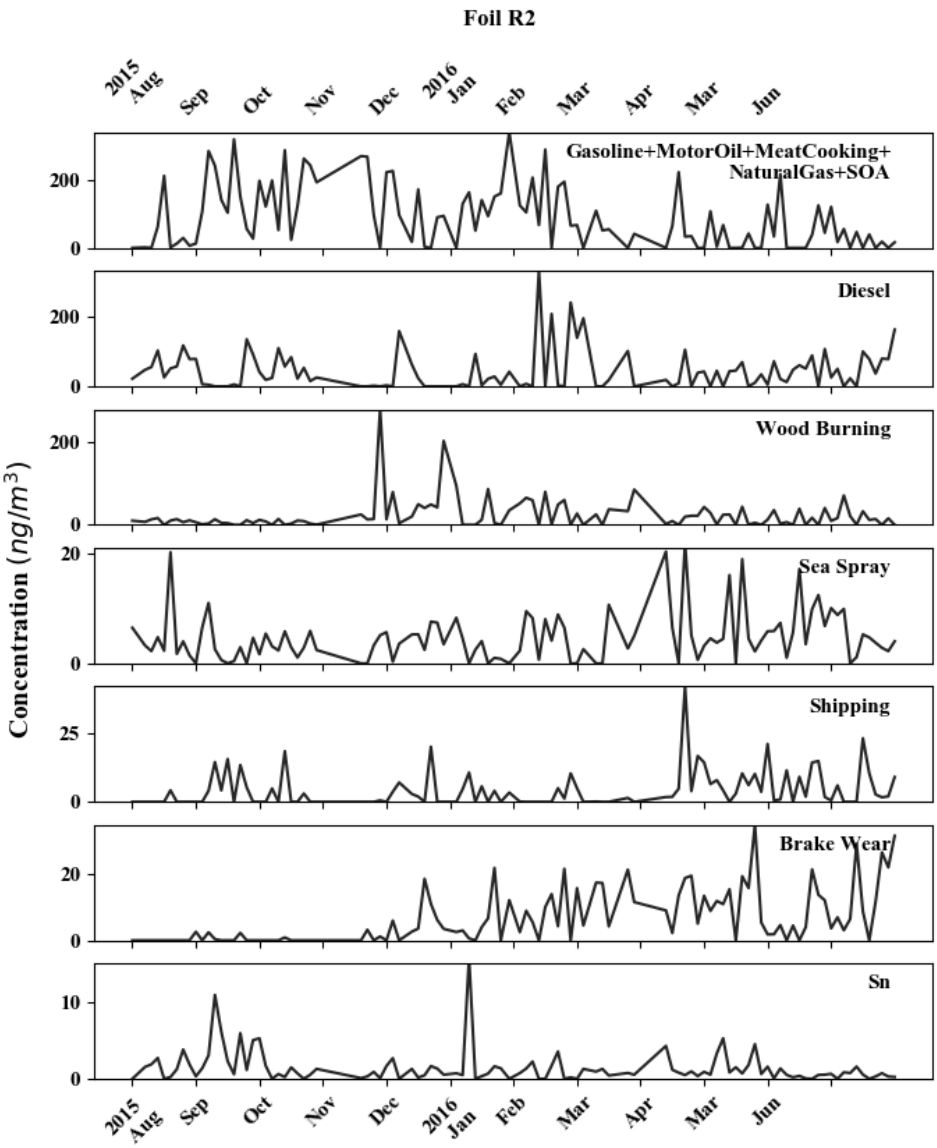

Figure 4.19. Time series for sources of foil R2 results at site EO.

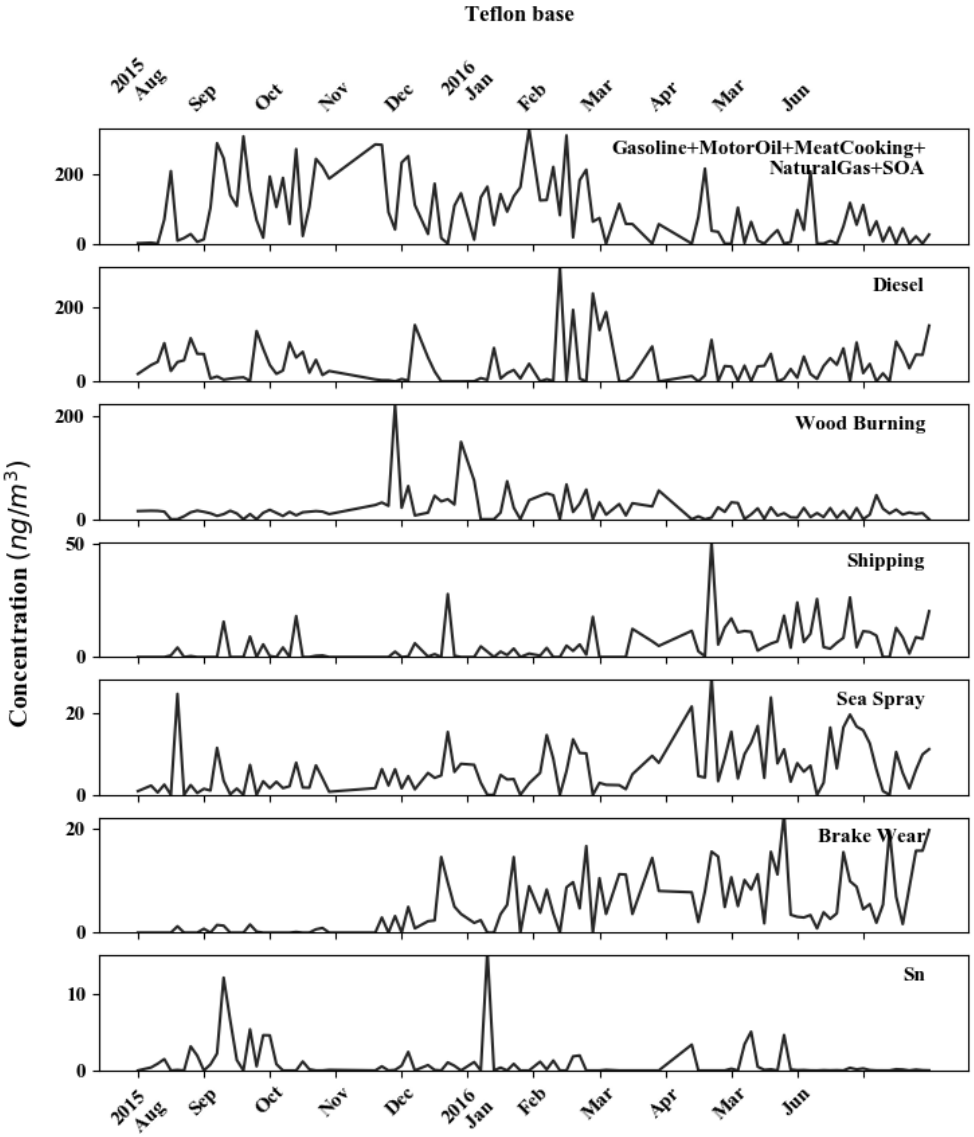

Figure 4.20. Time series for sources of Teflon base results at site EO.

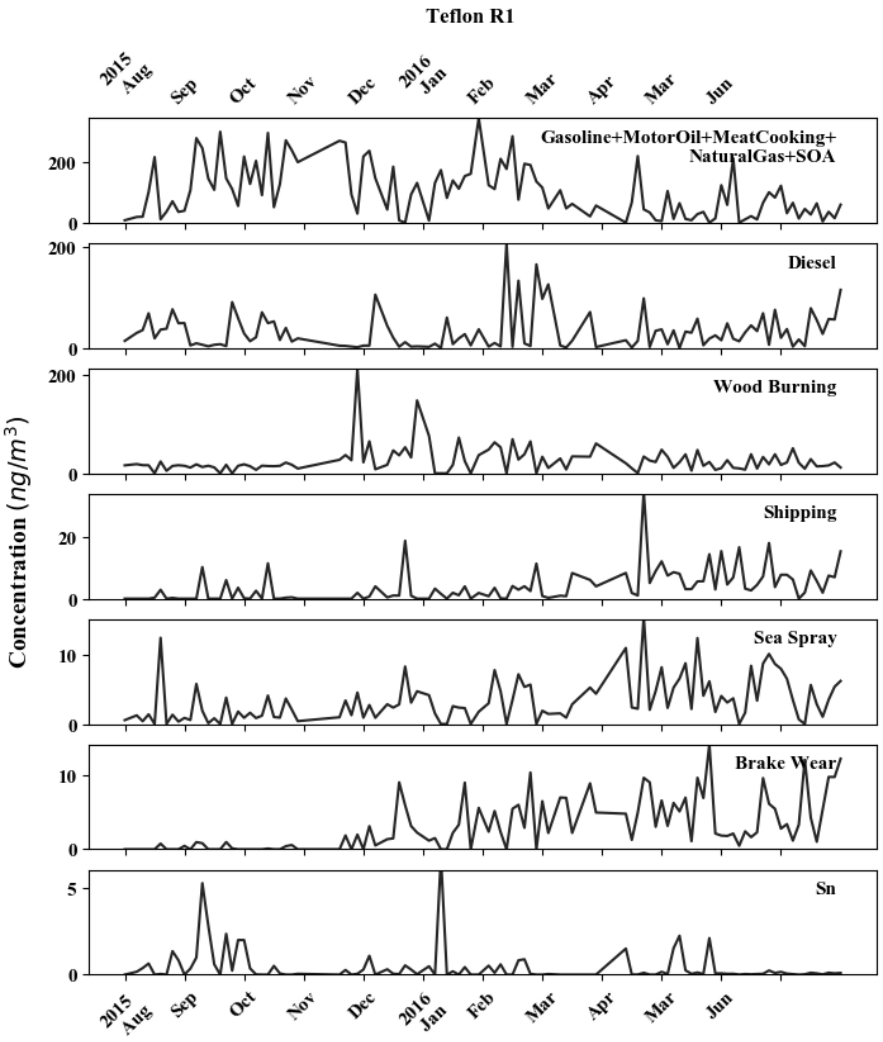

Figure 4.21. Time series for sources of Teflon R1 results at site EO.

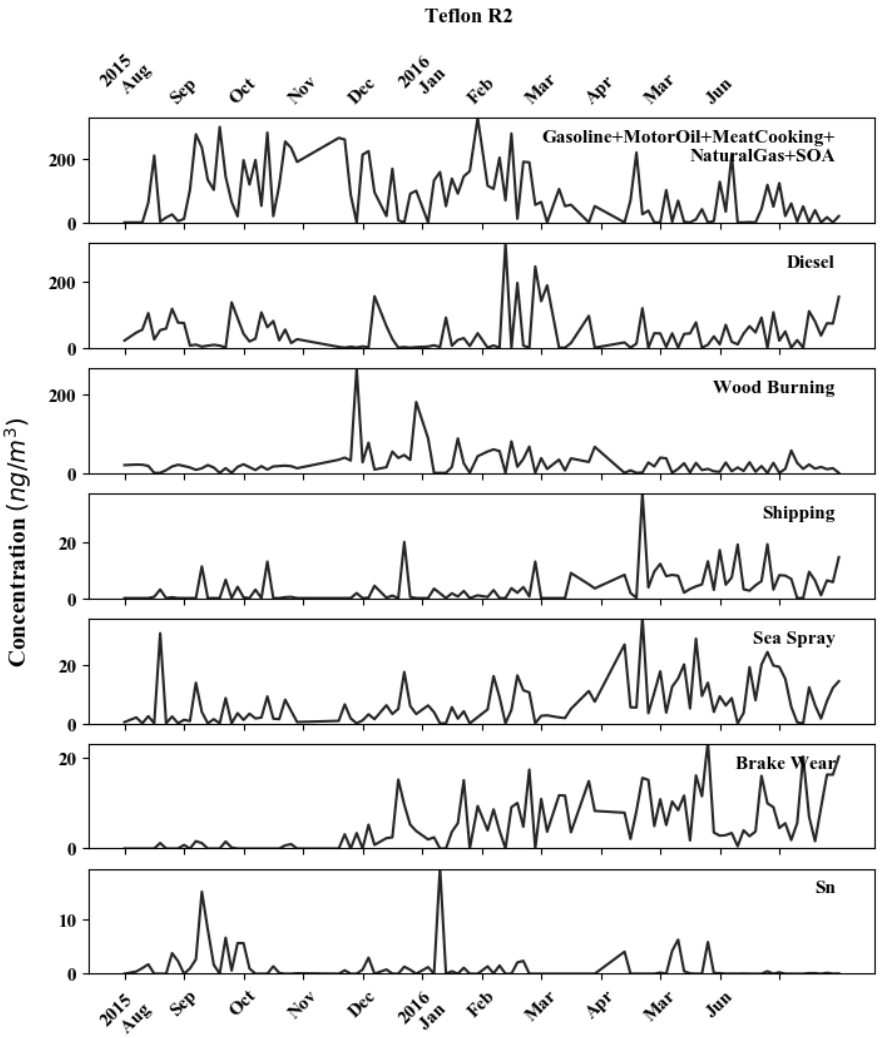

Figure 4.22. Time series for sources of Teflon R1 results at site EO.

Figure 4.23 summarizes $PM_{0.1}$ source apportionment results at the Los Angeles (LA) site using six different sampling and analysis configurations: Teflon+foil base, Teflon+foil R1, Teflon+foil R2, foil base, foil R1, and foil R2. All of the foil base, R1 and R2 solutions represent averages over the 30 input datasets that satisfied the Bootstrap quality control checks. The ranking of the dominant $PM_{0.1}$ sources remains constant in all solutions, but the absolute magnitudes of the source contributions changes as a function of the sampling and analysis configurations. Foil R1 has similar Factor 1 - Gasoline+Motor Oil+Meat Cooking+Natural Gas+SOA contribution

(46.2%±4.6%) as foil+Teflon R1(42.4%). Foil R1 has lower contribution from Factor 2 – Diesel+Motor Oil (31.1%±2.5%) than foil+Teflon R1 (35.3%). Factor 1 contributions to $PM_{0.1}$ are similar for foil R2 (29.7%±1.2%) and foil+Teflon R2 (26.7%), but Factor 2 contributions to $PM_{0.1}$ are smaller for foil R2 (37.4%±1.4%) than foil+Teflon R2 (45%). This discrepancy is caused by the fact that foil and foil+Teflon solutions have different EC3 loadings in Factor 1 and Factor 2 species profiles. The foil+Teflon PMF results are based on OC/EC measured from foil samples and elements from Teflon samples. The relatively humidity in LA was below 75% for the majority of the year, which may have exacerbated particle bounce on the foil MOUDIs vs. the Teflon MOUDIs [25]. Differential bounce may have caused a mismatch between OC/EC and element concentrations in the reference foil+Teflon PMF run at LA. It is notable that the Diesel $PM_{0.1}$ source contributions calculated by foil R1 and R2 (31.3%±2.5% and 36.2%±4.3%) are closer to values calculated by CMB (29%±4%) using molecular markers [15] than the values from foil +Teflon R1 and R2 (35.3% and 45%). $PM_{0.1}$ source contributions from Factors 3-7 are similar for foil and foil+Teflon PMF results. The foil base model results resemble those of foil R2 and the foil+Teflon base model results are similar to those of foil+Teflon R2. A typical behavior of base model is being similar to either R1 or R2 results.

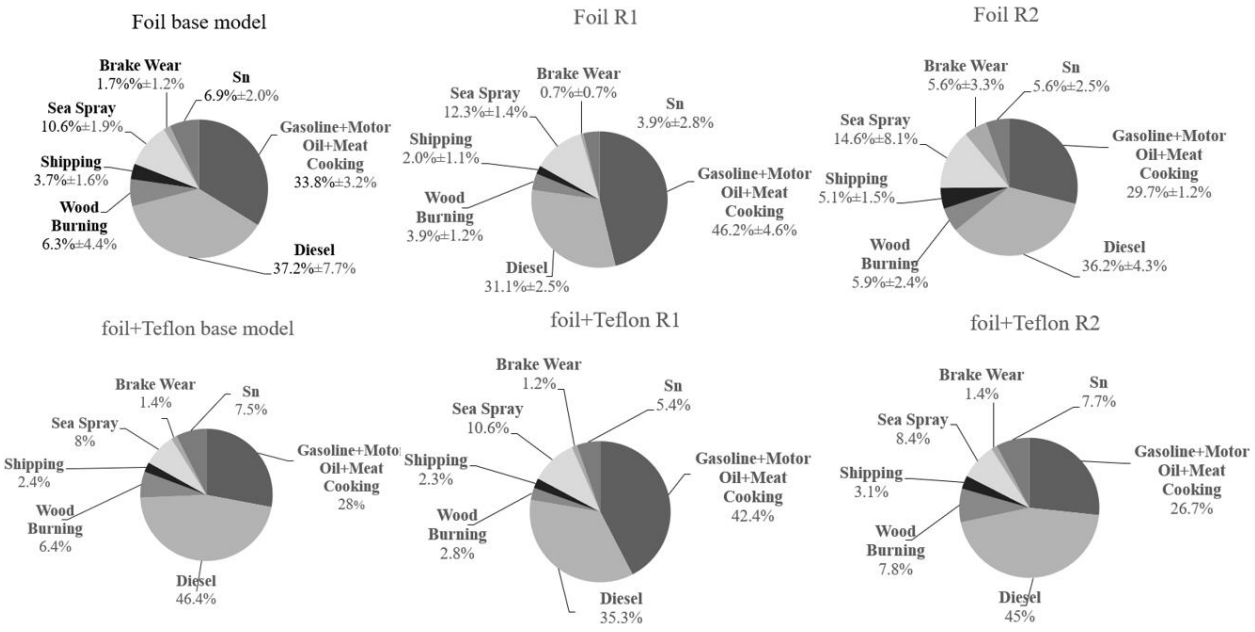

Figure 4.23. Source contributions to $PM_{0.1}$ of averaged foil PMF results R1 and R2, and of foil+Teflon base model, foil+Teflon R1 and foil+Teflon R2 at site Los Angeles. R1 results were generated from rotations of Fpeak value 0.1 or 0.2, and R2 results were generated from rotations of Fpeak value -0.1 or -0.2.

Figure 4.24 and Figure 4.25 summarize the $PM_{0.1}$ source apportionment results at the East Oakland (EO) site and San Pablo (SP) using the different sampling configurations. Calculated source contributions for foil vs. foil+Teflon R1, and foil vs. foil+Teflon R2 are very similar at these two locations, with small standard deviations for all sources. The results illustrated in Figure 4.24 and Figure 4.25 suggest that replacing measured Teflon $PM_{0.1}$ with simulated foil $PM_{0.1}$ had little effect on the PMF results at these two sites. This comparison also reveals that dropping some Weak Species while preserving Strong/tracer Species in PMF is unlikely to alter the results at these two sites.

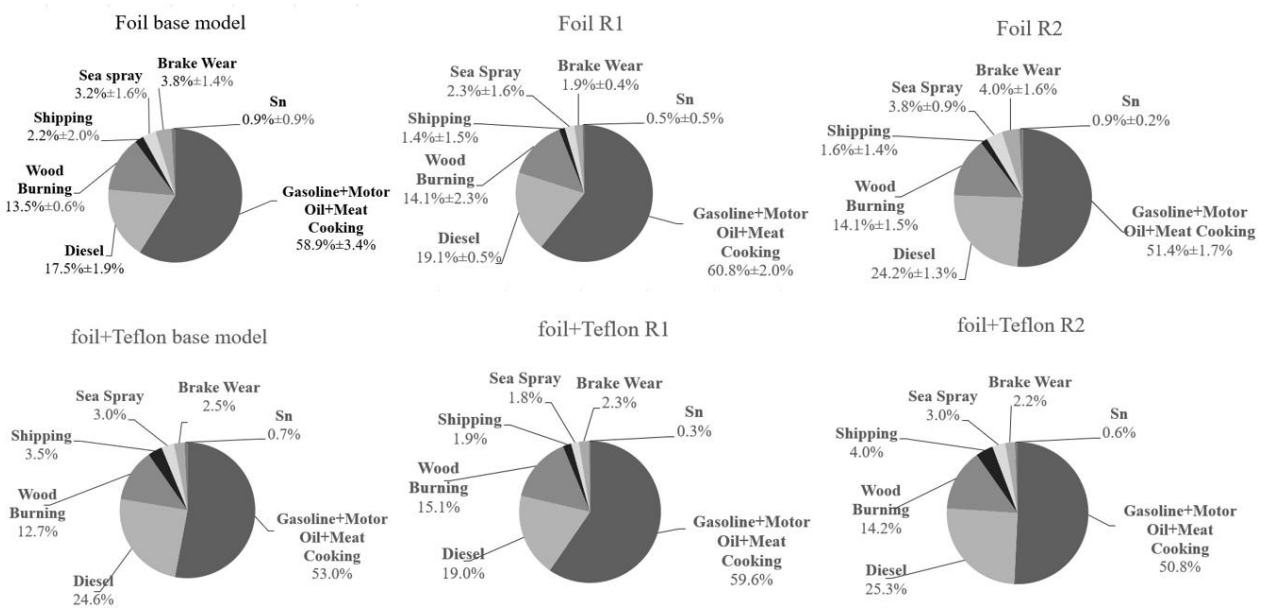

Figure 4.24. Source contributions to $PM_{0.1}$ of averaged foil PMF results R1 and R2, and of foil+Teflon base model, foil+Teflon R1 and foil+Teflon R2 at site East Oakland. R1 results were generated from rotations of Fpeak value 0.1 or 0.2, and R2 results were generated from rotations of Fpeak value -0.1 or -0.2.

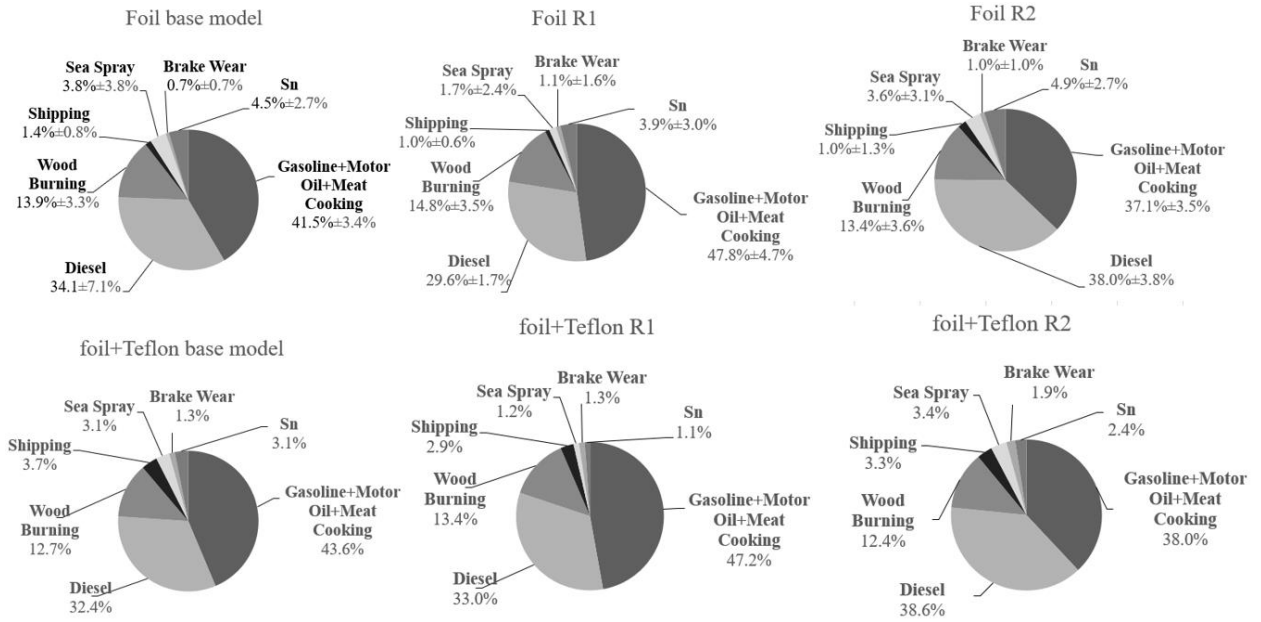

Figure 4.25. Source contributions to $PM_{0.1}$ of averaged foil PMF results R1 and R2, and of foil+Teflon base model, foil+Teflon R1 and foil+Teflon R2 at site San Pablo. R1 results were generated from rotations of Fpeak value 0.1 or 0.2, and R2 results were generated from rotations of Fpeak value -0.1 or -0.2.

Factor 1 and Factor 2 source contributions in the base model for both foil and foil+Teflon usually lie between their respective R1 and R2 PMF results at all three sites. The difference between base foil and base foil+Teflon results is usually larger than the difference between the R1 foil and R1 foil+Teflon results or the R2 foil and the R2 foil+Teflon results. For example, Factor 1 at EO accounts for 58.9%±3.4% of $PM_{0.1}$ mass in the base foil model and 53.0% of $PM_{0.1}$ mass in the foil+Teflon model (Δ=5.9%). In contrast, the Factor 1 contributions are 60.8±2.0% in R1 foil and 59.6% in R1 foil+Teflon (Δ=1.2%), while factor 1 contributions are 51.4%±1.7% in R2 foil and 50.8% in R2 foil+Teflon (Δ=0.6%).

Paatero *et al.* introduced G-Space plots to compare rotation results by plotting pairs of source contribution factors; the "edge" of regions densely occupied by points in better rotation results will be more parallel to the axes, indicating the weak independence between these two factors that is often observed in real-world sources data [47]. In the current study, R2 improved the edges in G-Space plots for multiple pairs of sources, such as Sea Spray vs Shipping, Sea Spray vs Wood Burning, and Gasoline+others vs Diesel (Figures 4.26-4.28) whereas R1 either decreased or did not improve the edges in the G-Space plots. This finding suggests that R2 solutions are preferred for both foil and foil+Teflon configurations at all three sites.

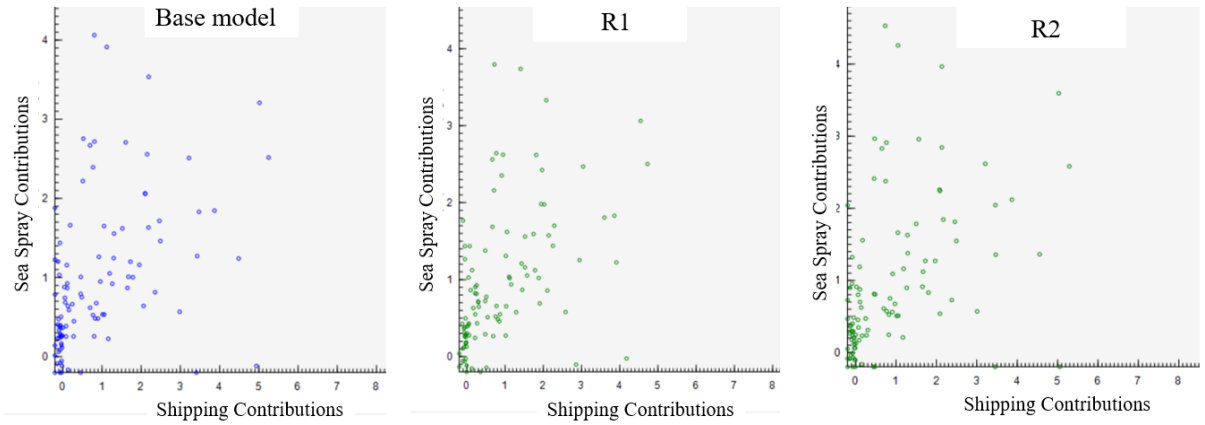

Figure 4.26. G-space plot example for sea spray vs shipping.

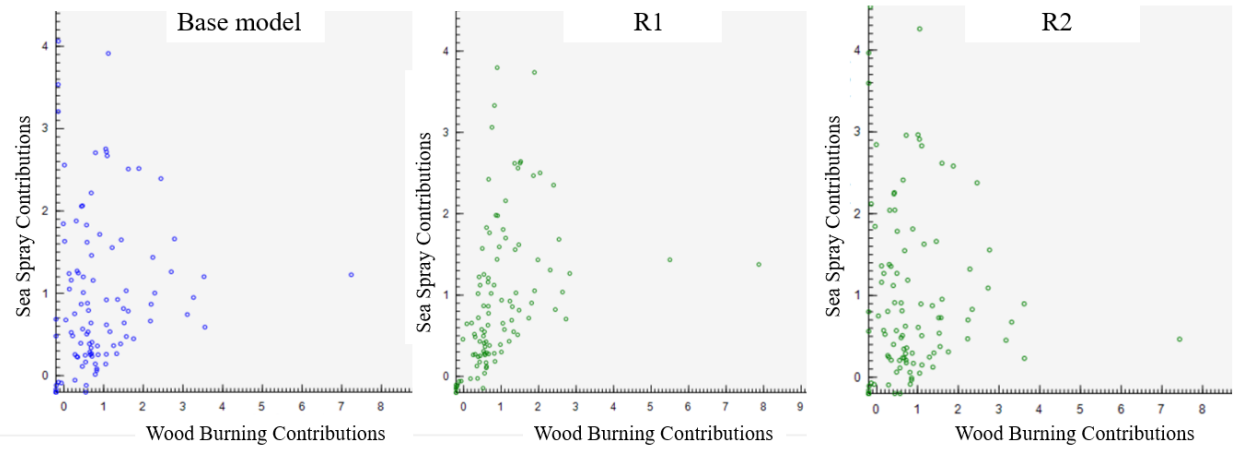

Figure 4.27. G-space plot example for sea spray vs wood burning.

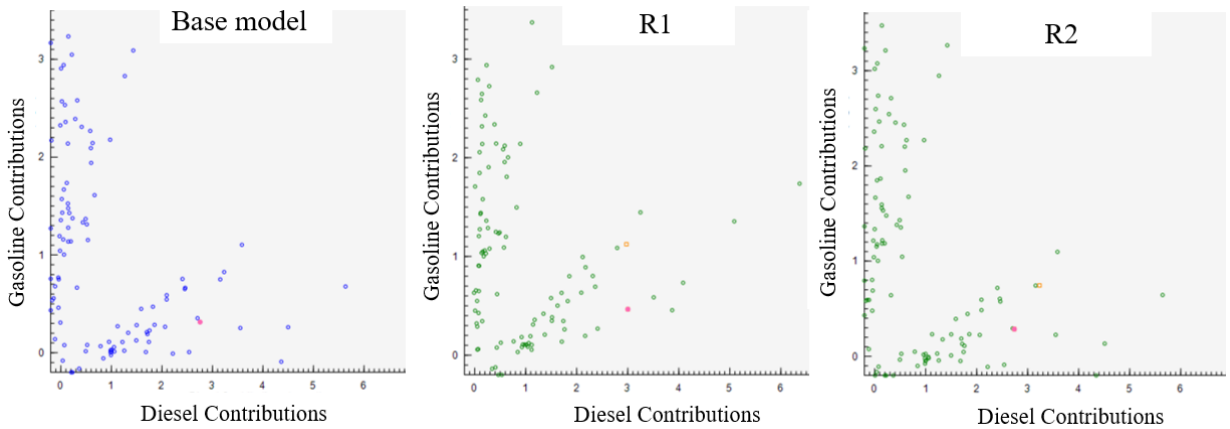

Figure 4.28. G-space plot example for gasoline vs diesel.

4.4 Conclusion

The current study modifies the extraction method developed for the analysis of elemental concentrations on Teflon substrates to work with foil substrates in order to test the feasibility of operating $PM_{0.1}$ sampling networks with a single cascade impactor. Results show that eighteen elements (Li, Na, Mg, K, Ti, V, Ga, As, Se, Br, Rb, Sr, Mo, Cd, Sn, Sb, Ba and Pb) in particles with diameters between 0.1 – 1.8 μm can be measured with similar accuracy using foil vs. Teflon substrates. Ten elements (Li, K, V, Br, Rb, Mo, Cd, Sn, Sb, and Ba) in "quasi-ultrafine" particles with diameter between 0.1 – 0.18 μm show good agreement between the foil and Teflon substrates. Elemental concentrations measured using foil substrates are typically lower than corresponding measurements on Teflon substrates, possibly due to enhanced bounce on the foil impaction surface.

Positive Matrix Factorization (PMF) conducted on 30 simulated foil $PM_{0.1}$ datasets spanning a full year of measurements generated two types of source apportionment results based on positive and negative rotations (R1 and R2) that explore the ambiguity in the solution. PMF results from the foil datasets identify the same rank order of $PM_{0.1}$ source contributions when compared to results from the foil+Teflon dataset. At one of the analyzed sites, the detailed $PM_{0.1}$ contributions from one of the sources changes by as much as 10% when only foil samples are analyzed, while the other sites show very similar $PM_{0.1}$ source breakdown between foil and foil+Teflon results. This level of variability is unlikely to affect the design of emissions control programs that seek to improve air quality by reducing ultrafine particle concentrations.

The difference between the foil PMF vs. the foil+Teflon PMF results for $PM_{0.1}$ source contributions are likely caused by enhanced particle bounce associated with relative humidity below 75%. Differential bounce between Teflon vs. foil impaction surfaces affects studies carried out with foil+Teflon configurations as well as studies carried out with only foil configurations.

Future sampling projects may consider investigating anti-bounce coatings that do not interfere with downstream chemical analysis, or controlling the relative humidity inside the impactor to reduce particle bounce.

The consistency between foil and foil+Teflon PMF results shows that $PM_{0.1}$ monitoring using a single cascade impactor loaded with foil substrates is feasible. A traditional $PM_{0.1}$ sampling network covering four sites based on a 3-day averaging time operating over a one-year period would require startup and maintenance costs for two cascade impactors, labor maintaining sampling network, Teflon substrates, and foil substrates. The adoption of a network design using a single cascade impactor equipped with foil substrates reduces all costs by approximately 50%. Future studies should consider the adoption of $PM_{0.1}$ sampling network using a single MOUDI loaded with foil substrates as a strategy to reduce the barriers towards enhanced monitoring of ultrafine particles.

4.5 Acknowledgements

This work was funded by the California Air Resources Board under Project #13-418. The statements and conclusions in this paper are those of the authors and not necessarily those of the sponsors. The mention of commercial products, their source, or their use in connection with material reported herein is not to be construed as actual or implied endorsement of such products.

4.6 References

1. Schwarze, P., et al., *Particulate matter properties and health effects: consistency of epidemiological and toxicological studies.* Human & experimental toxicology, 2006. **25**(10): p. 559-579.
2. Pope III, C.A. and D.W. Dockery, *Health effects of fine particulate air pollution: lines that connect.* Journal of the air & waste management association, 2006. **56**(6): p. 709-742.
3. Elder, A. and G. Oberdörster, *Translocation and effects of ultrafine particles outside of the lung.* Clinics in occupational and environmental medicine, 2005. **5**(4): p. 785-796.

4. Geiser, M., et al., *Ultrafine particles cross cellular membranes by nonphagocytic mechanisms in lungs and in cultured cells.* Environmental health perspectives, 2005. **113**(11): p. 1555.
5. Cabada, J.C., et al., *Mass size distributions and size resolved chemical composition of fine particulate matter at the Pittsburgh supersite.* Atmospheric Environment, 2004. **38**(20): p. 3127-3141.
6. Ondov, J.M., et al., *Baltimore Supersite: Highly time- and size-resolved concentrations of urban PM2.5 and its constituents for resolution of sources and immune responses.* Atmospheric Environment, 2006. **40**: p. S224-S237.
7. Zheng, M., et al., *Seasonal trends in PM2. 5 source contributions in Beijing, China.* Atmospheric Environment, 2005. **39**(22): p. 3967-3976.
8. Houthuijs, D., et al., *PM10 and PM2. 5 concentrations in Central and Eastern Europe:: Results from the Cesar study.* Atmospheric Environment, 2001. **35**(15): p. 2757-2771.
9. Baldauf, R.W., et al., *Ultrafine Particle Metrics and Research Considerations: Review of the 2015 UFP Workshop.* International journal of environmental research and public health, 2016. **13**(11): p. 1054.
10. Xue, W., et al., *Positive matrix factorization of ultrafine particle mass (PM0. 1) at three sites in California.* Science of The Total Environment, 2020. **715**: p. 136902.
11. Marple, V.A., K.L. Rubow, and S.M. Behm, *A microorifice uniform deposit impactor (MOUDI): Description, calibration, and use.* Aerosol Science and Technology, 1991. **14**(4): p. 434-446.
12. Misra, C., et al., *Development and evaluation of a personal cascade impactor sampler (PCIS).* Journal of Aerosol Science, 2002. **33**(7): p. 1027-1047.
13. Marple, V.A., et al., *Low flow rate sharp cut impactors for indoor air sampling: design and calibration.* Japca, 1987. **37**(11): p. 1303-1307.
14. Venecek, M.A., et al., *Characterization of the 8-stage Rotating Drum Impactor under low concentration conditions.* Journal of Aerosol Science, 2016. **100**: p. 140-154.
15. Xue, J., et al., *Seasonal and Annual Source Appointment of Carbonaceous Ultrafine Particulate Matter (PM0. 1) in Polluted California Cities.* Environmental science & technology, 2018. **53**(1): p. 39-49.
16. Xue, W., et al., *Day-of-week patterns for ultrafine particulate matter components at four sites in California.* Atmospheric Environment, 2019: p. 117088.
17. Herner, J.D., P.G. Green, and M.J. Kleeman, *Measuring the trace elemental composition of size-resolved airborne particles.* Environmental Science & Technology, 2006. **40**(6): p. 1925-1933.
18. Ham, W.A., et al., *Size Distribution of Health-Relevant Trace Elements in Airborne Particulate Matter During a Severe Winter Stagnation Event: Implications for Epidemiology and Inhalation Exposure Studies.* Aerosol Science and Technology, 2010. **44**(9): p. 753-765.
19. Kuwayama, T., C.R. Ruehl, and M.J. Kleeman, *Daily trends and source apportionment of ultrafine particulate mass (PM0. 1) over an annual cycle in a typical California City.* Environmental science & technology, 2013. **47**(24): p. 13957-13966.
20. Eller, P.M., *NIOSH manual of analytical methods*. Vol. 94. 1994: Diane Publishing.
21. Norris, G., et al., *EPA Positive Matrix Factorization (PMF) 5.0 fundamentals and User Guide Prepared for the US Environmental Protection Agency Office of Research and Development, Washington, DC.* Inc., Petaluma, 2014.

22. Reff, A., S.I. Eberly, and P.V. Bhave, *Receptor modeling of ambient particulate matter data using positive matrix factorization: review of existing methods.* Journal of the Air & Waste Management Association, 2007. **57**(2): p. 146-154.
23. Dzubay, T., L. Hines, and R. Stevens, *Particle bounce errors in cascade impactors.* Atmospheric Environment (1967), 1976. **10**(3): p. 229-234.
24. Yamamoto, N., et al., *Broad range observation of particle deposition on greased and non-greased impaction surfaces using a line-sensing optical microscope.* Journal of aerosol science, 2002. **33**(12): p. 1667-1679.
25. Chen, S.-C., et al., *The influence of relative humidity on nanoparticle concentration and particle mass distribution measurements by the MOUDI.* Aerosol Science and Technology, 2011. **45**(5): p. 596-603.
26. Pandolfi, M., et al., *Trends analysis of PM source contributions and chemical tracers in NE Spain during 2004–2014: a multi-exponential approach.* Atmospheric Chemistry and Physics, 2016. **16**(18): p. 11787-11805.
27. Gillette, D.A., et al., *Emissions of alkaline elements calcium, magnesium, potassium, and sodium from open sources in the contiguous United States.* Global Biogeochemical Cycles, 1992. **6**(4): p. 437-457.
28. Kleeman, M.J., J.J. Schauer, and G.R. Cass, *Size and composition distribution of fine particulate matter emitted from wood burning, meat charbroiling, and cigarettes.* Environmental Science & Technology, 1999. **33**(20): p. 3516-3523.
29. Turn, S., et al., *Elemental characterization of particulate matter emitted from biomass burning: Wind tunnel derived source profiles for herbaceous and wood fuels.* Journal of Geophysical Research: Atmospheres, 1997. **102**(D3): p. 3683-3699.
30. Richard, A., et al., *Source apportionment of size and time resolved trace elements and organic aerosols from an urban courtyard site in Switzerland.* Atmospheric Chemistry and Physics, 2011. **11**(17): p. 8945-8963.
31. Querol, X., et al., *Source origin of trace elements in PM from regional background, urban and industrial sites of Spain.* Atmospheric Environment, 2007. **41**(34): p. 7219-7231.
32. Lin, Y.-C., et al., *Characteristics of trace metals in traffic-derived particles in Hsuehshan Tunnel, Taiwan: size distribution, potential source, and fingerprinting metal ratio.* Atmospheric Chemistry and Physics, 2015. **15**(8): p. 4117-4130.
33. Adachi, K. and Y. Tainosho, *Characterization of heavy metal particles embedded in tire dust.* Environment international, 2004. **30**(8): p. 1009-1017.
34. Pavlovic, J., J. Kinsey, and M. Hays, *The influence of temperature calibration on the OC–EC results from a dual-optics thermal carbon analyzer.* Atmospheric Measurement Techniques, 2014. **7**(9): p. 2829-2838.
35. Cao, J., et al., *Characterization of roadside fine particulate carbon and its eight fractions in Hong Kong.* Aerosol Air Qual. Res, 2006. **6**(2): p. 106-122.
36. Liu, W., et al., *Enhanced source identification of southeast aerosols using temperature-resolved carbon fractions and gas phase components.* Atmospheric Environment, 2006. **40**: p. 445-466.
37. Zhu, C.-S., et al., *Characterization of carbon fractions for atmospheric fine particles and nanoparticles in a highway tunnel.* Atmospheric Environment, 2010. **44**(23): p. 2668-2673.
38. Pereira, E., et al., *Airborne measurements of aerosols from burning biomass in Brazil related to the TRACE A experiment.* Journal of Geophysical Research: Atmospheres, 1996. **101**(D19): p. 23983-23992.

39. Johansson, C., M. Norman, and L. Burman, *Road traffic emission factors for heavy metals.* Atmospheric Environment, 2009. **43**(31): p. 4681-4688.
40. Querol, X., et al., *PM speciation and sources in Mexico during the MILAGRO-2006 Campaign.* Atmospheric Chemistry and Physics, 2008. **8**(1): p. 111-128.
41. Abbasi, S., et al., *A study of airborne wear particles generated from organic railway brake pads and brake discs.* Wear, 2011. **273**(1): p. 93-99.
42. Namgung, H.-G., et al., *Generation of nanoparticles from friction between railway brake disks and pads.* Environmental science & technology, 2016. **50**(7): p. 3453-3461.
43. Roper, W., *Toxicological profile for tin.* US department of health and human services, agency for toxic substances and disease registry, 1992.
44. Venecek, M.A., X. Yu, and M.J. Kleeman, *Predicted ultrafine particulate matter source contribution across the continental United States during summertime air pollution events.* Atmospheric Chemistry and Physics, 2019. **19**(14): p. 9399-9412.
45. Gugamsetty, B., et al., *Source Characterization and Apportionment of PM10, PM2.5 and PM0.1 by Using Positive Matrix Factorization.* Aerosol and Air Quality Research, 2012. **12**(4): p. 476-491.
46. Shirmohammadi, F., et al., *Fine and ultrafine particulate organic carbon in the Los Angeles basin: Trends in sources and composition.* Sci Total Environ, 2016. **541**: p. 1083-1096.
47. Paatero, P., et al., *A graphical diagnostic method for assessing the rotation in factor analytical models of atmospheric pollution.* Atmospheric Environment, 2005. **39**(1): p. 193-201.

5.0 Conclusions

5.1 Day-of-Week Patterns for Ultrafine Particulate Matter Components at Four Sites in California

A comprehensive analysis of the day-of-week trends for fifteen components of ultrafine particulate matter was conducted over an annual cycle at four sites in California. This analysis reveals location-specific patterns along with important general trends. A comparison between different elements at the same location identified ultrafine components with highest concentrations on weekdays (Group I(M-F)), weekends (Group II(S-M)), or during the early week (Group III(M-W)). Across the most heavily urban sites, Group III(M-W) always contains EC (diesel engines). Across all sites, Group II(S-M) always contains K and Rb (biomass combustion). Ultrafine OC, and 11 other trace components did not display strong day-of-week concentration patterns, suggesting that multiple sources contribute to these ultrafine components.

A paired t-test constructed using measurements on weekends compared to measurements immediately preceding or immediately following the weekend confirms that ambient ultrafine particle concentrations associated with diesel engines (EC) are highest on weekdays while ambient ultrafine particle concentrations associated with biomass combustion (K and Rb) are highest on weekends in California. These weekly cycles in ultrafine particulate matter source contributions may have implications for public health.

A detailed trend analysis for the same element at different locations shows that the two closest sampling locations (SP and EO) have the great number of ultrafine particle components with identical weekly trends, but even at these locations only 3 out of 15 components displayed the exact same day-of-week profiles. Less similarity was observed in measured day-of-week profiles for ultrafine particle elements at other sites. This suggests that the details of ultrafine particle

concentrations at each sampling site reflect the mixture of sources immediately adjacent to that site. By extension, individual neighborhoods across California will each experience unique day-of-week concentration profiles for ultrafine particle components that reflect the surrounding sources.

5.2 Positive Matrix Factorization of Ultrafine Particle Mass ($PM_{0.1}$) at Three Sites in California

Three-day average samples of $PM_{0.1}$ collected over a full year at San Pablo, East Oakland, and Los Angeles were analyzed using Positive Matrix Factorization to identify source contributions at each location. Seven $PM_{0.1}$ sources were identified: Factor1-Gasoline+Motor Oil+Meat Cooking+Natural Gas+SOA, Factor 2- Diesel+Motor Oil, Factor 3-Wood Burning, Factor 4-Shipping and other heavy fuel oil combustion, Factor 5-Sea Spray, Factor 6-Sb Brake Wear, and Factor 7-Sn. They each contributes to 30.9-53.0%, 25.1-44.8%, 5.9-11.9%, 2.3-3.1%, 3.5-8.0%, 1.1-2.8%, and 0.5% to 7.0% to total $PM_{0.1}$. Wood Burning contributions to $PM_{0.1}$ were highest in the winter season when residential wood combustion was active. The monthly-averaged $PM_{0.1}$ source apportionment results calculated by PMF in the current study are consistent with the $PM_{0.1}$ source apportionment results calculated using CMB, showing the robustness of the PMF method. EC3, K and Rb, V, Br, and Sb were used as tracers for Factor 2-6 respectively. It's the first time that Shipping and Brake Wear were identified by PMF for $PM_{0.1}$ because of the use of V and Sb. Diesel source by a sub-fraction of EC(EC3), Brake Wear identified by Sb, and Wood Burning identified by Rb were not seen in previous literature, either. The higher time resolution inherent with in PMF method may help infer source characteristics.

5.3 Comparison of size-resolved PM elements measured using aluminum foil and Teflon impaction substrates: implications for ultrafine particle source apportionment and future sampling networks

The current study modifies the extraction method developed for the analysis of elemental concentrations on Teflon substrates to work with foil substrates in order to test the feasibility of operating $PM_{0.1}$ sampling networks with a single cascade impactor. Results show that eighteen elements (Li, Na, Mg, K, Ti, V, Ga, As, Se, Br, Rb, Sr, Mo, Cd, Sn, Sb, Ba and Pb) in particles with diameters between 0.1 – 1.8 μm can be measured with similar accuracy using foil vs. Teflon substrates. Ten elements (Li, K, V, Br, Rb, Mo, Cd, Sn, Sb, and Ba) in "quasi-ultrafine" particles with diameter between 0.1 – 0.18 μm show good agreement between the foil and Teflon substrates. Elements' concentrations measured using foil substrates are typically lower than corresponding measurements on Teflon substrates, possibly due to enhanced bounce on the foil impaction surface.

Positive Matrix Factorization (PMF) conducted on 30 simulated foil $PM_{0.1}$ datasets spanning a full year of measurements generated two types of source apportionment results based on positive and negative rotations (R1 and R2). PMF results from the foil datasets identify the same rank order of $PM_{0.1}$ source contributions when compared to results from the foil+Teflon dataset. At one of the analyzed sites, the detailed $PM_{0.1}$ contributions from one of the sources changes by as much as 10% when only foil samples are analyzed, while the other sites show very similar $PM_{0.1}$ source breakdown between foil and foil+Teflon results. This level of variability is unlikely to affect the design of emissions control programs that seek to improve air quality by reducing ultrafine particle concentrations.

The difference between the foil PMF vs. the foil+Teflon PMF results for $PM_{0.1}$ source contributions are likely caused by enhanced particle bounce associated with relative humidity

below 75%. Differential bounce between Teflon vs. foil impaction surfaces affects studies carried out with foil+Teflon configurations as well as studies carried out with only foil configurations. Future sampling projects may consider investigating anti-bounce coatings that do not interfere with downstream chemical analysis, or controlling the relative humidity inside the impactor to reduce particle bounce.

The consistency between foil and foil+Teflon PMF results shows that $PM_{0.1}$ monitoring using a single cascade impactor loaded with foil substrates is feasible. A traditional $PM_{0.1}$ sampling network covering four sites based on a 3-day averaging time operating over a one-year period would require startup and maintenance costs for two cascade impactors, labor maintaining sampling network, Teflon substrates, and foil substrates. The adoption of a network design using a single cascade impactor equipped with foil substrates reduces all costs by approximately 50%. Future studies should consider the adoption of $PM_{0.1}$ sampling network using a single MOUDI loaded with foil substrates as a strategy to reduce the barriers towards enhanced monitoring of ultrafine particles.